University of ZurichUZH

Opportunities and limitations of digital elevation models derived from optical stereo satellite imagery over Grosser Aletschgletscher, Switzerland

GEO 511 Master's Thesis

Author
Andrin Schmidli
17-550-518

Supervised by
Prof. Dr. Michael Zemp

Faculty representative
Prof. Dr. Michael Zemp

30.01.2025
Department of Geography, University of Zurich

Master Thesis of

Andrin Schmidli

andrin.schmidli@uzh.ch

Opportunities and limitations of digital elevation models derived from optical stereo satellite imagery over Grosser Aletschgletscher, Switzerland

Contact Details

Submitted by: **Andrin Schmidli**

University of Zürich

Wülflingerstrasse 324

CH-8408 Winterthur, Switzerland

andrin.schmidli@uzh.ch

Supervised by: **Dr. Michael Zemp**

University of Zürich

Winterthurerstrasse 190

CH-8057 Zürich, Switzerland

michael.zemp@geo.uzh.ch

Contents

Preface

This master's thesis symbolises the culmination of an interesting and insightful study period. After completing a Bachelor's degree in Geography and History at the University of Zürich, I pursued a Master's degree in Physical Geography at the same university. Glaciology has always been my favourite specialisation. One of the highlights of my studies was the course 'GEO851', which focused on glacier mass balance measurement and analysis under the supervision of Dr. Michael Zemp. At the end of this course, several potential topics for master's theses were presented. Although it was too early for me to decide at the time, I found the topics particularly intriguing. As a result, I knew exactly where to inquire when the time came to explore a fascinating subject for my thesis.

In this thesis, I aim to investigate the possibilities and limitations of using freely available tools and data. Given the scarcity of satellite-derived glaciological data for research purposes in universities, the *Satellite pour l'Observation de la Terre* (SPOT) – a satellite data from the French space agency – stood out to me as a promising option. Dr. Michael Zemp introduced me to Dr. Livia Piermattei, whose guidance proved invaluable. With her assistance, the stereo images provided for free were processed into Digital Elevation Models (DEMs). Using Python, I was able to process this data into measurable surface height changes, enabling an exploration of the opportunities and challenges associated with using a satellite not originally specialised for glaciology.

I would like to thank Dr. Michael Zemp for the opportunity to write this master's thesis under his supervision. Without his guidance and feedback, tackling a topic in a field relatively unfamiliar to me would have been an overwhelming task. His encouragement and insightful discussions inspired new ideas and fostered progress after every meeting.

Furthermore, I would like to thank Dr. Livia Piermattei. Without her expertise in processing the SPOT5 stereo images and providing Pléiades data, this thesis would not have been possible in its current form. Her support with coding and data usage was invaluable, especially during moments when I encountered challenges.

Zürich, January 2025   Andrin Schmidli

Summary

This thesis investigates the potential of SPOT5 and Pléiades satellite platforms as alternatives to Advanced Spaceborne Thermal Emission and Reflection Radiometre (ASTER) for glacier monitoring, particularly in the Aletsch Glacier area. With ASTER nearing its operational end, identifying new platforms capable of generating high-resolution Digital Elevation Models is critical for continued monitoring of glaciological changes. This study employs open-source software, specifically the Ames Stereo Pipeline (ASP), to process stereo imagery, perform DEM co-registration, and generate difference DEMs for analysing glacier surface height changes. By integrating SPOT5 and Pléiades datasets, the research evaluates their temporal and spatial capabilities for monitoring short-term and seasonal glacier dynamics. The methodology emphasises reproducibility and accessibility, using Python-based workflows to ensure consistent data processing and rigorous uncertainty quantification. Results demonstrate that SPOT5 and Pléiades datasets can achieve sufficient resolution and coverage for detecting glacier surface variations, making them viable successors to ASTER. However, challenges remain regarding radar signal penetration and seasonal data availability. The findings underscore the importance of refining processing workflows and integrating robust uncertainty assessments to enhance the reliability of glaciological applications. This work contributes to the understanding of how emerging satellite platforms can support glacier monitoring in response to climate change and offers pathways for improving global cryospheric studies.

Zusammenfassung

Diese Arbeit untersucht das Potenzial der Satellitenplattformen SPOT5 und Pléiades als Alternativen zu ASTER für die Überwachung von Gletschern, insbesondere im Gebiet des Aletschgletschers. Da ASTER das Ende seiner Betriebszeit erreicht, ist es entscheidend, neue Plattformen zu identifizieren, die in der Lage sind, hochauflösende digitale Höhenmodelle (DEMs) zu erstellen, um die kontinuierliche Überwachung glaziologischer Veränderungen sicherzustellen. In dieser Studie wird Open-Source-Software, insbesondere die Ames Stereo Pipeline, eingesetzt, um Stereo-Bilddaten zu verarbeiten, DEMs zu co-registrieren und Differenz-DEMs zu erstellen, um Veränderungen der Gletscheroberflächenhöhe zu analysieren. Durch die Integration von SPOT5- und Pléiades-Datensätzen wird deren zeitliche und räumliche Eignung für die Überwachung von kurzfristigen und saisonalen Gletscherdynamiken bewertet. Die Methodik betont Reproduzierbarkeit und Zugänglichkeit, indem Python-basierte Workflows verwendet werden, um eine konsistente Datenverarbeitung und eine rigorose Unsicherheitsbewertung zu gewährleisten. Die Ergebnisse zeigen, dass die Datensätze von SPOT5 und Pléiades ausreichende Auflösung und Abdeckung bieten, um Veränderungen der Gletscheroberfläche zu erkennen, und daher als geeignete Nachfolger von ASTER dienen können. Herausforderungen bestehen jedoch weiterhin hinsichtlich der Durchdringung des Radarsignals und der saisonalen Datenverfügbarkeit. Die Ergebnisse unterstreichen die Bedeutung der Verfeinerung von Verarbeitungsworkflows und der Integration robuster Unsicherheitsbewertungen, um die Zuverlässigkeit glaziologischer Anwendungen zu erhöhen. Diese Arbeit leistet einen Beitrag zum Verständnis, wie neue Satellitenplattformen die Gletscherüberwachung im Kontext des Klimawandels unterstützen können, und bietet Ansätze zur Verbesserung globaler Studien der Kryosphäre.

Glossary

Abbreviations

ASP	Ames Stereo Pipeline
ASTER	Advanced Spaceborne Thermal Emission and Reflection Radiometre
CNES	Centre National D'Etudes Spatiales
CRS	Coordinate Reference System
DEM	Digital Elevation Model
dDEM	Difference DEM
EGM	Earth Gravitational Model
EOS	Earth Observing System
EPSG	European Petroleum Survey Group
ESA	European Space Agency
GIS	Geographic Information System
GLAMOS	Glacier Monitoring in Switzerland
HiRI	High Resolution Optical Imager
HRS	High Resolution Stereo imager
LIDAR	Light Detection and Ranging
NASA	National Aeronautics and Space Administration
NIR/VNIR	Near Infrared / Visible Near Infrared
NMAD	Normalized Median Absolute Deviation
RGI	Randolph Glacier Inventory
RMSE	Root Mean Square Error
SAR	Synthetic Aperture Radar
SPOT	Satellite pour l'Observation de la Terre
TIR	Thermal Infrared
UTM	Universal Transverse Mercator
VNIR	Visible Near Infrared
WGS	World Geodetic Systems

Important terms

Ames Stereo Pipeline

Open-source software designed for generating digital elevation models from stereo image pairs (Beyer et al., 2018).

Co-Registration

Process of aligning two or more datasets to a common coordinate system to spatially align them (Nuth & Kääb, 2011).

Cryosphere

The frozen water part of the earth. It includes sea ice, permafrost, ice sheets and glaciers (Cogley et al., 2011).

Digital Elevation Model

"Digital elevation models are gridded, numerical representations of surface elevation" (Hugonnet et al., 2022).

Geodetic Method

This method of measuring glacier surface elevation relies on repeated mapping of said glacier surface. To get a mass balance from this method information on the ice, firn, and snow density is needed. The measurements are usually made using theodolites or similar instruments, but today primarily with global satellites (Cogley et al., 2011).

Glacier Morphology

Refers to the study and description of the form, structure, and surface features of glaciers, including their size, shape, flow patterns, and interaction with surrounding landscapes.

Glaciological method

This method determines the mass balance of a glacier with measurements on-site by manual measurements of the ablation and accumulation. This usually is done with snow pits and measurement stakes (Cogley et al., 2011).

Hydrological year

An alternative way to divide a year, starting the first of October and ending the 30 of September, with the advantage of being in tune with the hydrological cycle (Cogley et al., 2011).

Hypsometry

The distribution of area with elevation, often used in glacier studies to understand topographical dynamics (Zemp et al., 2014).

Mass balance

The change of the mass in a glacier over a given time. The timespan is usually a year or a season (Cogley et al., 2011).

Panchromatic

A panchromatic image is a single-band grayscale image that combines information from the visible R, G, and B bands, resulting in a high spatial resolution image with no wavelength-specific information (Filchev et al., 2020).

Radiometric Resolution

The ability of a sensor to differentiate between different brightness levels influencing the detail that can be captured in an image (Berthier et al., 2023).

Resampling

Method to change the spatial resolution or reproject raster data using algorithms like nearest neighbour or bilinear interpolation (Beyer et al., 2018).

Stable Terrain

Areas unaffected by dynamic processes like glacier movement, used as a reference in geodetic analyses (Hugonnet et al., 2022).

Stereo Imagery

Using a pair or more images with the purpose of estimating the distortion (parallax) between them. The images are derived from different cameras in different viewpoints (Toutin, 2001).

1 Introduction

The world is facing an ever-warmer climate that has effects on a global scale. From rising global temperatures to shifting weather patterns, the impacts of climate change are far-reaching, touching nearly every corner of the Earth. Among the most visible signs of this warming is the cryosphere, the frozen water part of our planet undergoing dramatic changes. This warming climate accelerates the melting of ice sheets worldwide, disrupting the balance between ice accumulation and melting. This contributes to sea level rising and altering of ecosystems, impacting global weather patterns and freshwater resources. This global pattern of ice loss also extends to glaciers. While the melting of polar ice sheets garners significant attention due to their scale, smaller glacier systems around the world are also rapidly losing mass, with profound regional and global implications. Glaciers are an important indicator of climate change. Their changes in geometry, driven by shifts in temperature and precipitation, are very visible and provide critical insights into broader environmental transformations. Their rapid retreat has significant implications, particularly for freshwater availability, disaster risks, and sea-level rise, which affect millions of people worldwide (Berthier et al., 2023). Moreover, the loss of glacier mass directly impacts regional water cycles, altering seasonal runoff patterns and increasing water scarcity in already vulnerable areas. Glaciers like those in the Aletsch region also serve as vital water sources for hydropower, irrigation, and drinking water. Their retreat increases the risk of glacial lake outburst floods, posing substantial threats to nearby communities (Huss et al., 2024; Kennedy et al., 2024). Globally, glaciers are a major contributor to sea-level rise, accounting for approximately 21% of observed increases during the early 21st century (Hugonnet et al., 2021). These dynamics underscore the interconnectedness of glacier systems, where changes in one region can ripple outward, influencing global hydrology and sea levels. This underscores the necessity for consistent, high-quality glacier monitoring to understand their dynamics and mitigate their impacts on vulnerable coastal areas. With the climate crisis intensifying, the availability of precise, high-resolution datasets has become crucial for assessing glacier changes at regional and global scales (Piermattei et al., 2023).

Modern advancements in remote sensing technologies have enabled researchers to capture these changes in unprecedented detail, providing a wealth of data for analysing glacier behaviour and informing policy decisions. Modern monitoring efforts often focus on polar regions or small, isolated study areas, with limited freely available global datasets. This limits the spatial and temporal availability of spatial data. The ASTER platform, which has been a cornerstone for global glacier studies, is nearing the end of its operational lifespan, creating an urgent need for alternatives. Implementing SPOT5 as a successor offers an opportunity to continue deriving geodetic measurements at a global scale, with its ability to capture elevation changes reliably in complex terrains. Its combination with Pléiades data further enhances temporal resolution and spatial accuracy, bridging gaps where ASTER and other datasets fall short (Berthier et al., 2023; Berthier & Toutin, 2008). The hydrological year 2022/2023 marked a record-breaking global annual mass balance of -1.2 metres of water equivalent, the largest ice loss since records began in 1950. This loss, driven by severe negative balances in North America and Europe, equates to roughly five times the water volume of the Dead Sea, emphasising the accelerating impacts of climate change on glacier systems (Kennedy et al., 2024). High-resolution data from SPOT5 and Pléiades offer a means to monitor these changes more effectively, particularly in alpine regions where spatial variability in thinning is often underestimated (Piermattei et al., 2023).

Uncertainty in existing DEM measurements, caused by voids, interpolation errors, and seasonal variability, remains a critical challenge. Methods like stable terrain co-registration can significantly reduce these uncertainties, enhancing the reliability of SPOT5 and Pléiades workflows (Hugonnet et al., 2022; Mesa-Mingorance & Ariza-López, 2020). Addressing these issues is vital for understanding glacier dynamics and ensuring that monitoring efforts provide actionable insights for both research and policy. By leveraging the SPOT5 archive, combined with Pléiades and potential future data from SPOT6 and SPOT7, this research aims to address key challenges in global glacier monitoring. These efforts are essential for maintaining continuity in observations, refining methodologies, and providing the high-

resolution data necessary to tackle the pressing issues of glacier retreat and its consequences (Berthier, Kargel, et al., 2024; Kennedy et al., 2024).

1.1 Motivation and Objectives

On May 11th 2024, the ASTER aboard NASA's Terra satellite reached the end of its operational life after nearly 25 years. Four days later, engineers briefly revived it, but its expected retirement by 2027 marks the close of an era in global glacier monitoring. ASTER's high-resolution DEMs have been pivotal in documenting rapid changes in glaciers globally, from thinning ice to the formation of meltwater lakes (Abrams, 2000; Abrams et al., 2015). Its 15-metre spatial resolution for visible and near-infrared (VNIR), near-infrared (NIR) and short-wave infrared (SWIR) imaging, combined with its along-track stereo capability, allowed researchers to generate global DEMs and conduct glaciological studies across diverse regions, including polar areas and alpine environments (Abrams et al., 2015; NASA, 2004). However, ASTER has limitations, including gaps in temporal coverage, susceptibility to cloud interference, and moderate resolution compared to more recent technologies. These limitations, along with its anticipated decommissioning, raise the pressing question: what comes next?

Glaciers, being among the most visible indicators of climate change, underscore the urgency of this challenge. Their retreat contributes significantly to global sea-level rise, disrupts regional hydrology, and poses risks to downstream communities that rely on glacier-fed water resources (Hugonnet et al., 2021). Glaciers in the European Alps, such as Grosser Aletsch-, Oberaletsch-, and Mittelaletschgletscher, are vital to the region, serving as reservoirs for hydropower, irrigation, and drinking water. However, their accelerated melting not only diminishes these resources but also increases the risk of glacial lake outburst floods, which threaten communities and infrastructure downstream (Huss et al., 2024). Monitoring these glaciers with high precision and temporal consistency is essential for understanding their dynamics, predicting future changes, and managing associated risks effectively.

From this context, the motivation for this thesis emerged: to evaluate remote sensing platforms with the potential of an increase in use cases as successors to ASTER. Specifically, this study focuses on SPOT5 and Pléiades, platforms that hold potential for glacier monitoring but are yet to be fully leveraged. SPOT5, with its High-Resolution Stereoscopic (HRS) imaging capability, offers a 5-metre spatial resolution and a swath width of 120 kilometres, making it well-suited for capturing elevation changes in complex terrains. These features surpass ASTER's capabilities and enable the creation of DEMs with higher accuracy (Berthier & Toutin, 2008). However, SPOT5's temporal coverage is limited, spanning from 2002 to 2015, necessitating complementary datasets. Pléiades, launched in 2011, delivers sub-metre resolution imagery with an exceptional vertical precision of ±1 metre, enabling the detection of even subtle glacier changes. Its 12-bit radiometric range further enhances its ability to capture details in snow-covered and texture less areas (Berthier et al., 2014). Together, these platforms have the potential to bridge the gaps left by ASTER and address critical needs in glacier monitoring.

To achieve these objectives, this thesis applies advanced workflows for co-registration, DEM differencing, and uncertainty analysis, as outlined by Piermattei et al. (2023). Open-source software, particularly xDEM, underpins the methodology, providing a reproducible and accessible framework for analysing SPOT5 and Pléiades datasets. xDEM enables key processing steps, including stable terrain co-registration, bias correction, and uncertainty estimation, which are essential for ensuring the accuracy and reliability of glacier elevation change measurements (Hugonnet et al., 2023; Piermattei et al., 2023). By leveraging open-source tools, this research avoids the constraints of proprietary software and promotes transparency, allowing others to replicate and extend these methods.

Beyond its methodological contributions, this thesis addresses a critical knowledge gap in global glacier monitoring: the integration of newer, high-resolution datasets to continue the legacy of ASTER and ensure the availability of reliable DEMs for both research and policy applications. The focus on SPOT5 and Pléiades reflects a deliberate effort to explore underused resources and optimise their potential for

monitoring glacier dynamics at regional and global scales (Berthier et al., 2014; Piermattei et al., 2023). By comparing the performance of these platforms against ASTER benchmarks, this study seeks to identify viable long-term solutions for alpine glacier monitoring. Such efforts are essential for maintaining continuity in observations, refining methodologies, and providing high-resolution datasets critical for understanding glacier dynamics in a rapidly changing climate (Hugonnet et al., 2021).

1.2 Thematical Introduction

The SPOT5 archive was made publicly accessible in 2021 by the French Space Agency *Centre National D'Etudes Spatiales* (CNES), offering free access to high-resolution satellite imagery. This dataset, when combined with Pléiades, a newer high-resolution platform, enables the creation of a continuous time series for monitoring glacier changes, extending from SPOT5's operational period into the present. SPOT5 has proven highly effective in capturing elevation changes in steep and complex terrains, making it suitable for alpine environments and glacier monitoring (Bernat et al., 2023; Piermattei et al., 2023). However, its limitations in flat or featureless terrains and under persistent cloud cover highlight the need for complementary datasets to ensure consistent and accurate observations (Bernat et al., 2023). The integration of SPOT5 and Pléiades significantly enhances both temporal resolution and spatial accuracy, offering a robust solution to these challenges in glacier studies (Berthier, Lebreton, et al., 2024).

Table 1: List of the relevant satellites for this thesis and key facts about them. The facts are ordered by platform. Terra is the platform on which the ASTER instrument is mounted. In the following parts, the data derived from the HRS instrument on the SPOT5 platform and the HiRI instrument on the Pléiades platform will be called by their platforms

Plattform	Terra	SPOT5	Pléiades
Launch	1999	2002	2011
Accessibility	Public	Public	upon request
System used	ASTER	High-Resolution Stereoscopic	HiRI
Resolution [m]	15 (VNIR); 30 (SWIR); 90 (TIR)	10 (cross-track); 5 (along-track)	0.5 (Pan); 2 (Multispectral)
Repeat Cycle	16 days	26 days	26
Key Facts	ASTER is an instrument aboard the Terra Satellite.	The SPOT5 satellite is making use of different sensors, the High-Resolution Stereoscopic sensor being the most relevant.	Pléiades has a High-Resolution Imager (HiRI)

With ASTER nearing the end of its operational lifespan, attention has turned to SPOT5 and its successors, SPOT6 and SPOT7, as potential tools for future global glacier research. SPOT5's finer spatial resolution compared to ASTER provides distinct advantages, particularly for detecting changes in smaller or steeper glaciers, where details are critical (Hugonnet et al., 2021; Korona et al., 2009). Furthermore, workflows developed by Hugonnet et al. (2021) and Piermattei et al. (2023) underscore the necessity of accurate co-registration and robust uncertainty analysis when integrating datasets from multiple sensors. By leveraging the publicly accessible SPOT archive and employing tools like the Ames Stereo Pipeline for generating DEMs, this thesis examines the potential of SPOT5 as a successor to ASTER. By leveraging the publicly accessible SPOT archive and employing tools like the Ames Stereo Pipeline for generating DEMs, this thesis examines the potential of SPOT5 as a successor to ASTER. The stereo data were processed using the NASA ASP, an open-source software designed for deriving high-quality terrain models from visual images like stereogrammetry and photoclinometry. The ASP was originally developed to be used to derive information about planetary topography from long-range stereo images captured from orbit. After years of use under NASA supervision, it was first publicly released under an open-source license in October 2009 (Beyer et al., 2018). Additionally, Pléiades data extends these analyses, enhancing the capacity for long-term glacier monitoring and contributing to a deeper understanding of glacier dynamics (Berthier, Lebreton, et al., 2024; Beyer et al., 2018).

1.3 State of Research

Advancements in remote sensing technologies have significantly improved the capacity for glacier monitoring, enabling precise assessments of glacier dynamics, surface elevation changes, and mass balance. The ASTER satellite, operational since the year 2000, has been a foundational tool for glacier research due to its ability to generate DEMs with 30-metre resolution through stereo imagery. Hugonnet et al. (2021) combined ASTER data with the Randolph Glacier Inventory (RGI) to produce a comprehensive global dataset covering over 97% of inventoried glacier regions from 2000 to 2019. By processing and correcting nearly 500,000 DEMs, they provided reliable long-term elevation change data while minimising seasonal effects through robust inte rpolation methods. Validation against Ice, cloud, and land elevation satellite (ICESat) and Operation IceBridge measurements confirmed the reliability of these estimates, with no significant spatial or temporal biases. The study revealed a global glacier mass loss rate of 267 ±16 gigatonnes per year, contributing 21 ±3% to sea-level rise, with significant regional variations such as accelerated thinning in Northwestern America. These results have become a benchmark for glacier mass balance studies and a foundation for this thesis (Hugonnet et al., 2021; NASA, 2004).

ASTER nears the end of its operational life, and alternative platforms such as SPOT5 and Pléiades are emerging as potential successors. SPOT5's HRS sensor excels in capturing elevation changes in steep and complex terrains, generating DEMs with a vertical accuracy of ±6 metres for 90% of the data (Korona et al., 2009). The SPOT 5 stereoscopic survey of Polar Ice: Reference Images and Topographies (SPIRIT) mission demonstrated SPOT5's effectiveness in polar regions, highlighting its capability to detect the thinning and retreat of glaciers. However, challenges persist in flat, snow-covered areas where interpolation is required to fill gaps in data. Pléiades, launched later, provides sub-metre resolution with a vertical accuracy of ±1 metre, making it particularly effective for detecting fine-scale changes in snow and ice surfaces. Its advanced radiometric range enhances its ability to handle complex textures in snow-covered regions, complementing SPOT5 by extending the temporal coverage and improving the precision of glacier monitoring (Berthier et al., 2014; Berthier, Lebreton, et al., 2024; Korona et al., 2009).

DEM production and post-processing are critical components of glacier monitoring. Accurate co-registration is a cornerstone of DEM analysis, as misalignment between datasets can result in systematic errors that compromise the reliability of surface elevation change assessments. Nuth and Kääb (2011) proposed a robust co-registration framework involving the removal of shifts, correction of elevation-dependent biases, and adjustment for sensor-specific errors such as along-track and cross-track biases. This approach, which leverages stable terrain as a reference, has become widely adopted in glacier studies, ensuring the alignment of data from different sensors such as ASTER, SPOT5, and Pléiades. Similarly, Piermattei et al. (2023) highlighted the importance of stable terrain co-registration in reducing vertical and horizontal misalignments, emphasising its critical role in DEM post-processing (Nuth & Kääb, 2011; Piermattei et al., 2023).

DEM differencing, used to quantify surface elevation changes, requires careful treatment of data voids and biases. Piermattei et al. (2023) provided a comprehensive framework for DEM differencing that includes elevation-dependent corrections, void-filling techniques, and noise filtering. These processes ensure that systematic errors are minimized, enhancing the reliability of elevation change assessments. For example, DEM comparisons often involve correcting for variations in radar penetration or adjusting for temporal mismatches in acquisition dates, both of which are essential for robust glacier monitoring workflows (Berthier et al., 2023; Piermattei et al., 2023).

Addressing uncertainties is integral to improving the reliability of glacier monitoring studies. Hugonnet et al. (2022) introduced a spatial inference approach for uncertainty analysis that uses stable terrain to model spatial error structures. This approach incorporates variograms to account for terrain-specific and sensor-dependent variations, capturing both local and large-scale biases. By propagating these uncertainties into DEM analysis workflows, researchers can ensure that error estimates are robust and

reflective of real-world conditions. Zemp et al. (2013) also stressed the importance of addressing random and systematic errors in glacier mass balance studies, advocating for the alignment of geodetic and glaciological balances to reduce discrepancies over multi-annual periods (Hugonnet et al., 2022; Zemp et al., 2013).

SPOT5 and Pléiades represent complementary datasets that address many limitations of ASTER. SPOT5, with its extensive coverage during its operational period (2002–2015), provides detailed spatial and temporal variability in glacier mass balance, as demonstrated by Bernat et al. (2023). Pléiades builds on this foundation, offering unprecedented spatial precision for detecting subtle changes in alpine and polar environments. By integrating these datasets, researchers can create high-resolution time series that improve the understanding of glacier dynamics. This integration is particularly valuable for alpine regions, such as the Aletsch area, where spatial variability in thinning is often underestimated. The workflows developed by Hugonnet et al. (2021) and Piermattei et al. (2023) serve as a methodological baseline for this thesis, providing a comprehensive framework for DEM production, co-registration, and uncertainty analysis (Bernat et al., 2023; Hugonnet et al., 2021; Piermattei et al., 2023).

By leveraging the combined strengths of SPOT5 and Pléiades, this thesis aims to assess their potential as successors to ASTER for glacier monitoring in the Aletsch region. These platforms not only address critical gaps in the spatial and temporal resolution of glacier datasets but also enable the application of advanced workflows that enhance the reliability of surface elevation change assessments. This integrated approach contributes to a deeper understanding of glacier dynamics, informing both scientific research and policy development in the context of a rapidly changing climate.

1.4 Research Questions

This thesis addresses several critical research questions to evaluate the potential of SPOT5 data for glacier monitoring and compare it to established methods. By focusing on data quality, workflow optimization, and the integration of additional datasets like Pléiades, the study aims to assess the reliability and applicability of SPOT5-derived DEMs for detecting glacier surface elevation changes. Special attention is given to the effects of seasonality, co-registration on stable terrain, and the feasibility of monitoring smaller glaciers in the Aletsch region.

- How does the SPOT5 archive data compare to the ASTER data widely used for DEMs in terms of spatial resolution, vertical accuracy, and temporal coverage when calculating surface elevation change?
- What quality results, in terms of accuracy and reproducibility, can modern open-source Python tools like xDEM create when following the workflow for glacier change introduced by Piermattei et al. (2023)?
- How can stable terrain be used to develop Python code that minimises vertical and horizontal misalignments in DEM co-registration?
- How does the introduction of Pléiades data into the workflow, to extend the temporal range, impact the accuracy and consistency of elevation change detection?
- How does the use of DEMs sourced in different seasons impact the accuracy surface elevation change measurements?
- Do the higher resolution DEMs produced from SPOT5 and Pléiades enable the observation of smaller glaciers compared to the Aletsch Glacier? If so, what results are obtained when analysing smaller glaciers like the Mittelaletschgletscher and the Oberaletschgletscher?

The focus of the research questions is on key challenges when creating a workflow to utilise and validate new DEMs for measuring glacier surface elevation changes. These questions aim to determine if the SPOT5 archive can match or exceed the benchmarks established by ASTER, particularly in terms of spatial resolution and data reliability. The significance of this comparison lies in identifying a viable successor for ASTER, especially as it approaches the end of its operational lifespan (Hugonnet et al., 2021). Moreover, the workflows developed by Hugonnet et al. (2021) and Piermattei et al. (2023)

provide a foundation for this study, focusing on co-registration optimisation and robust uncertainty quantification, both essential for ensuring the accuracy of DEM differencing.

A critical component of this study is evaluating how stable terrain can be used to refine co-registration workflows. The ability to minimise vertical and horizontal misalignments through Python-based methods like xDEM is central to this research. By building on techniques such as the Nuth and Kääb (2011) algorithm, the thesis aims to provide insights into the scalability and reproducibility of open-source tools for glaciological applications. These tools are particularly important in academic contexts, where accessibility and flexibility are key (Hugonnet et al., 2022).

The integration of Pléiades data introduces an additional dimension to this research, offering a higher resolution and extended temporal coverage compared to SPOT5. Pléiades has been designed as a successor mission to the SPOT series by the CNES and the pictures taken rely on the HiRI taking images at visible and near-infrared wavelength. However, combining data from different sensors requires addressing challenges like differing spatial resolutions and keeping individual limitations in mind. In this case, both sensors used are stereoscopic in nature and use visible and near-infrared wavelengths. This thesis explores these challenges by assessing how Pléiades complements SPOT5 in capturing elevation changes, particularly for smaller glaciers that have often been neglected in large-scale studies (Bernat et al., 2023; Berthier et al., 2023). Understanding the potential for integrating these datasets also provides a preliminary foundation for the use of SPOT6 and SPOT7 in future studies (CNES, 2024).

Seasonal variability further complicates the interpretation of elevation changes. DEMs sourced from different seasons, such as spring or fall, capture glaciers in distinct mass-balance states. This thesis examines the impact of these seasonal differences on the quality and accuracy of results, drawing on insights from Huber et al. (2020), who highlight the importance of timing in DEM acquisitions (Huber et al., 2020). Identifying the optimal season for data collection is critical for minimising uncertainty in elevation change measurements and ensuring consistency across datasets.

Finally, applying this workflow to smaller glaciers, such as the Mittelaletschgletscher and Oberaletsch-, provides an opportunity to evaluate the scalability and limitations of the methods developed. Smaller glaciers present unique challenges, including higher susceptibility to sensor resolution limits and terrain-induced errors. However, their inclusion in this study broadens the scope of SPOT5 and Pléiades applications, highlighting the potential to extend these methods beyond large, well-studied glaciers like the Aletsch (Cogley et al., 2011). These findings aim to provide actionable insights for glacier monitoring in diverse contexts.

2 Theoretical Background

2.1 The Aletsch Area

The Grosser Aletschgletscher, located in the Bernese Alps of Switzerland, is the largest glacier in the European Alps. It spans an area of approximately 80 square kilometres and contains an estimated ice volume of 12 cubic kilometres, accounting for more than 20% of the total ice volume in the Swiss Alps (Jouvet & Huss, 2019). The glacier stretches over 20 kilometres in length and descends from the accumulation area near the Jungfraujoch to its terminus at approximately 1800 metres above sea level. Its size and unique topography, including a convergence of ice streams at the Konkordiaplatz, make it one of the most studied glaciers worldwide (GLAMOS, 2024).

The glacier's accumulation area is composed of three primary firn fields: the Grosser Aletschfirn, Jungfraufirn, and Ewigschneefeld. The Grosser Aletschfirn flows from the west and is itself fed by three ice streams, the Äbeni Flueh-Firn, Gletscherhornfirn, and Kranzbergfirn, all originating at altitudes above 3800 metres. From the northwest, the Jungfraufirn contributes ice from the south wall of the Mönch and the east wall of the Jungfrau, also beginning above 3800 metres. Finally, the Ewigschneefeld, originating from the east wall of the Mönch, is the final of the three. The smaller Grüneggfirn, beginning below the Grünegghorn at approximately 3700 metres, joins the glacier on its eastern side before the tongue descends towards the Rhône valley (Swisstopo, 2024).

The Mittelaletschgletscher, situated between the Grosser Aletsch and Oberaletschgletscher, is a smaller glacier in the region with an area of approximately seven square kilometres and a length of fewer than 5.5 kilometres as of 2011 (GLAMOS, 2024). The glacier is south-facing and was connected to the Grosser Aletschgletscher until the 1970s. Its accumulation area originates near the Aletschhorn and Dreieckhorn, at altitudes around 3700 metres. The glacier tongue terminates at approximately 2300 metres above sea level, reflecting its retreat over recent decades (Swisstopo, 2024).

The Oberaletschgletscher is another prominent feature of the Aletsch region. It spans an area of just under 17.5 square kilometres and had a length of slightly over nine kilometres in 2011 (GLAMOS, 2024). Its two primary tributaries, the Oberaletschgletscher, originating from the southeast wall of the Aletschhorn, and the Beichgletscher, descending from the east wall of the Breithorn, converge at approximately 2500 metres above sea level. The glacier terminates at around 2150 metres, reflecting a significant retreat in response to warming temperatures.

The Grosser Aletschgletscher is not only a vital hydrological resource, contributing to the Rhône River's flow, but also a key indicator of climate change. Its retreat has been extensively studied, with recent models projecting significant changes throughout the 21st century. Jouvet and Huss (2019) modelled its evolution under various Representative Concentration Pathways (RCPs), revealing that even under the most moderate scenarios, substantial ice loss is expected. The glacier's tongue is anticipated to retreat by up to 12 kilometres by 2100, with only isolated ice bodies remaining above 3000 metres. This retreat will have far-reaching implications for regional water availability, tourism, and landscape evolution, including increased risks of slope destabilization and landslides triggered by the deglaciation process (Jouvet & Huss, 2019; Kos et al., 2016).

2.2 Measuring Glaciers from above

Satellite-based remote sensing has played a transformative role in glacier monitoring, evolving significantly over the decades. The journey began with the launch of the Landsat program in the 1970s, which provided the first large-scale, consistent imagery of glacierised regions. Landsat allowed researchers to map glacier extents and monitor changes over time, despite its limited spatial resolution and challenges such as frequent cloud cover (Gärtner-Roer et al., 2019; Racoviteanu et al., 2009).

In the 1990s, radar-based systems such as European Remote Sensing (ERS-1) Satellite introduced Synthetic Aperture Radar (SAR), enabling observation through clouds and during polar nights. This advancement proved invaluable for high-latitude regions, offering insights into glacier velocity and surface deformation. However, interpreting SAR data in areas with snow cover or debris presented ongoing challenges (Gärtner-Roer et al., 2019; Racoviteanu et al., 2009).

The early 2000s marked a leap forward with the introduction of ASTER and SPOT5. ASTER's stereo imaging capability provided repeatable, global coverage of glaciers with a spatial resolution of 15 metres, making it a foundational tool for studying glacier changes. SPOT5's HRS sensor complemented ASTER by enabling detailed mapping of glacier surfaces, particularly in steep and complex terrains, with a vertical accuracy of ±6 metres (Berthier & Toutin, 2008; Nuth & Kääb, 2011). However, both systems faced limitations, including susceptibility to cloud interference and relatively short operational lifetimes.

Recent advancements, exemplified by Pléiades, have introduced sub-metre resolution and improved radiometric capabilities. These innovations facilitate detailed studies of glacier morphology, enabling the detection of fine-scale changes and improving overall monitoring accuracy. Such capabilities are critical for addressing challenges such as debris-covered glaciers and rapidly changing ice margins (Berthier et al., 2014; Racoviteanu et al., 2009).

Despite these technological strides, challenges remain in satellite-based glacier monitoring. Cloud interference, polar night conditions, and difficulties in integrating multi-platform datasets continue to complicate global monitoring efforts. Nonetheless, the steady progression of satellite technology has provided increasingly robust tools for understanding glacier behaviour, offering essential insights into their responses to climate change and their role in the global water cycle (Gärtner-Roer et al., 2019; Nuth & Kääb, 2011; Racoviteanu et al., 2009).

2.2.1 The Geodetic Method

The geodetic method, rooted in early cartographic and photogrammetric techniques, has evolved into a cornerstone of glacier monitoring with the advent of satellite remote sensing. Initially relying on aerial photography, this method transitioned to digital workflows with the availability of satellite-based DEMs, enabling large-scale and long-term glacier studies (Kääb, 2002). By comparing DEMs from different times, the geodetic method calculates changes in glacier surface elevation, volume, and mass, offering a spatially comprehensive alternative to the point-based glaciological method (Nuth & Kääb, 2011; Zemp et al., 2013).

A key component of the geodetic method is the accurate co-registration of DEMs. Stable terrain is used as a reference to correct horizontal and vertical shifts, reducing errors caused by sensor biases or misalignment. This foundational step, described by Nuth and Kääb (2011), ensures that elevation differences represent real glacier changes. Uncertainty quantification, another defining feature, addresses errors stemming from DEM resolution, sensor characteristics, and terrain variability. Methods such as spatial inference modelling of error structures (Hugonnet et al., 2022; Nuth & Kääb, 2011) and corrections for radar penetration in snow and firn (Bannwart et al., 2024) further enhance reliability. Despite its strengths, the geodetic method faces challenges, including handling debris-covered glaciers, filling data voids, and reconciling differences in resolution or acquisition geometry between DEMs (Berthier et al., 2007; Racoviteanu et al., 2009). While it provides extensive spatial coverage, it depends heavily on high-quality datasets and robust processing workflows, making it computationally demanding. Compared to the glaciological method, which offers direct measurements of surface mass balance, the geodetic method excels in capturing long-term and large-scale trends but requires more indirect calculations. The geodetic method's integration of historical and modern datasets has transformed glacier studies. By combining diverse DEMs over broad regions, it provides critical insights into glacier responses to climate change, complementing field-based glaciological methods and advancing our understanding of glacier dynamics (Nuth & Kääb, 2011; Zemp et al., 2013).

2.2.2 Stereo Images and other measurement methods

Stereo imaging is one of the most significant advancements in glacier measurement, providing detailed data on surface elevation and morphology through paired images captured from slightly different angles. Historically, stereoscopic methods began with aerial photography, which laid the groundwork for the development of spaceborne applications (Kääb, 2002). Early satellite missions like SPOT1 and Landsat included stereo imaging capabilities, but it was the HRS sensor on SPOT5 that demonstrated the full potential of satellite-based stereo imagery for glacier monitoring (Berthier & Toutin, 2008). SPOT5 enabled the generation of DEMs with high spatial accuracy, revolutionising the ability to monitor elevation changes in steep and remote terrains.

Stereo imaging works by combining two images captured from different angles to generate a three-dimensional representation of the terrain. This method offers several advantages, including the ability to map large areas with high spatial resolution and to measure elevation changes over time. For glaciers, this has been instrumental in tracking surface thinning, mass loss, and dynamics (Berthier et al., 2023). Platforms like ASTER further refined stereo imaging, enabling near-global coverage with a spatial resolution of 15 metres. However, ASTER faced limitations, including data gaps due to cloud cover and issues with temporal frequency (Racoviteanu et al., 2009).

The challenges of stereo imaging lie in its reliance on clear skies and consistent lighting conditions, which can limit applicability in polar regions or during the winter season. Furthermore, debris-covered glaciers and snow-covered surfaces can reduce the accuracy of surface elevation measurements. Despite these challenges, stereo imaging has remained a cornerstone of glacier monitoring due to its balance of spatial resolution and global accessibility (Berthier & Toutin, 2008; Kääb, 2002).

Other measurement methods, including radar interferometry and laser altimetry, complement stereo imaging by addressing some of its limitations. Radar systems, such as those deployed on ERS-1 and Sentinel-1, operate independently of weather conditions and daylight, making them suitable for polar and cloudy regions. However, radar data often require complex corrections for signal penetration into snow and firn layers, as highlighted by Bannwart (2024). Laser altimetry, exemplified by ICESat and ICESat-2, offers highly precise elevation measurements but lacks the spatial coverage of stereo imaging, limiting its applicability for large-scale glacier studies (Bannwart et al., 2024; Berthier et al., 2023).

The historical progression of glacier measurement methods reflects a gradual integration of different techniques to overcome individual limitations. While stereo imaging has been pivotal for high-resolution surface mapping and elevation monitoring, integrating it with radar and altimetry data has improved temporal and spatial continuity. This combined approach ensures that challenges such as cloud cover, seasonal snow, and debris are addressed more effectively, providing a comprehensive picture of glacier dynamics over time (Racoviteanu et al., 2009; Zemp et al., 2014).

2.2.3 Big Cameras in Space

SPOT5 and Pléiades satellites have played pivotal roles in Earth observation, contributing to a wide range of applications beyond glacier monitoring. Launched in 2002, SPOT5 was designed to provide high-resolution imagery for uses such as urban planning, agriculture, forestry, and natural disaster assessment. Equipped with the High-Resolution Geometric and HRS sensors, SPOT5 could capture images with resolutions of 2.5 to 5 metres. This capability made it highly versatile for mapping diverse terrains, and its stereoscopic imaging was particularly suited for creating detailed three-dimensional representations of the Earth's surface. These features also made SPOT5 invaluable for tracking changes in mountainous regions, including glaciers, during its operational lifetime (Berthier & Toutin, 2008; ESA, 2024)

The Pléiades constellation, launched in 2011, further expanded the possibilities of satellite-based observation. With sub-metre resolution and enhanced radiometric capabilities, Pléiades enabled more detailed monitoring of urban growth, agricultural landscapes, and environmental changes, while also

proving highly effective for applications like disaster response and infrastructure assessment. Pléiades offered a significant advancement over SPOT5 in glaciology, providing higher precision for observing surface changes, crevasse formations, and glacier retreats. This improvement was particularly beneficial for alpine glaciers, where fine-scale observations are crucial for understanding complex dynamics (Airbus, 2025; Berthier et al., 2014; LEGOS, 2025).

The transition from SPOT5 to Pléiades highlights the evolution of satellite technology, with each system offering unique contributions. While SPOT5 was instrumental in providing a broader picture of Earth's surface at a moderate resolution, Pléiades has refined the focus, enabling more detailed and precise observations. Together, they have enhanced the ability to study glaciers alongside a wide array of other environmental and human systems, underscoring their broad impact on remote sensing (Berthier et al., 2014; Nuth & Kääb, 2011).

3 Data and Methods

3.1 The Aletsch Area Digitised

For this thesis, the most up-to-date data available at the time of writing was used. An overview of the data and their space in time can be found in Figure 1. The SPOT5 stereo images were obtained from the SPOT World Heritage archive and the DEMs were generated by Livia Piermattei, UZH/RSE, in collaboration with ScienteIT (UZH) using the Ames Stereo Pipeline (Beyer et al., 2018). These elevation models are high-resolution but contain some voids and outliers, particularly in areas where clouds were automatically removed. The Pléiades data, similarly processed, share these characteristics, offering detail with occasional gaps in coverage. The RAGMAC dataset, accessible online, was used primarily to develop my processing pipeline rather than for direct analysis, containing a variety of ASTER DEMs. For land cover classification, data from Copernicus was utilised. While this data provides valuable information, the resolution of 100 metres and the 2019-dated data set necessitated combining them with more detailed information from the RGI. The RGI, sourced directly from its website, offers a comprehensive dataset of glaciers larger than 0.01 square kilometres, providing all the necessary details for glacier analysis in the Aletsch region. The GLAMOS dataset from Huss, acquired with the support of my supervisor Michael Zemp, was also used to check the validity of my data. While this dataset is a simulation and thus not suitable for validation, it provides a valuable basis for comparisons. Finally, the ASTER data from Hugonnet et al. (2021) served as a foundation for a wide range of studies and is both temporally interpolated and validated. This makes it an excellent reference point for validating my findings in this thesis.

3.1.1 Elevations Measured from Space

The data from Hugonnet et al. (2021) was downloaded for this thesis. This data is provided as a timeline from 2000 to the end of 2019 as an interpolation at each pixel using the ASTER measurements available to create a continuous dataset. As this study used the RGI 6.0, the outlines had to be compared to the RGI 7.0 outlines used here for this thesis. They match the ones I used for the Aletsch Glacier, the Mittelaletsch- and the Oberaletschgletscher. Therefore, I used the data provided in this study, with the downside that the results are in millimetre water equivalent. There is no conversion to surface elevation change in millimetres for the specific glaciers provided. An error calculation can be downloaded for each dataset provided. It also provides change rate maps for different outlines in 5-year intervals (Hugonnet et al., 2021). The distribution of much of the ASTER data can be found in Figure 9. The ASTER data points were derived from the RAGMAC WG1 Glacier volume change intercomparison experiment (Braun et al., 2022).
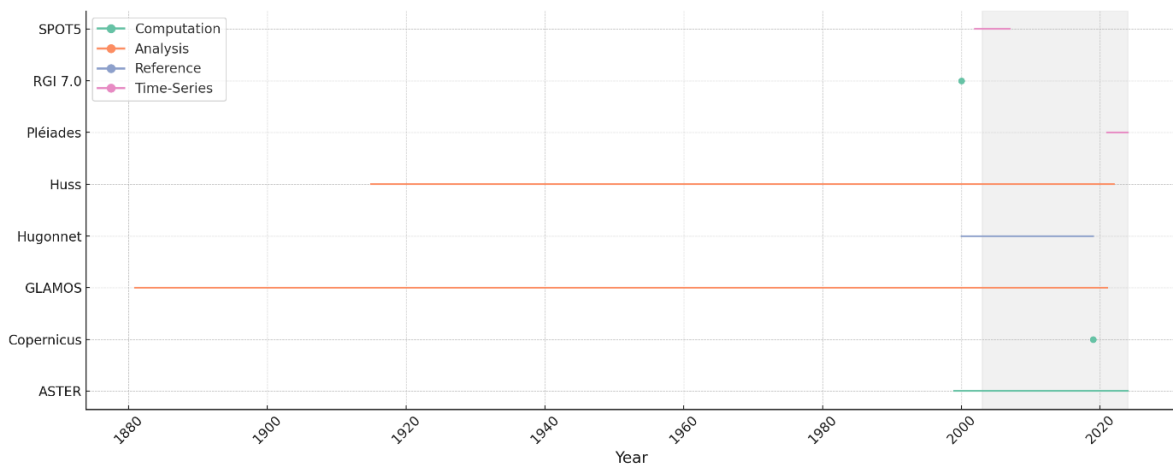

Figure 1: Temporal distribution of data used for this thesis. *The data included here ranges from the data used for the time series to additional data needed for computation to data used for reference and comparison. The time series temporal extend is marked by a light grey background. Huss stands for the GLAMOS (2022) model based on precipitation and temperature explained below. Hugonnet stands for the Hugonnet (2021) time series used as a reference. The rest of the data points represent the data introduced in Chapter 3.1.*

The numerical model output from Glacier Monitoring Switzerland (GLAMOS) (2022) was used to validate and understand the output. The model is based on precipitation and temperature data and was developed by Huss and colleagues at the GLAMOS. The output from this model represents a CSV file containing information about simulated daily accumulation and ablation over an extended period from 1915 to 2022 (GLAMOS, 2022). Because of the simulated nature of the model, it can only be used as a comparison. The model is trained using stake measurements on the glacier, some of the values had to be used with care at this point, as they contain positive ablation for example.

A further mass balance series provided by GLAMOS is an extensive dataset about many Swiss glaciers for some time from 1881 to 2020/2021, depending on the glacier data available. This extensive data series can also be accessed through their website. There is data available for many glaciers in Switzerland, but the specific data and its quality vary. The mass balance series gives an insight into the health of the glacier and is usually per hydrological year in millimetres water equivalent (GLAMOS, 2024). For the Grosser Aletschgletscher, there are extensive time series and data about length change (cumulative and periodic) and mass balance (yearly, winter and cumulative). This is also a welcome opportunity to validate the measurements from my geodetic method.

The SPOT5 data is at the centre of this thesis. Its task is to take Earth images from a sun-synchronous circular polar orbit. There are two instruments aboard that offer different modes at different resolutions. The data used in this thesis is derived from the HRS instrument. It operates in panchromatic mode using two cameras, pointing forward and backwards. This enables it to take stereo image pairs that show the relief of the earth pictures taken at a resolution from 2.5 or 5 metres. The results of the satellite observations are stereoscopic images (ESA, 2024). The SPOT5 satellite data is processed by the ASP. Stereo image pairs are found and out of these image pairs DEMs are calculated. A selection of images has been processed into DEMs for the period from 2002 to 2007 (Beyer et al., 2018).

The Pléiades data can be seen as a successor to the SPOT series. Because of the limited temporal coverage of SPOT5, Pléiades data is added to the DEM pool to extend the series into 2021 and 2024. The Pléiades data was kindly provided by Livia Piermattei through contact with Etienne Berthier (Berthier, Lebreton, et al., 2024). The DEMs provided were of higher resolution than the SPOT DEMs and suffered from very little voids, making these three DEMs a good reference.

The SPOT5 DEMs used in this thesis are primarily clustered around the years 2003–2007. This is why a time series from spring 2003 to spring 2007 has been created. Additionally, there is better SPOT5 data visible in spring, which led to the creation of a time series using only SPOT5 for the years 2003, 2004, 2005, and 2007. The Pléiades data are available for the years 2021 and 2024. These are used as an extension of the SPOT5 data, making it possible to create a time series from 2003 to 2024 for the spring series and from 2003 to 2021 for the fall series.

3.1.2 What is where?

To form outlines, I use the RGI 7.0, which aims to provide outlines for all glaciers bigger than 0.01 square kilometres as close as possible to the year 2000. The dataset is provided globally and can be downloaded for specific glacier-covered regions of the world. To get the outlines needed for the calculation of the Grosser Aletschgletscher, the central European dataset was used. The Grosser Aletschgletscher outline is dated the 13 August 2003. The same dataset was used for the Mittelaletsch- and the Oberaletschgletscher. These outlines, derived from the Landsat 5 thematic mapper (TM) and Sentinel-2 images, offer glacier boundaries at resolutions ranging from 30 to 90 metres, depending on the glacier size. For example, the Grosser Aletsch- is mapped at a 90-metre resolution, while the Mittelaletsch- and Oberaletschgletscher have outlines mapped at 30 metres (RGI 7.0 Consortium, 2023).

For the landcover classes, from the land monitoring service under Copernicus.eu, the 100-metre raster for the Land Cover 2019 was chosen, as it is the newest one available from a time series starting in 2005 and ending in 2019. The European Union's Copernicus Land Monitoring Service information Copernicus provides precise information on the global distribution of physical coverage of the earth's

surface. I am working with the Land Cover Change Version 3.0. The dataset can be downloaded using EPSG:4326 with the ellipsoid WGS 1984 projection. The crucial information for the thesis here is being able to differentiate stable terrain from unstable terrain and vegetation to maximise the quality of the co-registration (Copernicus, 2020).

3.2   Putting it all together

The processing of the data was done in two specific rounds. First through the ASP, where the SPOT5 stereo images were processed into DEMs. This step was done by Livia Piermattei's team at UZH. The pipeline is introduced in a descriptive manner in Figure 2 and was based on Beyer et al. (2018). The Pléiades pictures have also been provided by Livia Piermattei. Her contact with Etienne Berthier from the University of Toulouse allowed me to work with this data, provided in connection to Berthier, Lebreton, et al. (2024). As I received all data in a DEM format, I wrote my pipeline by relying heavily on open-source tools. I split my code into three distinct parts, with the first being the co-registration of datasets used for a timeline of a specific glacier of the Aletsch region to a reference DEM. The second step is the DEM differencing step, providing a reliable output for step three using the co-registered data from step one. The third step is the analysis, it has been separated from the first two steps to make it easier to adapt to additional analysis that might become relevant over time working with these data sets and eventual needs that come up over time when writing a thesis and analysing intermediate outputs
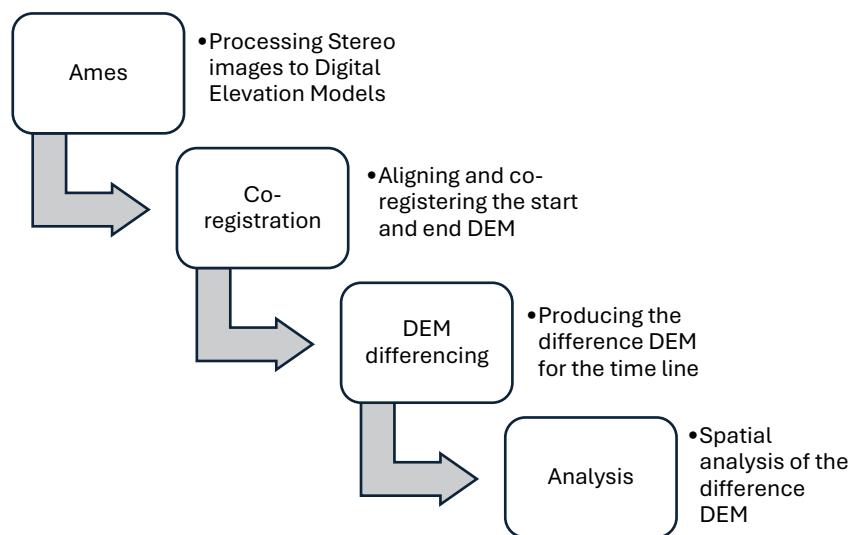

Figure 2: Four codes that convert the stereo images into glacier surface height change in millimetres per year. The four pipelines loosely follow the steps suggested by Piermattei et al. (2023). Additional info is to the right of the boxes, describing the purpose of a step. The Ames Stereo Pipeline produces the output data, that is processed by the three consecutive scripts developed for this thesis. First by the co-registration script, then by the DEM differencing script and lastly by the analysis script. The last three scripts can be found in the appendix.

3.2.1   Satellite to Computer: Ames Stereo Pipeline

The release of the ASP marked a shift toward accessibility and broader applications, including Earth observation. The data processing begins with refining the Rational Polynomial Coefficients (RPCs) of the satellite images. These coefficients are crucial for geolocation accuracy, essentially linking each pixel in the image to a specific real-world coordinate. To guide this adjustment, approximate minimum and maximum elevations of the area are used. This refinement ensures that the RPCs align closely with the true geometry of the Earth's surface. ASP's support for RPCs camera models allows it to process a variety of satellite data, including from SPOT5 and Pléiades. Once refined, each image in the stereo pair is re-projected into a unified coordinate system. This step is vital for aligning the images, enabling effective stereo matching.

Stereo matching is the process of identifying corresponding points in the two images, a key step in deriving 3D information. Advanced algorithms such as Semiglobal Matching (SGM) and More Global Matching (MGM) are employed. These methods are designed to create disparity maps, which quantify the differences in perspective between the two images. SGM and MGM enhance ASP's capability to resolve areas with low texture or repetitive patterns, surpassing earlier block-matching algorithms. Disparity maps serve as the foundation for constructing 3D point clouds, representing the terrain in high detail. The ASP is good at optimising these workflows by incorporating hierarchical, multi-resolution processing. This approach allows for the efficient handling of large datasets by working progressively from lower to higher resolutions. Additionally, ASP includes subpixel refinement techniques to ensure accuracy, addressing challenges like areas with low texture or significant occlusions. These refinements are essential for achieving sub-metre vertical accuracy, particularly in rugged or complex terrains. These refinements result in high-quality point clouds that capture intricate terrain details. The generated point clouds are then converted into DEMs. DEMs are gridded representations of the terrain, essential for various analyses. To ensure global consistency, each DEM is adjusted to the Earth Gravitational Model (EGM) 2008 geoid model, a standard for vertical referencing. This correction standardises the elevation data, aligning it with a global model rather than a local or satellite-specific reference. Finally, the DEMs undergo a co-registration process to align them with a high-resolution reference DEM, often derived from Light Detection and Ranging (LIDAR) data. Co-registration minimises discrepancies in position and ensures spatial consistency across the dataset. This step typically employs the Iterative Closest Point (ICP) algorithm, a method well-suited for aligning complex 3D datasets. The resulting DEMs provide accurate and standardised terrain data, forming a critical foundation for analysing glacier thickness changes and other geospatial phenomena central to this thesis (Beyer et al., 2018).

3.2.2 Creating a Pipeline

The script to process the SPOT5 and Pléiades data has been written over a period of several months. The script, made from three sub-scripts, can be found in the addendum of this thesis. The functions and goals of each script, and the tools used are described here but it will not go into any in-depth description of the coding process itself. The code was written by me with help from the Artificial Intelligence tool ChatGPT to streamline the process when needed. This way, a smooth data flow from start to finish was ensured, helping especially in making calculations of big datasets more efficient and reducing processing time. The code was written using the Anaconda Distribution version 3.12.3. An environment has been created and Spyder was chosen as the preferred user interface. The reason for that is prior experience with Spyder and the easily readable console output, the variable explorer and overall easy interfaces. Some of the primarily used libraries consist of xDEM, numpy, rasterio, geopandas, shapely, matplotlib and datetime. Taking a closer look at Piermattei et al. (2023), I used the "experiment configuration and general workflow for glacier elevation change assessment using DEM differencing [...]" (Piermattei et al., 2023). Especially important to this thesis is the third step in Figure 3, "Post-Processing" in the Piermattei's et al. (2023) paper. The following steps are named: Bias correction, DEM co-registration, noise filtering, void-filling, and DEM differencing. These steps have been introduced into my code as can be seen in the following subchapter (Piermattei et al., 2023).
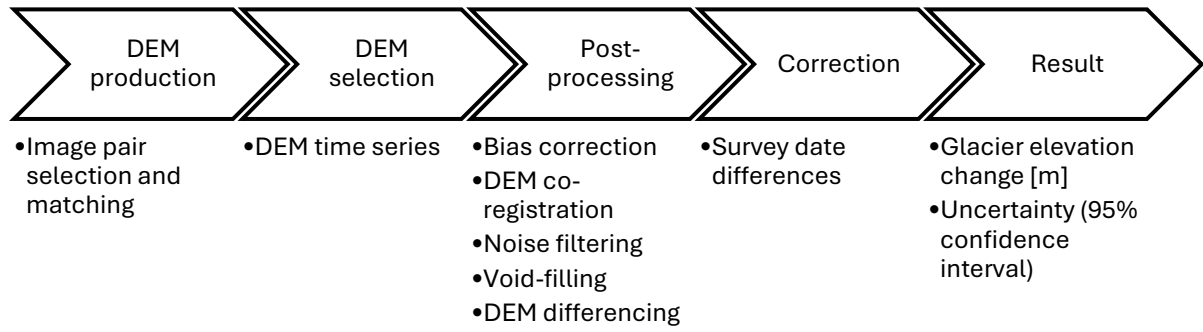
Figure 3: Steps of Piermattei et al. (2023) implemented into the code. The DEM production is done via the Ames Stereo Pipeline. The main steps used can be found in the arrows. The sub-steps taken in each section are listed below and chosen as important steps for the creation of the pipeline for this thesis. Each step can be found in some form in the final code. There are sub-steps of Piermattei et al. that are not used in this thesis and are not listed. Thie selection was done due to time constraints whilst preserving a meaningful output.

3.2.3 Ensuring a Perfect Match: Co-registering

The purpose of the workflow depicted in Figure 4 is to accurately align two Digital Elevation Models for subsequent analysis of surface elevation changes over glaciers. DEM co-registration is a critical step in glaciological studies, as even minor misalignments between DEMs can lead to significant errors in detecting and quantifying changes in surface elevation. This workflow takes a structured approach, starting with input data preparation, followed by spatial alignment, masking of unstable areas, co-registration, and different outputs along the way.

The first step in the workflow involves the preparation of input data. The two DEMs used include a reference DEM (REF DEM) and a to-be-aligned DEM (TBA DEM). The REF DEM represents the baseline for alignment. Due to the combination of SPOT5 and Pléiades, the latter has been chosen as the reference DEM due to its high quality, minimal voids and high resolution. The TBA DEM, requires alignment to the REF DEM to enable accurate comparisons. In addition to the DEMs, the additional data includes a global landcover raster and glacier outlines. The landcover raster, a 2019 global classification map, is used to identify stable terrain such as bare ground, which remains mostly unchanged over time and serves as a reliable reference for co-registration (Image 1). For this Herbaceous vegetation and Bare/Sparse vegetation have been selected as landcover classes to use as stable terrain to exclude any ice or snow-covered areas as well as vegetation. The glacier outlines delineate the glaciers' boundaries and exclude dynamic glacier regions from the co-registration process. This is done by adding a 200-metre buffer zone around the RGI glacier outlines. This buffer is intersected with the landcover classes, creating the final stable terrain used for co-registration.

Since the input datasets may have different coordinate reference systems (CRS), the workflow first ensures that all inputs are reprojected to the same CRS. The chosen CRS is the Universal Transverse Mercator (UTM) Zone 32N (EPSG:32632), which minimises distortion over the study area in the Swiss Alps. UTM coordinates are ideal for regions of limited extent, as they provide consistent units (metres), and reduced distortions compared to global coordinate systems like World Geodetic System (WGS) 84. A custom reprojection function checks the CRS of each dataset and reprojects it only if necessary. This step is done to save computational resources, as the code is already demanding large quantities of memory space. Along with reprojection, the spatial alignment of the DEMs is ensured by interpolating the TBA DEM onto the same grid structure as the REF DEM. Bilinear resampling is used for this step, as it provides a good balance between accuracy and smoothness by interpolating elevation values based on surrounding pixels. After reprojection and alignment, the workflow identifies areas of overlap between the two DEMs. An overlap mask is created to isolate regions where both DEMs have valid data, excluding any 'nan' values or areas outside the extent of the datasets. This ensures that all further

operations focus only on overlapping areas, avoiding artefacts at the boundaries of the datasets and is necessary to avoid clashes in later processes, that cannot handle 'nan' pixel values.
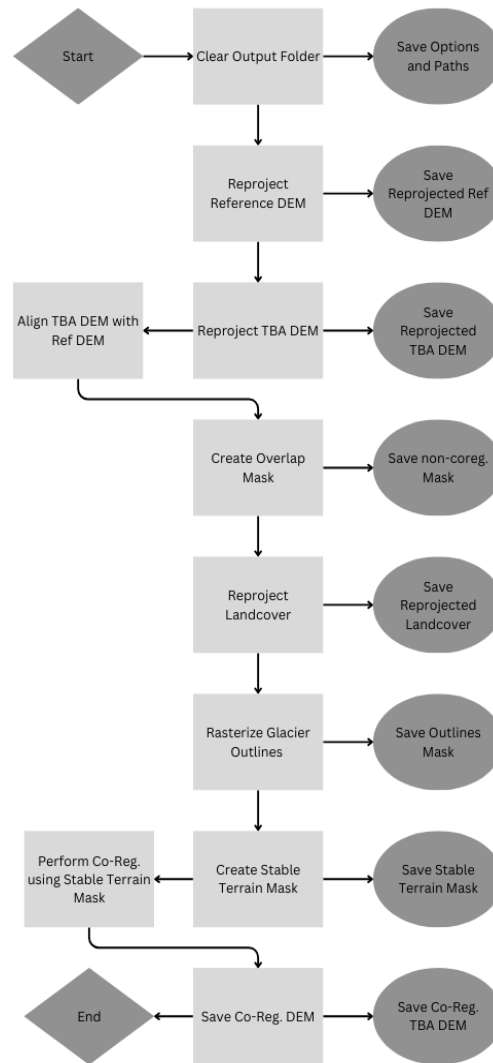

Figure 4: Flow chart of the Co-Registration process. *All the saved outputs of the code are illustrated as dark grey circles. They are used later in the code again for the co-registration process. The code ends at End. The main output is a reprojected and co-registered TIFF file of the input 'to be aligned' (TBA) DEM. It can be found in the final circle. Some of the intermediate outputs are saved for data interpretation. The code can be found in the appendix (Chapter 8.1).*

The co-registration itself is performed using the Nuth and Kääb algorithm, which is widely regarded as the standard for DEM alignment in glaciological studies (Piermattei et al., 2023). This algorithm iteratively minimises elevation differences between the two DEMs by applying small horizontal shifts to the TBA DEM. It analyses elevation differences over the stable terrain mask, fitting a transformation model to reduce systematic biases in the horizontal and vertical dimensions. A maximum of 10 iterations is used, balancing computational efficiency with alignment accuracy. More iterations might marginally improve the results but at a significant computational cost, while fewer iterations could fail to converge to an optimal solution. This can easily be adjusted, and tests have shown that more than 10 iterations do not change the result any more in a way that can be differentiated from noise or artefacts.

The final output of the workflow includes the co-registered DEM, which represents the TBA DEM aligned with the REF DEM. The co-registered DEM is saved with the same resolution, CRS, and metadata as the REF DEM, ensuring compatibility with further analyses. Additionally, the workflow generates masks for quality control, including the overlap mask and the stable terrain mask. These masks, which are created as a byproduct of the co-registration, provide insights into the areas used for said co-registration and allow for debugging or further refinement of the process. A PDF documenting

the parameters and file paths used in the workflow is also generated, providing a transparent record of the process for reproducibility. The numbers and parameters used in this workflow, such as the 200-metre buffer around glacier outlines and the 10 iterations for the Nuth and Kääb algorithm, were chosen based on trial and error. The buffer distance reflects what has been deemed unstable terrain by looking at the stereo images and identifying moraines and debris lining the glacier outlines. Using simple distance measurement tools, 200 metres have been determined to reliably exclude enough unstable terrain from the co-registration process without minimising the available stable terrain too much. The number of iterations for the co-registration algorithm was selected to strike a balance between accuracy and computational efficiency, as more iterations gave diminishing returns in alignment quality.
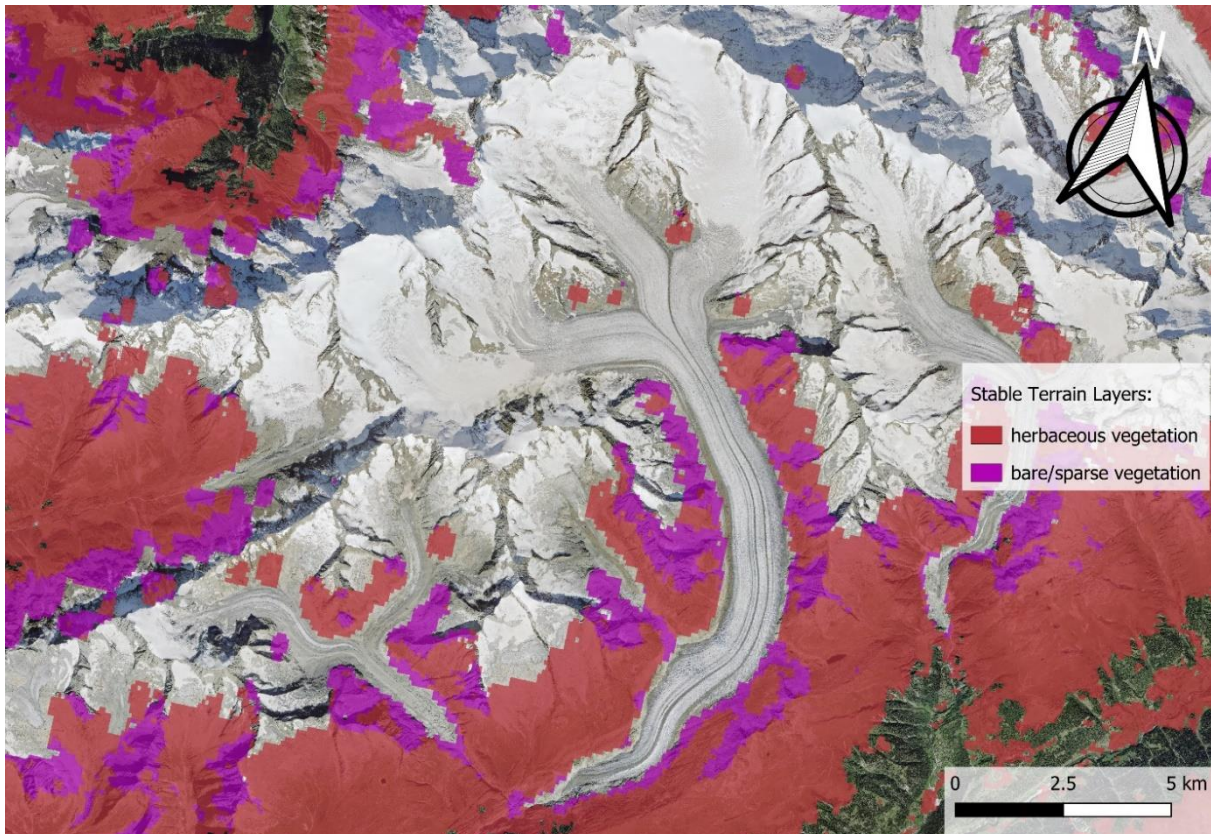

Image 1: Orthophoto overlaid with the Copernicus landcover classes chosen as stable terrain. *In purple is the bare/sparse vegetation and the red area is the herbaceous vegetation area. Both classes have been used for the creation of the stable terrain mask. Areas that are not pink or purple have a different classification in the Copernicus Land Cover Classes. This picture only includes the immediate vicinity of the Aletsch area with the stable terrain masks produced in the code being bigger. This screenshot helps to visualize the different terrains, slopes and aspects included in the stable terrain mask. Outside the masked area there is forest and vegetation as well as snow, ice and bare rock visible. As a result of the code an additional buffer area of 200 metres is later generated around glaciated areas classified using RGI 7.0, reducing the stable terrain mask further, as can be seen in Image 2.*

3.2.4 Bringing it together: DEM differencing

The DEM differencing workflow, shown in Figure 5, is designed to compute and refine the differential elevation changes between two DEMs, representing surface elevation dynamics over time. The process involves calculations and filtering techniques to ensure that the resulting dataset reflects reliable changes while excluding outliers and anomalies. This step is critical for the study of glaciated and non-glaciated regions, particularly for understanding elevation changes and glacier mass balance.

The input data consists of two co-registered DEMs: One representing the older snapshot and the other a more recent snapshot. These DEMs are pre-processed to ensure spatial alignment, making them suitable for direct comparison. Additionally, glacier outlines in shapefile from RGI format are provided to delineate the glacier area, enabling separate treatment of glaciated and non-glaciated regions. The newer DEM serves as the reference for this differencing workflow, with its spatial metadata determining the

alignment of all subsequent calculations. Starting with a first step in the process is the subtraction of the older DEM from the newer DEM, calculated on a pixel-by-pixel basis. This operation results in a differential DEM that quantifies elevation changes across the study area. However, raw differencing may include regions where data is missing in one or both DEMs, resulting in invalid values. To address this, an overlap mask is used for identifying pixels where both DEMs contain valid data. This ensures that only reliable overlapping regions are included in subsequent steps, with any non-overlapping or 'nan' areas excluded. The overlap mask is applied to the difference DEM, leaving a clean dataset focused on the area of interest.
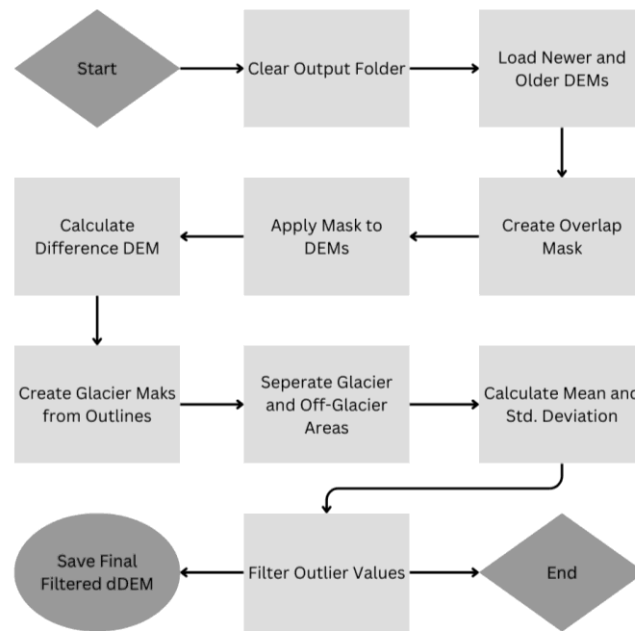

Figure 5: Flow chart for the difference DEM code. It starts at Start and runs through the necessary steps of loading the data, calculating the difference DEM, filtering outliers and saving it. The output can be seen in the figure as a dark grey circle is the difference DEM in TIFF format. The data loaded into this code is already co-registered from the previous script. The code can be found in the appendix (Chapter 8.1).

The difference DEM is then split into two subsets: on-glacier and off-glacier areas. For each subset, basic statistical metrics are calculated, including the mean and standard deviation of the elevation changes. These metrics provide a baseline for identifying and excluding outliers. Using a threshold based on three times the standard deviation, pixels with elevation changes significantly outside the expected range are flagged as outliers. For glacier-covered areas, this threshold is applied relative to the mean elevation change of the glacier subset, while for non-glacier areas, it is applied using the corresponding statistics for the terrain. This separation is crucial, as the elevation dynamics of glaciers often differ markedly from those of stable terrain, making it necessary to filter each region independently.

Outlier exclusion involves replacing the flagged values in the dDEM with 'nan', effectively removing them from further analysis. For glacier-covered areas, pixels with elevation changes exceeding three standard deviations above or below the mean are excluded, as they likely represent errors or extreme anomalies rather than true changes. Similarly, for non-glaciated regions, the same approach is applied, ensuring that anomalies such as misclassifications, sensor errors, or extreme noise are filtered out. By applying this process separately to the on-glacier and off-glacier subsets, the workflow maintains the integrity of the data while removing artefacts that could distort the analysis. Once the filtering is complete, the refined difference DEM is saved as the final output. This filtered dataset reflects the reliable elevation changes between the two periods, with outliers excluded and invalid regions masked. The output file retains the spatial metadata of the input DEMs, ensuring compatibility with further geospatial analysis. The choice of parameters in this workflow, such as the three-standard deviation threshold for outlier exclusion, is informed by statistical principles and practical considerations. The

three-sigma rule captures approximately 99.7% of data under a normal distribution, making it a robust choice for identifying extreme values while retaining valid changes. The separation of glaciated and non-glaciated regions further enhances accuracy, as it acknowledges the distinct characteristics of each area and avoids introducing biases into the filtering process. This provides a reliable method for quantifying surface elevation changes over time, ensuring that the results are robust and meaningful. By using an extra step for handling outliers and distinguishing between different terrain types, the workflow produces an interpretable dataset that forms the foundation for further analyses, such as glacier mass balance estimation or landscape evolution studies.

3.2.5 Understanding the Results: Analysis

Figure 6 represents a workflow for analysing glacier elevation changes through DEM differencing. The workflow incorporates methodologies for glacier analysis and statistical approaches that are calculated from geospatial processing, and in the end a documentation in the form of several PDF files saved to a desired output folder. It encapsulates a framework that reflects best practices in glaciology (Hugonnet et al., 2022).

The primary goal of this workflow is to quantify, analyse, and visualise changes in glacier surface elevation over time. The analysis is based on a differential DEM that represents the elevation differences between two points in time. The periods are specified by the user, ensuring flexibility in applying this workflow to various datasets. By inputting a start date and an end date, the temporal scope of the analysis can be set, thus fine-tuning the desired output. However, for my analysis, better results were obtained with the dates matching the ones of the input DEMs. The workflow also calculates annual rates of change, enabling a consistent comparison of elevation dynamics across different periods. The input datasets include besides the differential DEM, a stable terrain mask, a reference DEM, and glacier outlines. The difference DEM is pre-filtered to exclude outliers and anomalous values, ensuring a high-quality dataset for subsequent analyses. The stable terrain mask identifies regions unlikely to experience elevation changes, providing a reliable baseline for uncertainty quantification. Glacier outlines delineate the boundaries of glaciers, allowing the analysis to separate glacier-covered regions from stable terrain. Each input has been chosen to maximise the robustness and reliability of the results.

The first major component of the workflow is an uncertainty analysis. Uncertainty is inherent in DEM differencing due to factors such as sensor noise, interpolation errors, and alignment inaccuracies. The workflow explicitly addresses these uncertainties by analysing the stable terrain, where changes in elevation are expected to be minimal. By focusing on stable terrain, the workflow provides a benchmark against which glacier elevation changes can be compared. Statistical metrics such as the median, mean absolute deviation (MAD), normalized MAD (NMAD), root mean square error (RMSE), and standard deviation are calculated to quantify the variability in the difference DEM. These metrics provide a comprehensive picture of the data quality, highlighting potential biases and noise levels. The use of NMAD is particularly significant for this thesis. Unlike the standard deviation, NMAD is robust to outliers, making it well-suited for datasets where extreme values may distort the standard deviation. By scaling MAD with a factor of 1.4826, the NMAD is reached. The NMAD approximates the standard deviation for normally distributed data. In the same code, histograms are generated to visualise the distribution of elevation changes. Separate histograms are created for the stable terrain and the glacier-covered regions of the difference DEM, allowing me to compare their respective characteristics. Key metrics such as the mean, median and the zero-line are annotated on the plots. These visualisations serve a dual purpose: they provide immediate insights into the data distribution and facilitate quality control by highlighting potential anomalies.

The second major component of the workflow involves a hypsometric analysis, which examines elevation changes within specific elevation bands. Elevation bands are defined in 100-metre intervals, reflecting a resolution that balances granularity with computational efficiency. For each band, the workflow calculates metrics such as the median, mean, standard deviation, and total area covered by the difference DEM. This analysis reveals how elevation changes vary across different altitudes, providing

insights into glacier dynamics such as thinning at lower elevations or accumulation at higher elevations. The hypsometric analysis includes a bar chart, that depicts the distribution of elevation changes within each band. The lines in the graph are generated to show how the median and mean elevation differences vary across elevation bands. Error bars are included in the report to indicate variability within each band, highlighting the confidence intervals for the reported values. Additionally, there is a series of smaller hypsometry created, showing the distribution of pixels within each of the height bands, creating a small graph for each band. These plots are combined into a single output PDF for analysis. These plots use colourblind-friendly palettes to ensure accessibility.
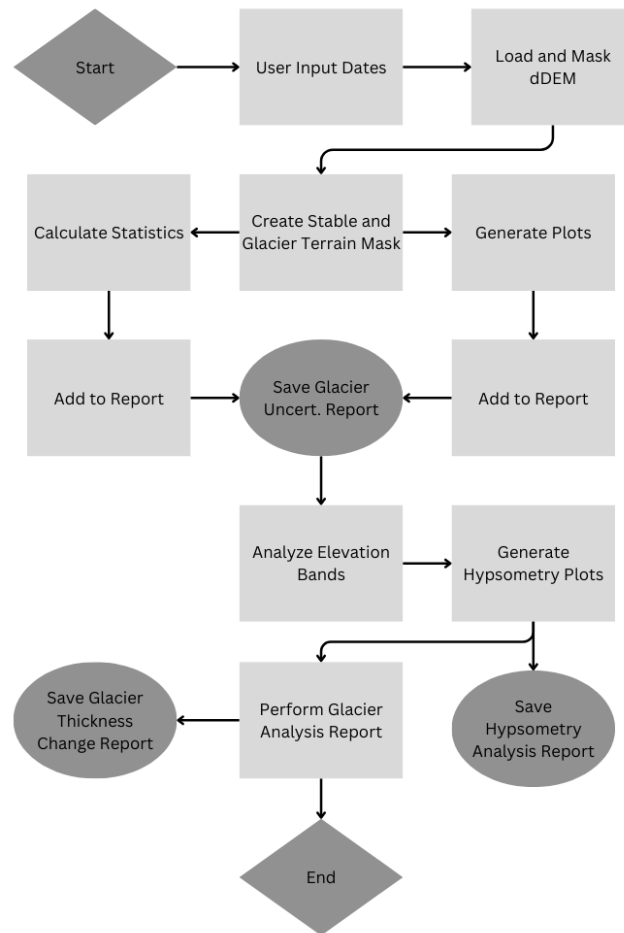

Figure 6: Flow chart of the process of creating the final analysis output in Python. *The analysis script creates three PDFs containing important information about the glaciers. These outputs can be seen in the figure as dark grey circles. The data flow is simplified but includes representations of major steps and flows from start to end implemented in the script. The code can be found in the appendix (Chapter 8.1). The output of this code creates the basis for the interpretation of the glacier surface height change of the glacier data that was used as input into the first script.*

The final component of the workflow is the glacier analysis, which focuses on glacier-covered regions. Using the glacier mask, the workflow isolates elevation changes specific to glaciers and calculates statistics such as the weighted mean and weighted median. These weighted measures account for the varying area of elevation bands, ensuring that the reported values accurately represent the glacier as a whole. The workflow also calculates annualised rates of change by dividing the total elevation difference by the time between the two DEMs. This normalisation enables consistent comparisons across glaciers or periods, providing a standardised measure of glacier thinning or accumulation.

The output of the script is a series of PDF reports that document the results in a clear and reproducible format. The main report includes summaries of the uncertainty analysis, histograms, and statistical metrics for stable terrain and glacier-covered regions. The hypsometric analysis generates additional plots and summaries, highlighting elevation band-specific dynamics.

The design of this workflow is supposed to be flexible and adaptable for different inputs while creating a reliable output. User inputs, such as the dates of the DEMs, allow the analysis to be tailored to specific datasets or study areas. At the same time, the use of statistical methods, masking, and clear documentation ensures that the results are scientifically sound and reproducible. The choice of parameters, such as the use of 100-metre elevation bands or NMAD for uncertainty quantification, reflects best practices in the field, informed by both theory and practical experience (Hugonnet et al., 2022).

4 Results

In this chapter, the results of this thesis will be presented. The goal is to present a comprehensive overview of all the results relevant for later interpretation of the main findings and to answer the research questions. The structure of this part will be as follows. The first results can be attributed to more general processes and findings outside of the pipeline created for this thesis. These results have been processed separately. After the results from the processing pipeline are presented. Additionally, information in the form of graphs can be found in the appendix (Chapter 8).

Before interpreting the results, it is crucial to recognize that datasets from other sources, such as Hugonnet et al. (2021), often express glacier mass change in millimeters water equivalent rather than millimeters of surface height change, as used in the present study. This distinction is significant because water-equivalent values account for the difference in density between ice and liquid water. Given that the density of glacier ice typically ranges from 850 to 910 kg/m³ (Zemp et al., 2013), compared to 1000 kg/m³ for water, the mm w.e. values tend to be systematically lower. Consequently, direct comparisons between datasets require careful consideration of these density differences to avoid misinterpretation.

4.1 The Glaciers in Numbers

The Grosser Aletsch is already being researched extensively. One of the projects is an accumulation and ablation simulation by Huss et al. (GLAMOS, 2022). Figure 7 is an extensive plot from the hydrological year 2000 to 2022. The cyclic behaviour in cumulative mass balance highlights the clear distinction between winter accumulation periods and summer ablation phases, driven by temperature and precipitation variability. The trend to more extreme events with time reflects the growing sensitivity of the glacier system to external climatic forcing. In the fall of 2004, there is hardly any mass balance loss visible in the graph. 2014 and 2015 also stand out by showing minimal negative values, indicating relatively mild ablation seasons. Additionally, there is a gradual downward trend in cumulative mass balance over the two aforementioned decades. In late 2019, there is a big spike in the form of a big negative mass balance. The very negative value in fall 2019 coincides with a point cloud of accumulation values staying exceptionally close to the zero-millimetre water equivalent line. However, the ablation values seem to get strongly negative for a short moment. In fall 2021, there is once more very little melt simulated, followed by 2022, where the graph ends in the second most negative value. There were no values available that go past 31.09.2022.
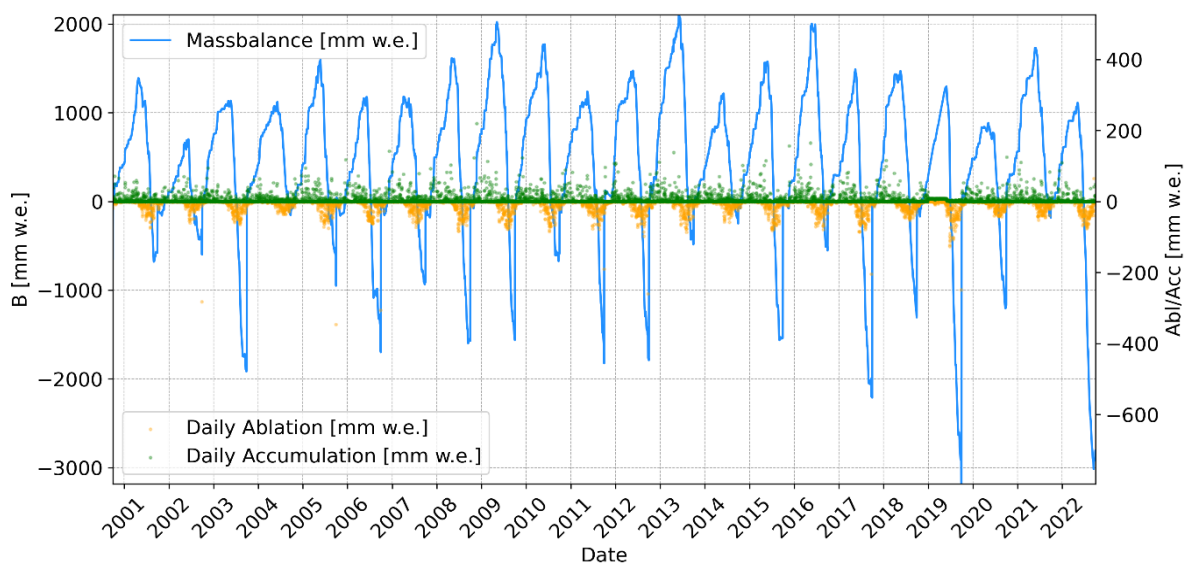

Figure 7: Plot of GLAMOS (2022) numerical model for the Aletsch glacier used for comparison. The x-axis ticks represent the first of January of each year respectively. The graph contains two separate y-axes to make the data more readable. The blue line shows the cumulative mass balance derived from the daily accumulation and ablation values shown in green and. orange respectively. The massbalance (B) is the product derived from the ablation and accumulation values that are also displayed in this graph.

The simulated values of Figure 7 can be cross-checked with the values provided by GLAMOS (1881–2023), visible in Figure 8. This annual mass balance series is derived from on-site measurements and data from the Federal Office of Topography. This mass balance series shows all negative values for the time of 2000–2024. The minimum negative value occurs in late 2021, corresponding to the hydrological year 2022, with -2982 millimetre water equivalent (mm w.e.). The largest value in the mass balance graph is recorded in late 2022, representing the hydrological year 2023, with -114 mm w.e.. Years such as 2003, 2011, and 2018 also display distinct mass loss events.
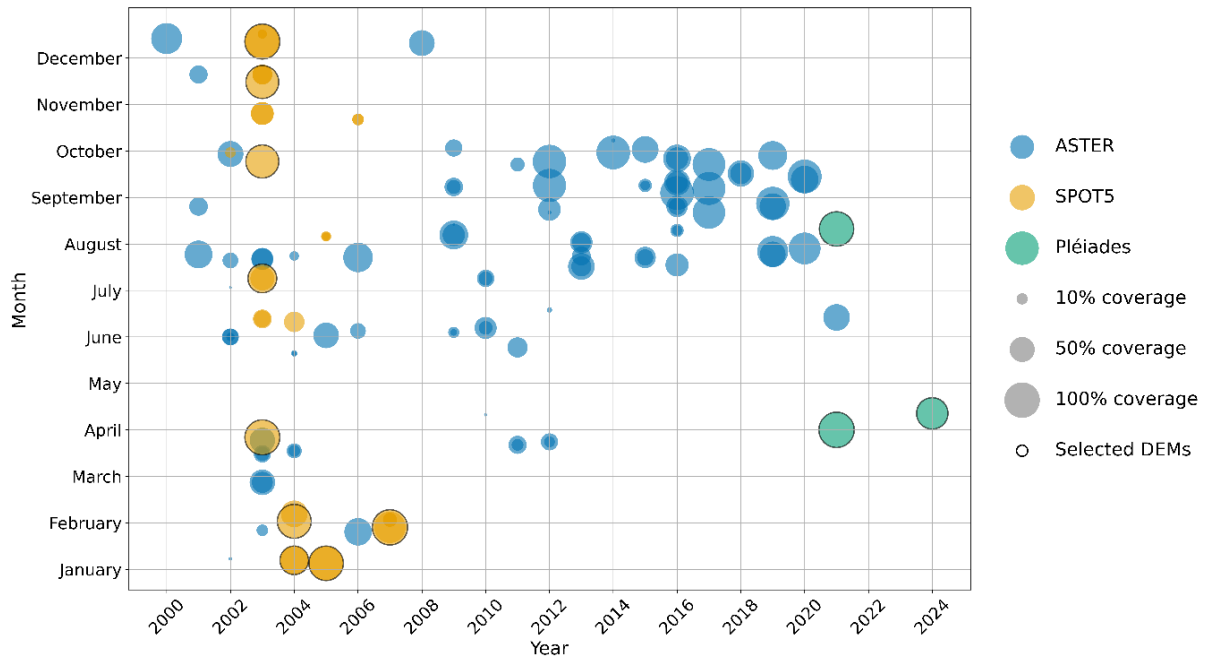

Figure 8: Aletsch glacier coverage in DEMs calculated as a percentage of valid data within RGI 7.0 outlines. The SPOT5 DEMs are marked in orange, with the ones processed for this thesis indicated by a black circle surrounding them in the figure. Pléiades data is green, the ASTER colour is blue. Circle sizes are proportional to the percentage they are representing, as shown in the legend on the right. The SPOT5 data is clustered in the first half of the graph whilst the Pléiades data is only available for 2021 and 2024 for this thesis. The ASTER data derived from RAGMAC is spread over the whole period.

The Aletsch glacier region is analysed using several DEMs from three distinct platforms, two of which have been processed in this thesis. Looking at Figure 9, there is a widespread selection of digital elevation models. There is a total of 12 DEMs marked as selected. The group consists of 9 SPOT5 DEMs and 3 Pléiades DEMs. The selected DEMs for SPOT5 and Pléiades all show coverage of 64% and above, with only three being below 80% and 5 below 90%, respectively.
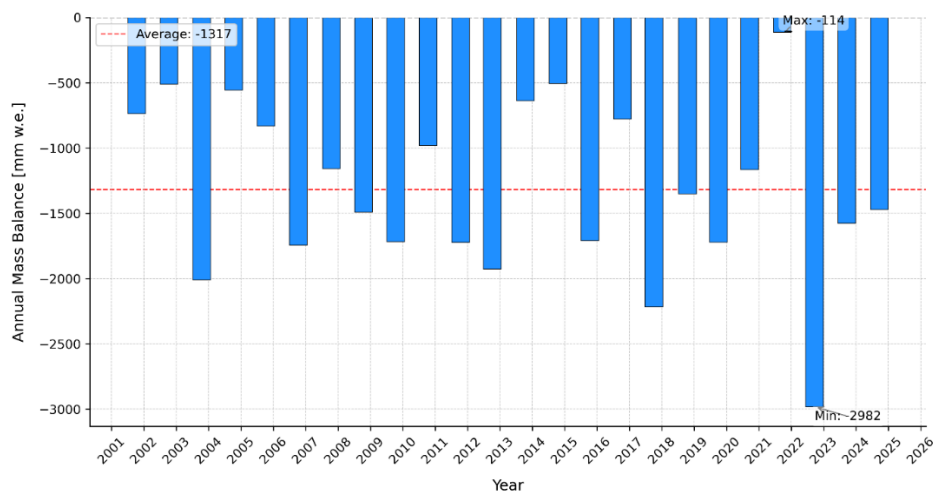

Figure 9: Mass balance for the Grosser Aletschgletscher from GLAMOS (2024). The x-axis represents the years whilst the y-axis represents the annual mass balance (B) in mm w.e. for the Grosser Aletschgletscher. The red line shows the average mass balance over this period. Annotations can be found about the years with the maximum and minimum mass balance.

23

The DEMs were processed using the aforementioned self-developed pipeline. A key component of this process is the co-registration of two DEMs, which requires the identification of stable terrain (details can be found in Figure 5). The stable terrain was selected based on a mask that encompasses a bounding box covering all three glaciers relevant to this thesis. A depiction of this can be seen in Image 2, where the entire area is displayed as a raster file, with valid areas specifically highlighted in green. The selected stable terrain area was determined using a buffer around the RGI 7.0 outlines and Copernicus land cover classes to exclude glacier-covered regions. Further details about this selection process are provided in the methodology section. The stable terrain mask area comprises 114,733,682 pixels in the EPSG:32632 projection (WGS 84 / UTM Zone 32N, with metres as the unit of measurement). Of this, the valid stable terrain area covers just over 121.3 square kilometres, while the invalid, non-stable terrain area amounts to approximately 337.6 square kilometres. The stable terrain raster includes three glaciers: the Grosser Aletschgletscher, the Mittelaletschgletscher, and the Oberaletschgletscher. For context, the areas of these glaciers, as measured via the RGI 7.0 outlines, are 81.78 square kilometres for the Grosser Aletschgletscher, 7.50 square kilometres for the Mittelaletschgletscher, and 19.29 square kilometres for the Oberaletschgletscher.
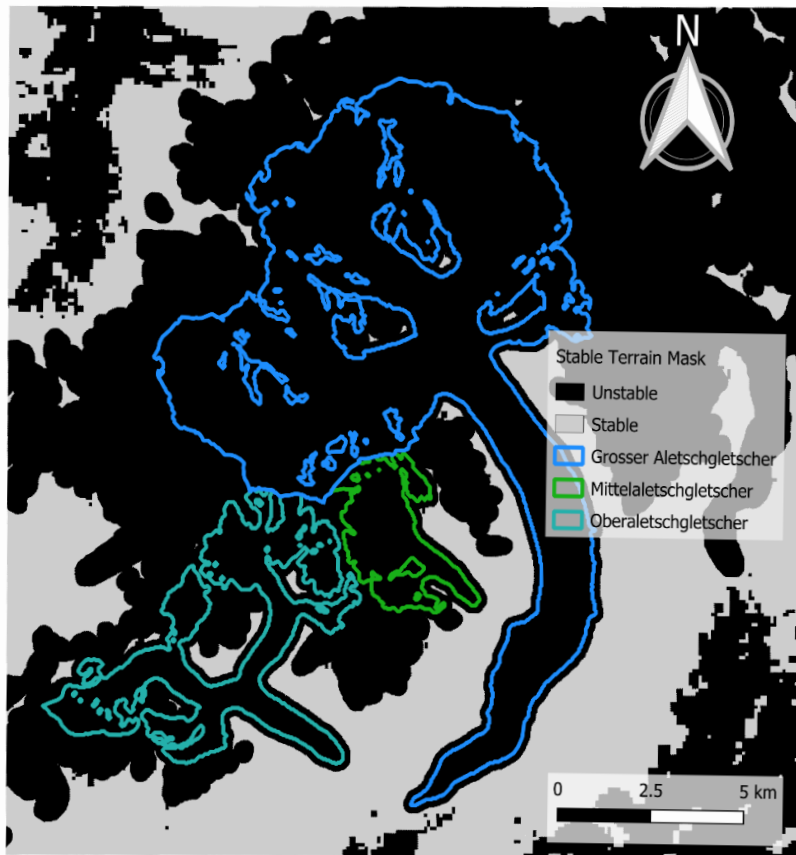

Image 2: Raster of stable terrain created from the RGI 7.0 glacier outlines. *The Grosser Aletschgletscher is displayed in blue, the Mittelaletschgletscher in green, and the Oberaletschgletscher in turquoise. The glacier outlines with a 200-metre buffer combined with the Copernicus land cover classes form the unstable terrain, visible in a black hue. The grey area is the remaining area, designated as stable terrain area, used for the co-registration process. The black area is excluded from stable terrain calculations.*

The three glaciers discussed in this thesis are very different in size. To later understand the effect of the minimum and maximum heights of the glaciers, Figure 10 shows the minimum and maximum elevation pixels derived from a mask created using the RGI 7.0 outlines for all DEMs used. It is important to remember that no filter has been applied. This visualisation shows that each of the glaciers looked at closer in this thesis starts and ends at different elevations above sea level. The lowest pixels are, on average, at 1657 metres above sea level (masl) for the Grosser Aletschgletscher, 2438 masl for the Mittelaletschgletscher, and 2235 masl for the Oberaletschgletscher. The highest points are 4138 masl for the Grosser Aletschgletscher, 4105 masl for the Mittelaletschgletscher, and 3842 masl for the

Oberaletschgletscher. There are minimal differences over the years for the minimum and maximum elevations for each glacier due to the use of static outlines. The highest maximum values for all three glaciers are observed in the first Pléiades DEM from 31.03.2021 (Aletsch: 4207 masl, Mittelaletsch: 4164 masl, Oberaletsch: 3872 masl), even when compared to the oldest SPOT5 DEM from 26.03.2003 (Aletsch: 4134 masl, Mittelaletsch: 4095 masl, Oberaletsch: 3859 masl). This is different for the minimum values, where no such significant variations occur. The mean elevation value, calculated from all pixels over the glacier terrain, shows no significant trend of decreasing over time. However, the minimum and maximum pixel values have decreased over time. Between the first and last DEM, the minimum and maximum pixel values for the Grosser Aletschgletscher have decreased by 78 and 100 metres, for the Mittelaletschgletscher by 62 and 139 metres, and for the Oberaletschgletscher by 46 and 80 metres. The Grosser Aletschgletscher ends at the lowest elevation of the three glaciers, while the Mittelaletschgletscher ends at the highest elevation. The Grosser Aletschgletscher also starts at the highest elevation, while the Oberaletsch Glacier starts at the lowest elevation.
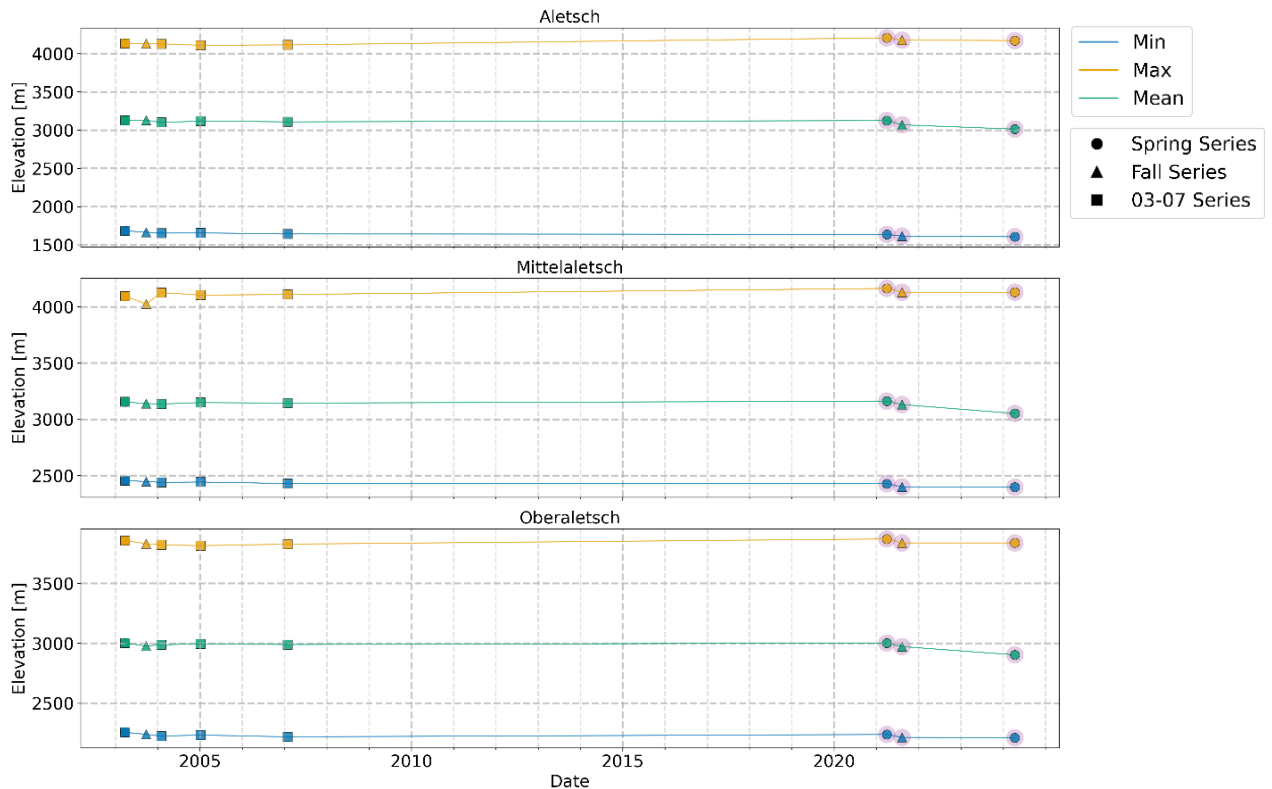

Figure 9: Display of the minimum, maximum and mean of each used DEM out of a multi-year series plotted to check the data for outliers. The colours indicate blue for minimum, yellow for maximum and green for mean. The shape of the marker indicates the series it has been used for. The circle is for the spring series, the triangle for the fall series and the square for the 2003 to 2007 series. Each subplot is for a glacier, from the top it is the Grosser Aletsch Glacier, the Mittelaletschgletscher and the Oberaletschgletscher. All DEMs here have been sourced from SPOT5 data except for the one with a purple shade, indicating Pléiades data. The Spring Series and 03-07 Series share a dot, on 26.03.2003, explaining why only the square is visible.

Figure 11 displays the slope and aspect distributions of the Grosser Aletschgletscher. The slope (A) is predominantly concentrated in the 0–10° range, showing that the Grosser Aletschgletscher is relatively flat. A secondary peak appears in the 20–30° range, with steeper slopes becoming progressively less common. Slopes exceeding 40° are rare. The Grosser Aletschgletscher has the highest concentration of pixels relative to the total pixels over the glacier area in the flattest slope category. The aspect distribution (B) peaks between 170° and 200°, indicating a primarily south-facing orientation (with south at 180°). Significant pixel counts are also observed between 70° and 170°, corresponding to east and southeast-facing aspects across large parts of the glacier. The lowest frequencies occur around 0°, indicating minimal surface area facing north.
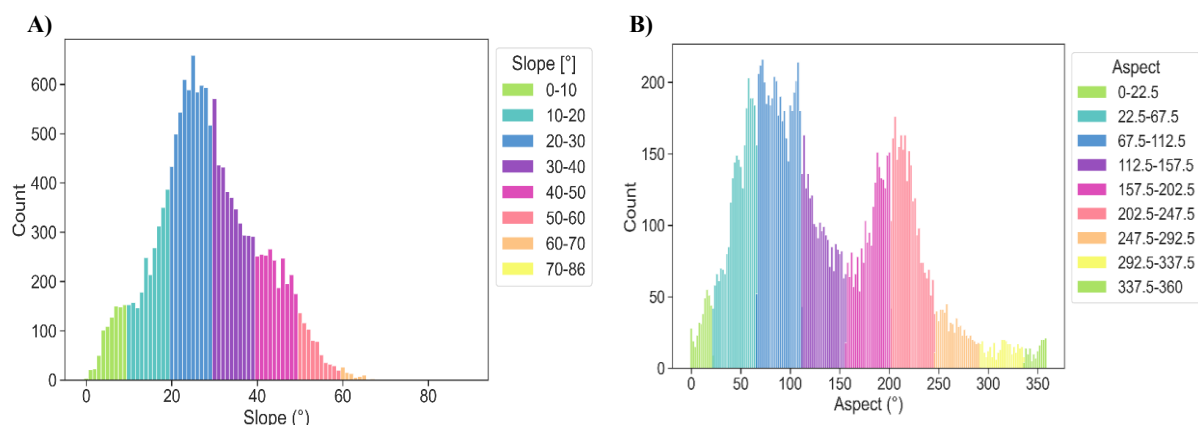
Figure 10: Histogram of the slope (A) and aspect (B) of the Mittelaletschgletscher area calculated from a SPOT5 DEM from 26.03.2003. *The x-axis contains the slope for graph A and the aspect for graph B. The y-axis shows the pixel count for each degree. The colours help visualise 10-degree steps in graph A, with 0 degrees being horizontal. In graph B, each colour is 45-degrees, 22.5 degrees left and right of the cardinal and ordinal directions.*

Figure 12 presents the slope and aspect distributions of the Mittelaletschgletscher. The slope distribution (A) shows a clear concentration of pixels in the 20–30° category, accounting for a significant portion of the glacier surface. In contrast, the 0–10° range has a much lower frequency, suggesting a steeper overall terrain compared to the Grosser Aletschgletscher. The slope frequency decreases steadily beyond 30°, with slopes in the 40–50° range still moderately represented. Slopes exceeding 50° are uncommon, with minimal glacier area observed above 60°. The aspect distribution (B) reveals two prominent patterns. The first consists of several smaller peaks between 50° and 110°, showing that a significant portion of the glacier faces east. The second, more substantial peak occurs between 200° and 230°, reflecting a dominant southwest-facing orientation. North-facing aspects (0–22.5° and 337.5–360°) are virtually absent, consistent with the glacier's overall alignment.
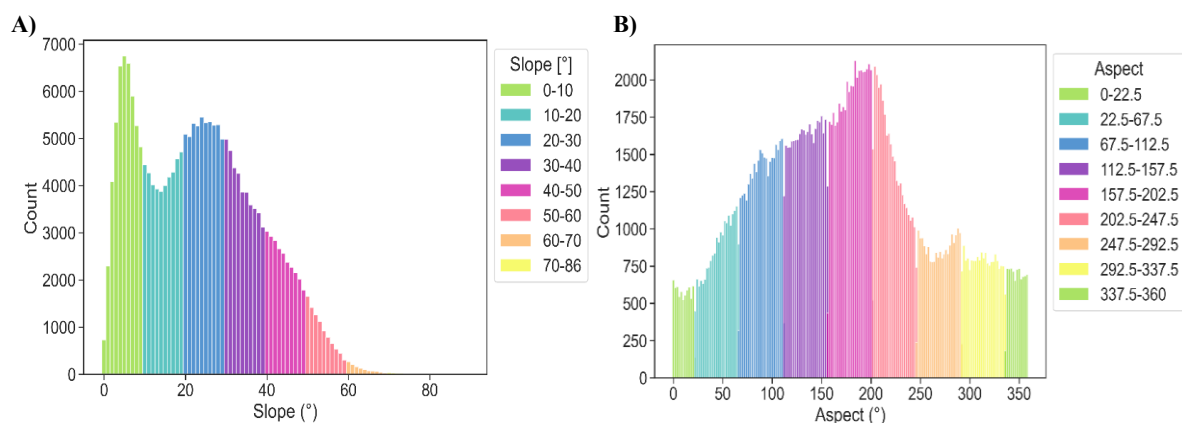

Figure 11: Histogram of the slope (A) and aspect (B) of the Grosser Aletschgletscher area calculated from a SPOT5 DEM from 26.03.2003. *The x-axis contains the slope for graph A and the aspect for graph B. The y-axis shows the pixel count for each degree. The colours help visualise 10-degree steps in graph A, with 0 degrees being horizontal. In graph B, each colour is 45-degrees, 22.5 degrees left and right of the cardinal and ordinal directions.*

In Figure 13 the same data is presented for the Oberaletschgletscher. The slope distribution (A) shows a small peak in the 0–10° range, followed by a slight indentation and a dominant peak at approximately 30°. This is then followed by a steady decline in pixel counts as slopes increase toward 60°. The Oberaletschgletscher exhibits a high concentration of slopes in the 20–40° range. The aspect (B) shows a distribution of pixels facing all around the full 360 degrees. The first peak occurs between 200° and 230°, indicating a significant southwest-facing surface. The second peak lies between 320° and 340°, showing a substantial northwest-facing orientation. Unlike the Grosser Aletsch and Mittelaletschgletscher, the Oberaletschgletscher has a considerable portion of its surface oriented toward northwest, while the share of north-facing slopes remains limited.
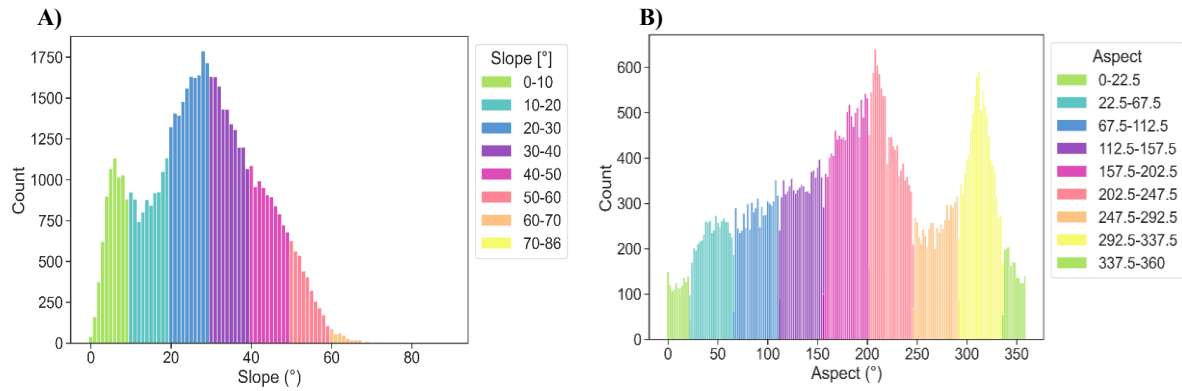
Figure 12: Histogram of the slope (A) and aspect (B) of the Oberaletschgletscher area calculated from a SPOT5 DEM from 26.03.2003. *The x-axis contains the slope for graph A and the aspect for graph B. The y-axis shows the pixel count for each degree. The colours help visualise 10-degree steps in graph A, with 0 degrees being horizontal. In graph B, each colour is 45-degrees, 22.5 degrees left and right of the cardinal and ordinal directions.*

4.2 The Seasons and their Results

The results of the pipeline developed with open-source tools are displayed here. They are structured into three major parts, a spring series and a fall series, consisting of a mix of SPOT5 and Pléiades DEMs, and a 2003-2007 yearly series, only using SPOT5 derived DEMs. These series are displayed in Figure 26. Additionally, there is a sub-year series presented in chapter 4.2.4., which yielded inaccurate results for reasons that will be examined in detail later. Some of its results are displayed in this section to analyse the pipelines' limitations.

4.2.1 Spring Series

The Spring Series consists of two difference DEMs (dDEM). These time series were derived from three DEMs: one SPOT5 DEM and two Pléiades DEMs. The first SPOT5 stereo image was taken on March 26 2003, the second DEM was originally taken by Pléiades on March 31 2021, and the third DEM is also derived from Pléiades data from April 11 2024. These two resulting time series have been analysed for each of the three glaciers in the Aletsch area.

The results of the Spring Series are presented in Table 2. The analysed Orthophotos show that the snow cover was consistent for all three data acquisition dates. The glaciers and the surrounding area were fully covered in snow in the SPOT5 and the two Pléiades pictures. Upon closer examination of the satellite images (Appendix Image 3), no differences can be identified for further analysis.

Table 2: Results derived from the self-developed pipeline for the spring series. *They are grouped by glacier and date. The abbreviations stand for Stable Terrain, Glacier Terrain, Normalised Median Absolute Deviation, Root Mean Square Error (RMSE). Bin stands for the results calculated using 100-metre bins and interpolation.*

Name	Aletsch		Mittelaletsch		Oberaletsch	
Start Date	26.03.2003	31.03.2021	26.03.2003	31.03.2021	26.03.2003	31.03.2003
End Date	31.03.2021	11.04.2024	31.03.2021	11.04.2024	31.03.2021	11.04.2024
Area [km²]	81.78	81.78	7.5	7.5	19.29	19.29
ST Median [m]	0.01	0.01	0.01	0.01	0.01	0.01
ST NMAD [m]	4.1	1.86	4.1	1.86	4.1	1.86
ST RMSE [m]	7.57	2.09	7.57	2.09	7.57	2.09
GT Median [m]	-15.85	-6.27	-12.83	-1.86	-20.83	-2.86
GT NMAD [m]	20.71	7.33	10.3	3.56	21.16	6.52
GT RMSE [m]	32.58	9.62	30.28	6.09	34.83	6.78
Bin Mean [mm.year]	-1328.44	-2122.08	-1132.96	-687.14	-1497.39	-938.69
Bin Median [mm.year]	-1332.24	-2238.47	-1103.06	-701.94	-1507.28	-982.07
95% [mm.year]	446.07	1202.85	446.07	1202.85	446.07	1202.85

Hugonnet and colleagues have collected surface changes with the respective uncertainty data until 2020 only, whilst the Pléiades brings the calculated dataset into 2024. The data is thus separated into two different time series, one spanning the years from 2003 to 2021 and the other one those from 2021 to 2024.

The same pair of dDEMs, covering an identical spatial extent, was utilised for all three glaciers, encompassing the entire Aletsch region, including the Grosser Aletschgletscher, Mittelaletschgletscher, and Oberaletschgletscher. As a result, the ST analysis yields consistent values across all glaciers, reflecting the uniform assessment of the same dataset (Appendix Images 27A, 31A, 35A). The ST median elevation difference is 0.01 meters, indicating successful co-registration between the DEMs. The NMAD values of 4.1 meters for the 2003–2021 period and 1.86 meters for the 2021–2024 period suggest varying levels of uncertainty, with the shorter observation period exhibiting lower variability. The RMSE values follow a similar pattern, with values of 7.57 meters and 2.09 meters, respectively, indicating an improvement in co-registration accuracy for the more recent period.

The GT analysis reveals higher median values, reflecting expected glacier surface changes. The Grosser Aletschgletscher exhibits median elevation changes of -15.85 meters for the longer period and -6.27 meters for the shorter period, while Mittelaletschgletscher shows changes of -12.83 and -1.86 meters, respectively. The Oberaletschgletscher experiences the most pronounced changes, with values of -20.83 and -2.86 meters, suggesting significant thinning across both periods. The NMAD values for glacier terrain are higher compared to stable terrain, ranging from 10.3 to 21.16 meters for the longer period and 3.56 to 7.33 meters for the shorter period, reflecting the dynamic nature of glacier surfaces. RMSE values for GT are similarly variable, with values of 30.28 to 34.83 meters for the 2003–2021 period and 6.09 to 9.62 meters for the 2021–2024 period.

The binned calculations of glacier surface elevation changes, expressed in millimetres (mm) per year, show that the Grosser Aletschgletscher experienced a mean change of -1328.44 mm/year over the longer period, increasing to -2122.08 mm/year in the shorter period. Mittelaletschgletscher exhibits a lower magnitude of change, with values of -1132.96 mm/year and -687.14 mm/year, respectively. Oberaletschgletscher shows the highest rate of surface lowering, with values of -1497.39 mm/year and -938.69 mm/year, respectively. The median values of the binned calculations closely align with the mean values, reinforcing dataset consistency. The uncertainty estimates, represented by the 95% confidence intervals, show values of 446.07 mm/year for the longer period and 1202.85 mm/year for the shorter period across all three glaciers, indicating a higher degree of uncertainty for the shorter observation period. The longer observation period (2003–2021) provides a more consistent trend in surface height changes, with lower uncertainty values. In contrast, the shorter time series (2021–2024) shows greater variability and higher uncertainty. Among the three glaciers, the Mittelaletschgletscher exhibits the smallest surface height change, whereas the Oberaletschgletscher demonstrates the largest. The Grosser Aletschgletscher falls between the two in terms of elevation change magnitude.

Figure 14, shows the Grosser Aletschgletscher surface height change. The plot comprises both the pipeline calculated data as well as the one from Hugonnet et al. (2021). The detailed numbers have been detailed in Table 2. Hugonne's uncertainty, depicted as a grey box, is greater in value than the calculated uncertainty, which is represented by a blue box instead. It's also noticeable that the shorter time series has a higher uncertainty. Instead, the calculated data for surface height changes is negative for both time series, from 2003 to 2021 and from 2021 to 2024.
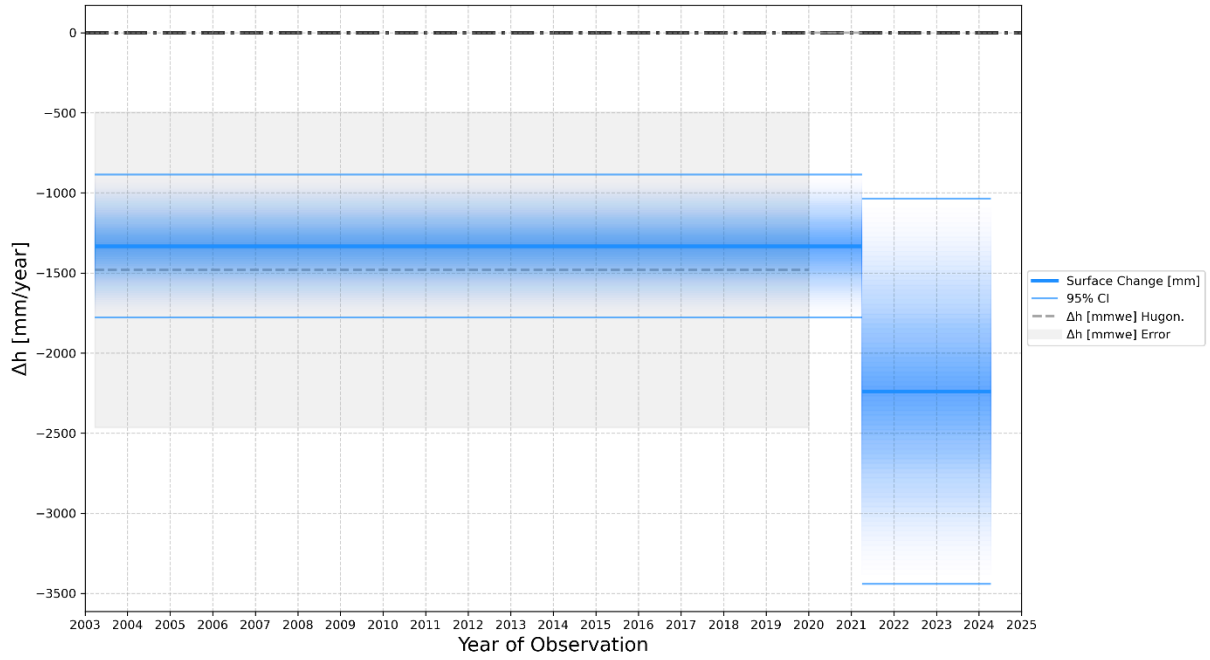
Figure 13: Graph showing the surface height change derived from the pipeline and Hugonnet et al. of the Grosser Aletschgletscher. Blue is the value calculated from the difference DEMs with the uncertainty indicated as the two surrounding bars. The grey dotted line is the difference in millimetre water equivalent for the Aletsch Glacier over the same period by Hugonnet et al. (2021). The grey box in the background is the uncertainty calculated for the same period.

Figure15, depicts Mittelaletschgletscher's surface height changes in the spring series. Hugonnet's group uncertainty reaches slightly over the zero line, their surface height changes values and those calculated from the pipeline have similar values upon comparison/relate closely to each other. The calculated uncertainties derived from the pipeline and are firmly in the negative space for the first time series spanning 2003 to 2021. Instead, the time span from 2021 to 2024, while being slightly above zero is still mostly negative indicating a slight decrease in the glacier's surface height.
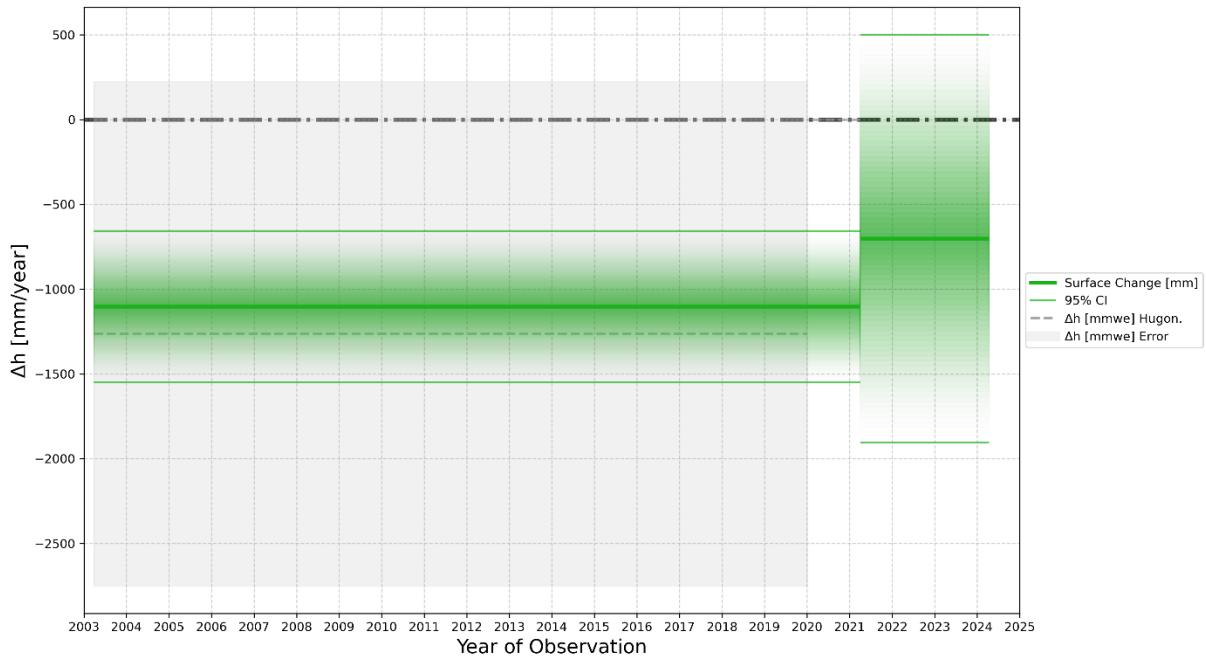

Figure 14: Graph showing the surface height change derived from the pipeline and Hugonnet et al. of the Mittelaletschgletscher. Green is the value calculated from the difference DEMs with the uncertainty indicated as the two surrounding bars. The grey dotted line is the difference in millimetre water equivalent for the Mittelaletschgletscher over the same period by Hugonnet et al. (2021). The grey box in the background is the uncertainty calculated for the same period.

Finally, Figure 16, represents the spring series of the Oberaletschgletscher, it is noticeable that both Hugonnet's uncertainty as well as the one calculated from the pipeline are both consistently negative and the surface height changes are similar in value for the whole 2003-2021 series. Instead, the uncertainty for the 2021-2024 period is over the zero line but mostly includes negative values. Instead, the calculated surface height changes, while still under the zero line, are slightly less negative in comparison to both surface changes from the previous period.

Figure 15: Graph showing the surface height change derived from the pipeline and Hugonnet et al. of the Oberaletschgletscher. *Turquoise is the value calculated from the difference DEMs with the uncertainty indicated as the two surrounding bars. The grey dotted line is the difference in millimetre water equivalent for the Oberaletsch Glacier over the same period by Hugonnet et al. (2021). The grey box in the background is the uncertainty calculated for the same period.*

4.2.2 Fall Series

Table 3 summarizes all collected data output of the fall series. Its analysis, as presented in Table 3, is based on a single difference DEM, which combines one SPOT5 DEM and one Pléiades DEM, covering the period from September 2003 to August 2021. A close look at the satellite pictures reveals that at the time of the data acquisition of the first and second DEM –with SPOT5 and Pléiades respectively–, the surface of the Grosser Aletsch glacier was snow free from its tongue up to the Konkordiaplatz. The snow cover starts about 200 vertical metres above the Konkordiaplatz and is almost identical for both DEMs in terms of extent. Similarly, for the Mittelaletschgletscher and the Oberaletschgletscher, large parts of snow accumulation areas have very little differences in coverage between the two orthophotos. Additionally, Oberaletschgletscher's ablation area is made by ice and debris only. A slight difference can be made out in the northernmost extents of the Oberaletschgletscher under the Sattelhorn, where the accumulation area has some snow-free zones (Image 4).

As the same difference DEM was used for all three glaciers, their stable terrain statistics are identical. The median elevation difference over stable terrain is 0.12 meters, indicating minimal vertical offset between the two DEMs. The normalised median absolute deviation is 5.26 meters, reflecting moderate variability in elevation differences, while the root mean square error is 42.00 meters. Over the glacier terrain, the Grosser Aletschgletscher shows a median elevation change of -13.42 meters, the Mittelaletschgletscher exhibits a smaller negative change of -8.51 meters, and the Oberaletschgletscher

demonstrates the greatest change with -21.24 meters. The NMAD values for the glacier terrain range

Variable	Aletsch	Mittelaletsch	Oberaletsch
Start Date	24.09.2003	24.09.2003	24.09.2003
End Date	10.08.2021	10.08.2021	10.08.2021
Area [km²]	81.78	7.5	19.29
ST Median [m]	0.12	0.12	0.12
ST NMAD [m]	5.26	5.26	5.26
ST RMSE [m]	42	42	42
GT Median [m]	-13.42	-8.51	-21.24
GT NMAD [m]	24.89	16.8	27.63
GT RMSE [m]	31.75	31.79	33.78
Bin Mean [mm.year]	-1022.57	-759.89	-1254.72
Bin Median [mm.year]	-1041.79	-790.38	-1253.81
95% [mm.year]	576.66	576.66	576.66

from 16.80 meters for Mittelaletsch to 27.63 meters for Oberaletsch, indicating spatial variability in elevation changes. The RMSE values range from 31.75 to 33.78 meters, reflecting variations in topographic complexity across the glaciers. The annual surface height change calculations show mean values of -1022.57 mm/year for Aletsch, -759.89 mm/year for Mittelaletsch, and -1254.72 mm/year for Oberaletsch. Median values are consistent with these trends, with Aletsch at -1041.79 mm/year, Mittelaletsch at -790.38 mm/year, and Oberaletsch at -1253.81 mm/year. The 95% confidence interval for all glaciers is 576.66 mm/year, indicating the range of uncertainty in the calculated values.

In Figure 17, while Hugonnet's time series is shorter than the calculated one, it can be seen that for the Grosser Aletschgletscher both datasets contain firmly negative values indicating melt. Additionally,
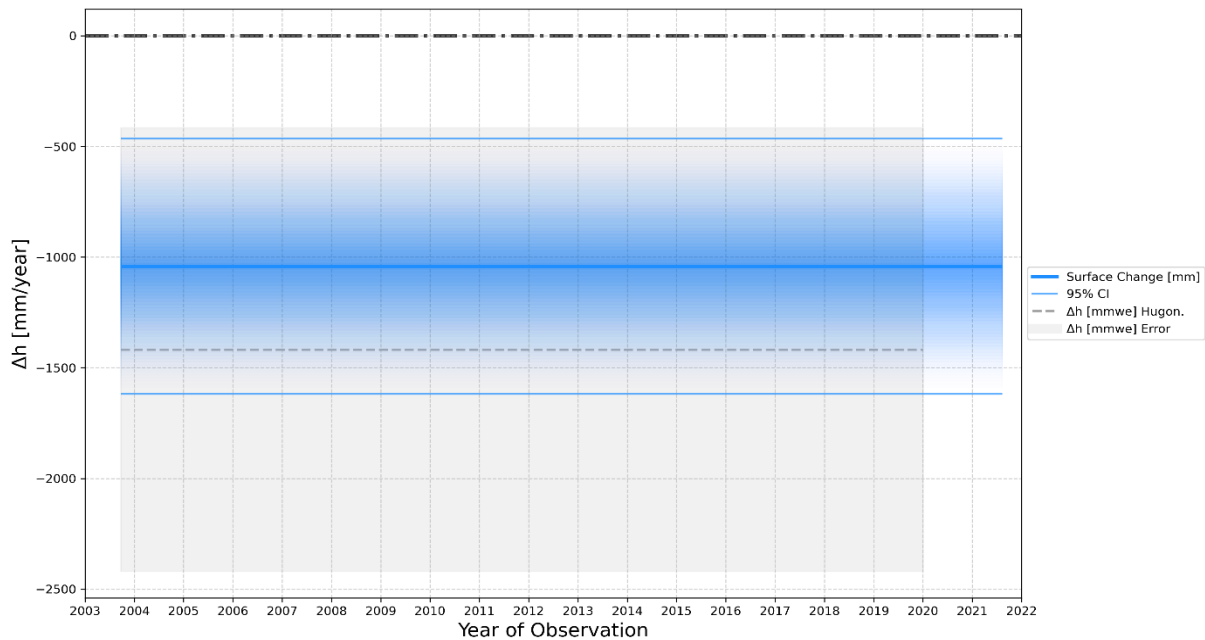

*Figure 16: Graph showing the surface height change derived from the pipeline and Hugonnet et al. of the **Grosser Aletschgletscher.** The blue line is the value calculated from the difference DEMs with the uncertainty indicated as the two surrounding bars. The grey dotted line is the difference in millimetre water equivalent for the Grosser Aletsch glacier over the same period by Hugonnet et al. (2021). The grey box in the background is the uncertainty calculated over the same period.*

Hugonnet's data is more negative in comparison to the pipeline's, both in terms of uncertainty and surface changes.

Next, Figure 18 presents the same two datasets for the Oberaletschgletscher. The uncertainty of Hugonnet's data is reaching into the positive elevation change, whilst the calculated surface height changes uncertainty is in the negative. Furthermore, Hugonnet's time series has slightly more negative height changes compared to the calculated ones.
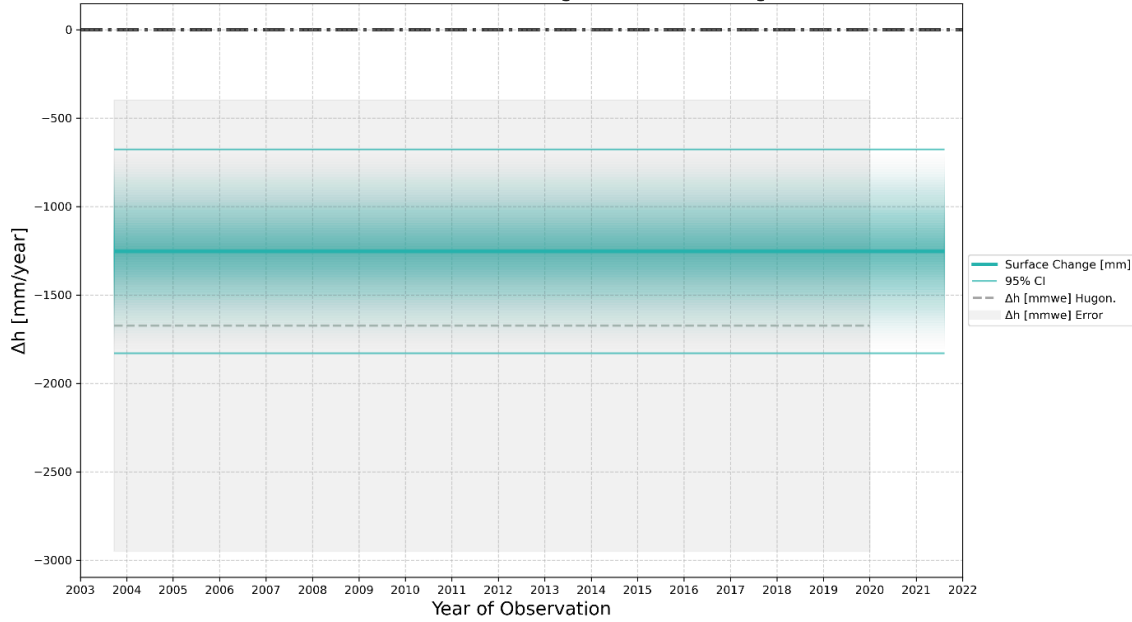

Figure 17: Graph showing the surface height change derived from the pipeline and Hugonnet et al. of the Oberaletschgletscher. The turquoise line is the value calculated from the difference DEMs with the uncertainty indicated as the two surrounding bars. The grey dotted line is the difference in millimetre water equivalent for the Oberaletschgletscher over the same period by Hugonnet et al. (2021). The grey box in the background is the uncertainty calculated over the same period.

Finally, Figure 19 follows the same principle as the two previous figures and displays the same two data sets for the Mittelaletschgletscher. Once more, Hugonnet's uncertainty is greater than the calculated uncertainty and for both data sets the values for heigh changes during the respective periods are strictly negative, with the pipeline's output being closer to zero in comparison.
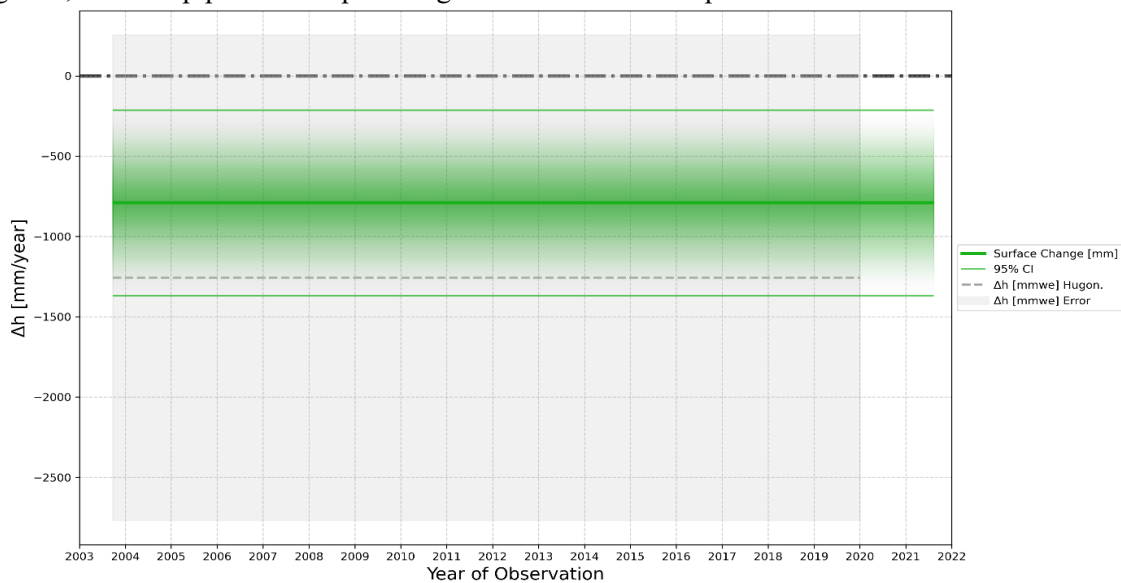

Figure 18: Graph showing the surface height change derived from the pipeline and Hugonnet et al. of the Mittelaletschgletscher. The green line is the value calculated from the difference DEMs with the uncertainty indicated as the two surrounding bars. The grey dotted line is the difference in millimetre water equivalent for the Mittelaletschgletscher over the same period by Hugonnet et al. (2021). The grey box in the background is the uncertainty calculated over the same period.

4.2.3 Yearly Series

The time series from 2003 to 2007, summarized in Table 4, consist of three consecutive difference DEMs derived from four SPOT5 DEMs, being taken at the end of March 2003, February 2004, January 2005 and the end of January 2007. There is no valid DEM for 2006, creating the need to disregard one year. The values have been calculated over stable terrain and glacier terrain. Furthermore, the table depicts the weighted mean and median, uncertainty and a 95% confidence interval.

Table 4: 2003-2007 time series for the Grosser Aletsch-, Mittelaletsch- and Oberaletschgletscher. They are grouped by glacier and date. The abbreviations stand for Stable Terrain (ST), Glacier Terrain (GT), Normalised Median Absolute Deviation (NMAD), Root Mean Square Error (RMSE). Bin stands for the results calculated using 100-metre bins and interpolation.

Name	Aletsch			Mittelaletsch			Oberaletsch		
Start Date	26.03.03	01.02.04	04.01.05	26.03.03	01.02.04	04.01.05	26.03.03	01.02.04	04.01.05
End Date	01.02.04	04.01.05	28.01.07	01.02.04	04.01.05	28.01.07	01.02.04	04.01.05	28.01.07
Area [km²]	81.78	81.78	81.78	7.5	7.5	7.5	19.29	19.29	19.29
ST Median [m]	0.02	-0.01	-0.05	0.02	-0.01	-0.05	0.02	-0.01	-0.05
ST NMAD [m]	3	2.36	1.83	3	2.36	1.83	3	2.36	1.83
ST RMSE [m]	4.78	3.58	2.87	4.78	3.58	2.87	4.78	3.58	2.87
GT Median [m]	-4.28	-0.75	-3.03	-4.46	-1.16	-2.61	-4.06	-2.01	-3.16
GT NMAD [m]	3.74	3.23	3.9	2.95	2.51	3.19	3.33	2.99	3.89
GT RMSE [m]	6.56	4.01	5.21	6.29	3.57	4.7	6.02	4.2	5.02
Bin Mean [mm.yr]	-5019	-755	-1447	-5469	-855	-1411	-4755	-1906	-1390
Bin Median [mm.yr]	-4895	-672	-1494	-5085	-1092	-1432	-4759	-1999	-1409
95% [mm.yr]	6884	4999	1738	6884	4999	1738	6884	4999	1738

The analysis of the 2003–2007 series is based on three difference DEMs, which were generated using input DEMs acquired during the winter and spring periods. Two of the three dDEMs cover an approximate one-year interval, while the third spans over a two-year time frame. The orthophotos that were used to produce the DEMs for this time series, all show a full snow cover for the general Aletsch area that was used for the calculations. With one exception being the first satellite image (Image 5), where only the first 1.5 kilometres approximately of the Grosser Aletschgletscher were snow free.

The results derived from the ST mask indicate a high degree of agreement between the DEMs, with a low median elevation difference across all glaciers, as shown in Table 4. For the Grosser Aletschgletscher, the ST median values range from 0.02 to -0.05 meters, suggesting that the co-registration process was effective. The NMAD values, which range from 1.83 to 3.00 meters, indicate that localised discrepancies exist, but remain within an acceptable range for glacier studies. Similarly, the RMSE values, varying between 2.87 and 4.78 meters, further support the conclusion that systematic errors are minimal, confirming the robustness of the co-registration. For the Mittelaletschletscher, the results show consistent patterns with a median ST value of 0.02 to -0.05 meters, an NMAD ranging from 1.83 to 3.00 meters, and RMSE values between 2.87 and 4.78 meters, aligning closely with the observations made for the Aletsch Glacier. These findings confirm the overall reliability of the DEM differencing process for this glacier. The Oberaletschgletscher follows a similar trend, with ST median values between 0.02 and -0.05 meters, an NMAD ranging from 1.83 to 3.00 meters, and RMSE values between 2.87 and 4.78 meters. The consistency of these values across all three glaciers implies that the ST mask effectively captured stable regions, contributing to reliable co-registration and error analysis.

Over glacier terrain, the calculated median values demonstrate the expected negative trends due to glacier thinning. For Aletsch Glacier, the median values range from -4.28 to -0.75 meters, while Mittelaletschgletscher exhibits values between -4.46 and -1.16 meters, and Oberaletschgletscher ranges from -4.06 to -2.01 meters. These values suggest spatial variability in glacier thinning, with Mittelaletschgletscher showing the least change and Oberaletschgletscher the greatest. The NMAD values for GT, ranging from 2.51 to 3.90 meters, highlight areas with higher variation due to dynamic

glacier processes, while RMSE values between 3.57 and 6.56 meters further emphasise the expected heterogeneity within the glacierised areas.

The binned calculations for surface height changes provide valuable insights into glacier thinning rates. The mean values for Aletsch Glacier range from -5019 to -1447 mm/year, for Mittelaletschgletscher from -5469 to -1411 mm/year, and for Oberaletschgletscher from -4755 to -1390 mm/year. The close agreement between the bin mean and median values across all glaciers suggests stable datasets with minimal influence from outliers. The uncertainty analysis, expressed as the 95% confidence interval, is consistent across all glaciers at 6884 mm/year for the upper bound and 4999 mm/year for the lower bound in most cases. This indicates a robust assessment of uncertainty and suggests a high level of confidence in the calculated glacier changes.

In Figure 20, for the Grosser Aletschgletscher in the period from 2003 to 2007, the uncertainties of both the pipeline output as well as Hugonnet's data derived an uncertainty spread into the positive area of the graph. Instead, the last period from 2005 to 2007 has the smallest reach into the accumulation territory. Furthermore, for the first two time series the calculations for the surface elevation changes reflect a melting trend, in agreement with both the pipeline output and Hugonnet's data. The third time series, which encompasses roughly two years, has almost overlapping values in terms of surface elevation changes when comparing the two data sets, indicating once more a melting trend confirmed by both.
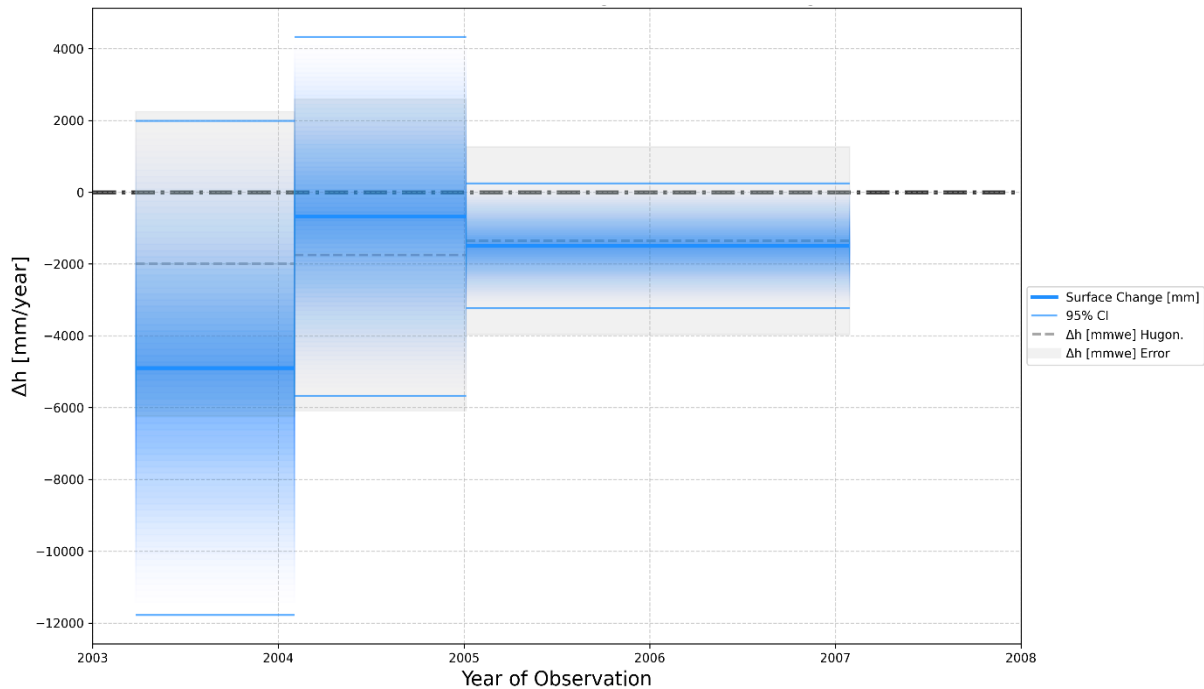

Figure 19: Time series of the surface elevation change calculated in the pipeline and derived from Hugonnet et al. for the years 2003, 2004, 2005 and 2007 for the Grosser Aletschgletscher including uncertainties. *The blue centre line shows the surface elevation change in millimetres per year. The outer blue lines show the upper and lower 95% confidence interval for the surface elevation change. The grey dotted line is Hugonnet et al. (2021) melt rate in millimetres of water equivalent per year. The grey box is the uncertainty calculated for the change in water equivalent, taken from Hugonnet et al. (2021).*

Figure 21 depicts again various similarities between the pipeline output and Hugonnet's data, although this time for the Oberaletschgletscher. In terms of uncertainty the first period shows the higher calculated uncertainty, with a wide spread spanning more in the negative area of the graph compared to Hugonnet's data. Instead, the pipeline's output for uncertainty of the other two periods seem to be more aligned with Hugonnet's data. Furthermore, the closer alignment in surface elevation changes values can be observed

in the periods from 2004 to 2005 and 2005 to 2007, while we observe a bigger spread for the first period. derived uncertainty.
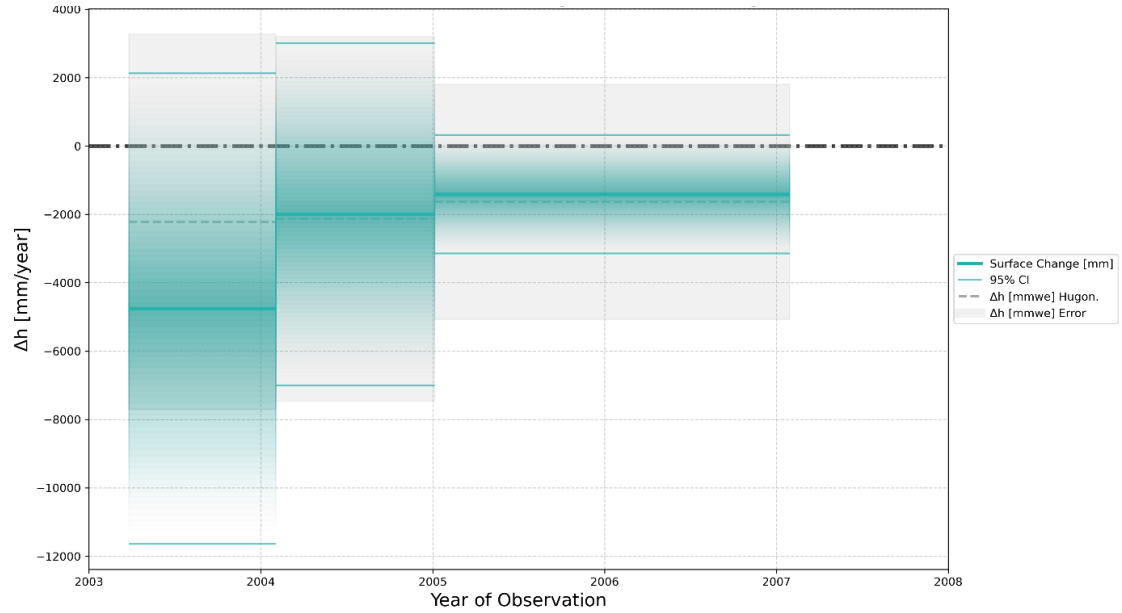

Figure 20: Time series of the surface elevation change calculated in the pipeline and derived from Hugonnet et al. for the years 2003, 2004, 2005 and 2007 for the Oberaletschgletscher including uncertainties. The turquoise centre line shows the surface elevation change in millimetres per year. The outer turquoise lines show the upper and lower 95% confidence interval for the surface elevation change. The grey dotted line is Hugonnet et al. (2021) melt rate in millimetres of water equivalent per year. The grey box is the uncertainty calculated for the change in water equivalent, taken from Hugonnet et al. (2021).

Finally, Figure 22 shows strong similarities between the pipeline output and the Hugonnet's data for the Mittelaletschgletscher too, in both the uncertainty and the derived glacier surface elevation change. Overall, there is a similar pattern as with the two previous Figures, with the first period from 2003 to 2004 having the poorest alignment for both studied variables between the two data sets. For the other periods, the pipeline derived uncertainties slim are lower compared to Hugonnet's, while the glacier's surface elevation changes are only slightly different in comparison.
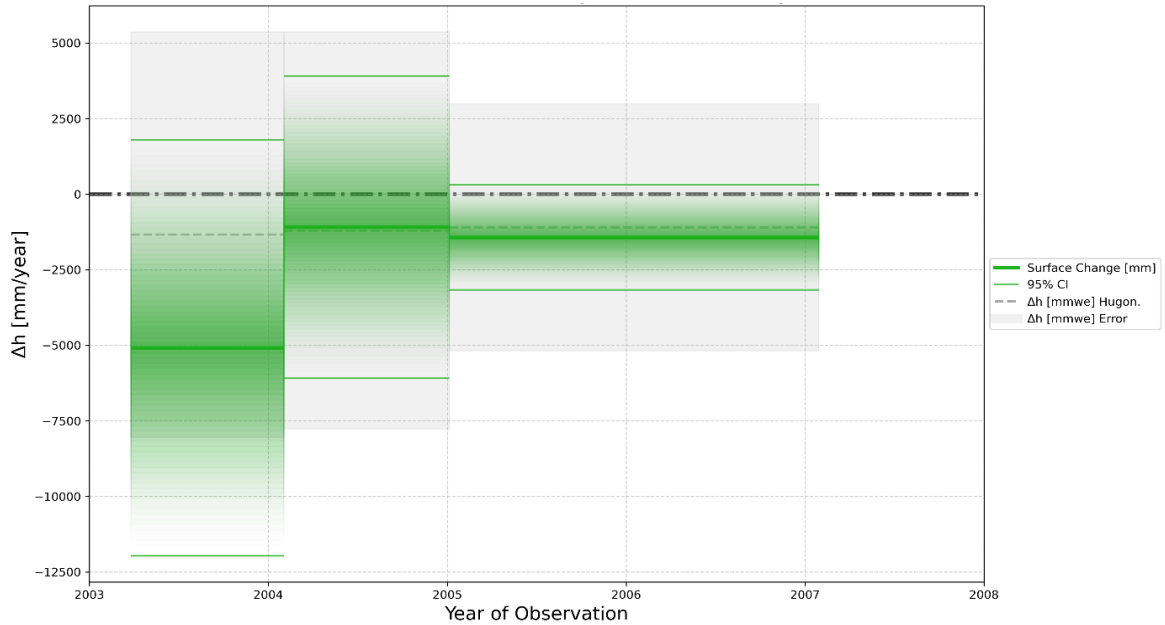

Figure 21: Time series of the surface elevation change calculated in the pipeline and derived from Hugonnet et al. for the years 2003, 2004, 2005 and 2007 for the Mittelaletschgletscher including uncertainties. The green centre line shows the surface elevation change in millimetres per year. The outer green lines show the upper and lower 95% confidence interval for the surface elevation change. The grey dotted line is Hugonnet et al. (2021) melt rate in millimetre of water equivalent per year. The grey box is the uncertainty calculated for the change in water equivalent, taken from Hugonnet et al. (2021).

4.2.4 Sub-Year Series

The sub-year series has been an experiment looking into the potential applications this pipeline could offer in terms of maximizing temporal resolution. It consists of SPOT5 DEMs from March 26 2003 to July, September, November December and then January and February 2004. The results have been calculated and taken into consideration with uncertainties. The sub-year series was run for all three glaciers in the Aletsch area.

In Figure 23, the sub-year series can be seen, combining Hugonnet data in grey with the output of the pipeline for the Grosser Aletschgletscher. The output of the data shows big uncertainties, increasing with shorter time series, which is also true for Hugonnet's data. Additionally, there are also incongruences in terms of surface elevation changes. Finally, it's also not possible to generate an annual trend based on the output of the pipeline.
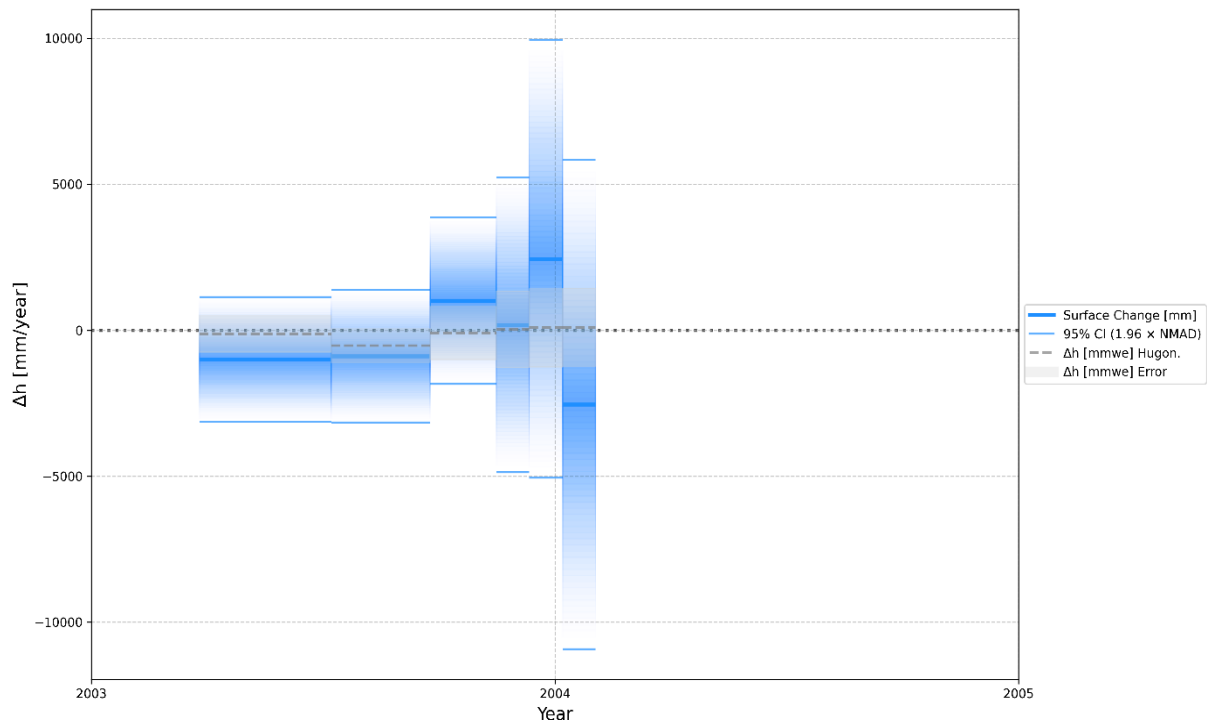

Figure 22: This figure shows a sub-year time series for March, July, September, November and December 2003 and January and February 2004 for the Grosser Aletschgletscher. On the x-axis is the time whilst the x-axis is the delta height (Δh) in millimetres per month. The blue centre line shows the surface elevation change in millimetres per year. The outer blue lines show the upper and lower 95% confidence interval for the surface elevation change. The grey dotted line is Hugonnet et al. (2021) melt rate in millimetres of water equivalent per year. The grey box is the uncertainty calculated for the change in water equivalent, taken from Hugonnet et al. (2021).

The sub-year series in Figure 24 shows the pipeline output for the Mittelaletschgletscher. Where uncertainties are great in value and inversely proportional to the length of each time series and the surface elevation changes are inconsistent throughout the timeline displayed in the graph. Once more, the data does not exhibit any observable yearly trend.
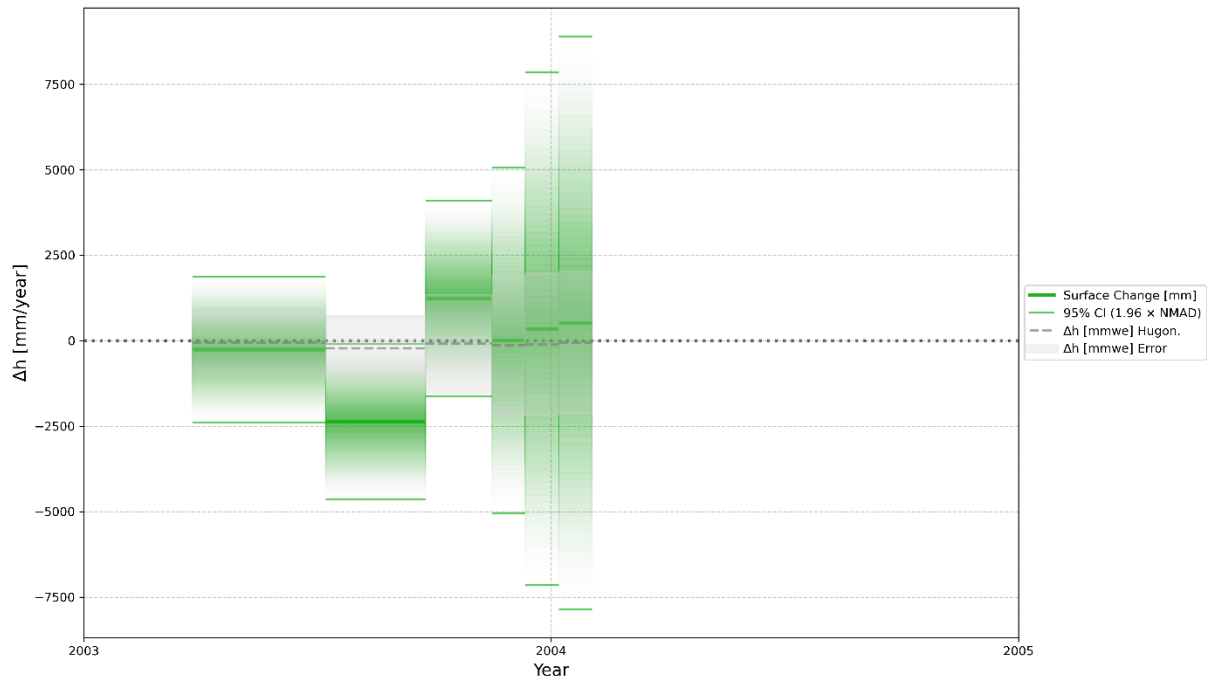
Figure 23: This figure shows a sub-year time series for March, July, September, November and December 2003 and January and February 2004 for the Mittelaletschgletscher. On the x-axis is the time whilst the x-axis is the delta height (Δh) in millimetres per month. The green centre line shows the surface elevation change in millimetres per year. The outer green lines show the upper and lower 95% confidence interval for the surface elevation change. The grey dotted line is Hugonnet et al. (2021) melt rate in millimetres of water equivalent per year. The grey box is the uncertainty calculated for the change in water equivalent, taken from Hugonnet et al. (2021).

For the Oberaletschgletscher, the sub-year data plotted can be seen in Figure 25. The uncertainty bands have a large range and are increasing with the shorter periods chosen, while the delta height is once more inconsistent throughout the year with no seasonal trend visible. In this case too, the pipeline's output is very different compared to Hugonnet's data.
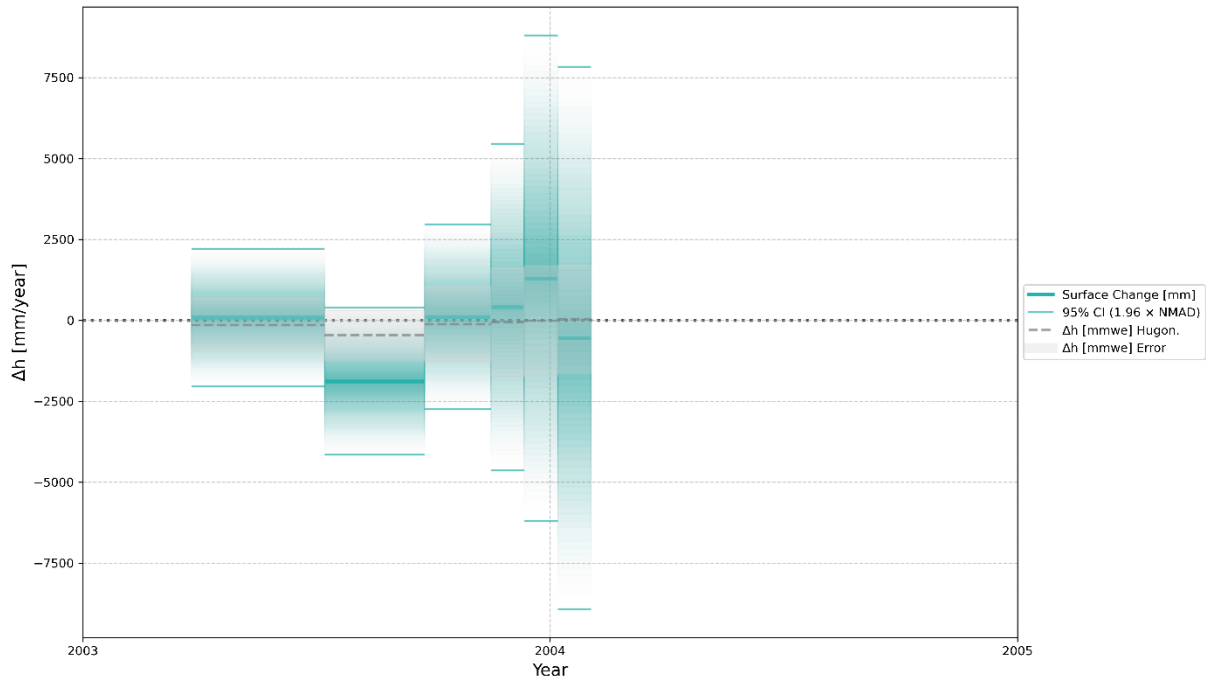

Figure 24: This figure shows a sub-year time series for March, July, September, November and December 2003 and January and February 2004 for the Grosser Oberaletschgletscher. On the x-axis is the time whilst the x-axis is the delta height (Δh) in millimetres per month. The turquoise centre line shows the surface elevation change in millimetres per year. The outer turquoise lines show the upper and lower 95% confidence interval for the surface elevation change. The grey dotted line is Hugonnet et al. (2021) melt rate in millimetres of water equivalent per year. The grey box is the uncertainty calculated for the change in water equivalent, taken from Hugonnet et al. (2021).

To summarize, as shown in Figure 23, the uncertainties values for the Grosser Aletschgletscher are high and inversely proportional to the length of time series' surrounding the calculated data. The same values are slightly smaller but still substantial and following the same rends in Figures 24 and 25, respectively Mittelaletsch- and Oberaletschgletscher. In comparison, Hugonnet et al.'s (2021) error calculations show a significantly smaller uncertainty than the pipeline's. Furthermore, for all three figures, it is not possible to make out a clear seasonal cycle. The 95% confidence interval is derived from a scaled NMAD. Additionally, in the Aletsch series, the July to September line is showing less melt than the prior line from March to July, which is unusual. Comparing this to the Mittelaletsch- and Oberaletschgletscher, the most melt can be found in the July to September time series. Finally, the January to February 2024 time series of the Grosser Aletsch- and the Oberaletschgletscher also appear unusual, as they show a negative surface change where one would expect a glacier-wide increase in surface change.

5 Discussion

The data used in this thesis was collected from multiple sources, including SPOT5 and Pléiades datasets, the RGI 7.0, and Copernicus landcover classes. SPOT5 images were inspected for cloud cover before use, and those selected exhibited minimal voids, particularly over the Aletsch region. The Pléiades data, similarly of high quality, had slightly fewer voids than SPOT5. SPOT5 provides a ground resolution of five metres, while Pléiades offers a finer resolution of two metres for the data used in this thesis. To maintain compatibility between datasets, SPOT5 data were upscaled to match the Pléiades resolution, ensuring no information was lost during processing. While this increased the overall pixel count, the analysis is ultimately constrained by SPOT5's five-metre resolution, which cannot be overlooked. This decision to upscale was critical in preserving the fidelity of the Pléiades data, aligning with recommendations from Berthier et al. (2023) on maintaining comparability in multi-sensor DEM analyses.

Another factor influencing data quality is the RGI 7.0. It is important to note that these outlines are static and were created in 2003. For consistency, the 2003 outlines were used throughout the analysis, ensuring that the full glacier extent is captured, even for later DEMs. However, this approach assumes glacier shrinkage over time, potentially leading to overestimating the glaciated area for more recent datasets. For larger glaciers, like the Grosser Aletschgletscher, this is primarily an issue in the ablation area, where the glacier retreats and becomes slimmer. This assumption introduces a potential bias, particularly when interpreting results from smaller glaciers, where area changes have a proportionally greater impact on volume estimates, as noted in studies like Hugonnet et al. (2021).

The Copernicus landcover dataset, with a 100-metre resolution and approximately 80% classification accuracy, was employed to identify stable terrain. The stable terrain mask, created by combining the RGI outlines with a 200-metre buffer and the Copernicus landcover classifications, covered an area of over 120 square kilometres. This approach successfully excluded glaciated and vegetated regions, providing a reliable baseline for co-registration. The co-registration was further strengthened by the high resolution of the DEMs and unified grid structures, ensuring low normalised median absolute deviation and root mean square error values. This methodology aligns with Hugonnet et al. (2022), who emphasised the role of large, carefully defined stable terrain masks in achieving robust co-registration for glacier studies.

The temporal distribution of the DEMs posed a significant challenge. The SPOT5 data is clustered between 2003 and 2007, limiting its utility for constructing a long-term time series. To address this, Pléiades data from 2021 and 2024 were incorporated to extend the timeline. However, the large gap between these datasets introduces difficulties in capturing potential short-term climatic variations and may impact the reliability of results in certain periods. Despite this, the inclusion of Pléiades allowed for a more comprehensive analysis of glacier changes over time, albeit with some limitations in temporal consistency. This trade-off between temporal coverage and dataset resolution mirrors the challenges faced in previous studies, such as Piermattei et al. (2023), and highlights the need for further investment in regularly updated, high-resolution DEM archives.

While these datasets provide a robust basis for analysing glacier surface elevation changes, their limitations must be acknowledged. The resolution mismatch between SPOT5 and Pléiades, though addressed by upscaling, may introduce minor inconsistencies in the differencing results. Additionally, the reliance on static outlines from 2003 could overestimate glacier areas for later DEMs, especially given the known retreat of glaciers like the Aletsch. Despite these challenges, the stable terrain mask ensured reliable co-registration and minimised systematic errors, supporting the validity of the derived results. These findings demonstrate the importance of carefully aligning datasets in multi-sensor workflows to ensure compatibility, as emphasised in Table 5.

Table 5: Overview of geographical data, listing datasets resolution, temporal coverage, strengths and some limitations for a subset of the data.

Dataset	Resolution	Temporal Coverage	Strengths	Limitations
SPOT5	5 m	2003-2007	Minimal voids; reliable over study area	Clustered in time; limited temporal range
Pléiades	2 m	2021, 2024	High resolution; minimal voids	Large temporal gaps; limited availability
RGI 7.0	30m, 90m	2003	Comprehensive glacier outline	Static; potential overestimation for later DEMs
Copernicus	100m	2019	Reliable stable terrain classification	Moderate classification accuracy (80%)

5.1 Grosser Aletschgletscher

For the Grosser Aletschgletscher, the results vary depending on the time series analysed. The sub-year series does not exhibit consistent patterns of melt, likely because the observed changes are too small to be reliably detected within such short time intervals. This is compounded by relatively large uncertainties, which obscure any potential yearly fluctuations. The 2003 to 2007 series align reasonably well with the results of Hugonnet et al. (2021), though uncertainties occasionally extend beyond the zero line, particularly in shorter intervals where melt would otherwise be expected.

Among the series analysed, the most robust results are observed in the longer time series. Both the Spring and Fall Series, combining SPOT5 and Pléiades DEMs, present consistent melt rates for the years 2003 to 2021, with the Spring Series suggesting an acceleration in melt from 2021 to 2024. This observed trend aligns with broader climatic tendencies, as highlighted in the GLAMOS mass balance records and the GLAMOS (2022) climatic simulations. The observed increase in melt rates for the Spring Series from 2021 onward is consistent with regional climatic trends noted in Hugonnet et al. (2021), particularly the intensification of negative glacier mass balances driven by warm summers and reduced winter snow accumulation in the Alps (Hugonnet et al., 2021). When comparing these results to Hugonnet et al. (2021), there appears to be a good fit. The longer series, particularly those spanning multiple years, produce reliable outputs that surpass uncertainty thresholds, even when using generously calculated 95% confidence intervals. These results compare favourably with ASTER-derived outputs and reinforce the validity of the SPOT5 and Pléiades integration.

It is noteworthy that the DEMs used in the Spring Series were captured while the glacier and much of the stable terrain were snow-covered. This introduces potential biases due to variable snow thickness, as snow-covered surfaces can reduce the accuracy of elevation change measurements, a challenge noted in Berthier et al. (2023). Despite this, the Spring Series time series from 2003 to 2021 estimates approximately 300 millimetres more melt than the Fall Series. This discrepancy, however, lies well within the uncertainty bands. Best practices in glacier monitoring advocate for using digital elevation models captured at the end of the hydrological year. Thus, the Fall Series is likely the more reliable representation of melt trends, though it is reassuring that the NMAD values over stable terrain and the overall differences between the two series are minimal.

In this context, the Grosser Aletsch results emphasise the strengths of integrating SPOT5 and Pléiades DEMs to produce longer time series. This approach captures large-scale melt patterns effectively but highlights the limitations of sub-annual intervals and the influence of acquisition timing on data accuracy. Future research might benefit from integrating auxiliary datasets, such as meteorological data or snow models, to better address seasonal biases and refine the reliability of sub-annual measurements.

5.2 Mittelaletschgletscher

For the Mittelaletschgletscher, the sub-year series exhibits substantial uncertainties, making it challenging to discern any seasonal cycles. This is likely due to the short intervals between observations, which hinder the clear detection of small-scale changes in surface height. This aligns with observations from Piermattei et al. (2023), who emphasise the critical role of temporal spacing in capturing reliable glacier dynamics using DEM differencing methods (Piermattei et al., 2023). Similar to the findings for the Grosser Aletschgletscher, these results suggest that sub-year datasets are less suited to reliably capture glacier dynamics using the current pipeline. The 2003 to 2007 series provide more reliable results, although some uncertainties persist, particularly in the 2003 to 2004 interval. This period exhibits a notably poor fit with ASTER-derived data, likely stemming from challenges in co-registration or data coverage for that specific timeframe.

However, subsequent intervals, especially the 2005 to 2007 dDEM, demonstrate smaller uncertainties and align well with ASTER data. These findings corroborate Hugonnet et al.'s (2021) assertion that spatial and temporal gaps in DEM coverage can influence the robustness of glacier change estimates (Hugonnet et al., 2021). The longer time spans in these intervals appear to mitigate the proportional influence of uncertainties, reinforcing the idea that longer observation periods enhance the reliability of glacier monitoring data. The longer time series also reveal notable trends. The Fall Series estimates an annual melt of fewer than 800 millimetres, while the Spring Series indicates slightly more than 1100 millimetres of melt per year from 2003 to 2021. The Spring Series aligns more closely with the ASTER data from Hugonnet et al. (2021), further supporting its reliability. This highlights the effectiveness of integrating high-resolution SPOT5 and Pléiades datasets, as discussed by Berthier et al. (2023), in resolving discrepancies and improving temporal consistency in glacier elevation change analyses (Berthier et al., 2023; Hugonnet et al., 2021). Interestingly, the Spring Series also displays a decline in melt rates for the 2021 to 2024 interval, which is unexpected given the strong negative mass balance recorded in 2022. These results highlight both the strengths and limitations of different temporal approaches.

The sub-year data lack the robustness to identify trends, while the 2003 to 2007 series demonstrate improved alignment with expected patterns, particularly in its longer intervals. The Spring and Fall Series, while differing slightly in estimated melt rates, both yield reliable insights into multi-year trends. Nonetheless, the unexpected decline in melt rates post-2021 suggests the need for further refinement in methodology and an exploration of complementary datasets, such as meteorological records, to contextualise and validate these findings. Future research should consider integrating auxiliary datasets, as recommended by Berthier et al. (2023), to address discrepancies and improve the reliability of elevation change estimates (Berthier et al., 2023; Hugonnet et al., 2021).

5.3 Oberaletschgletscher

The Oberaletschgletscher demonstrates patterns in surface height change that are broadly comparable to those observed in the Grosser Aletschgletscher and Mittelaletschgletscher. No clear pattern emerges to suggest that the Oberaletschgletscher consistently experiences more extreme changes in either direction compared to the others. The sub-year series, as with the other glaciers, exhibits a high degree of scatter around the zero-millimetre line, providing no discernible evidence of seasonal cycles. This aligns with the observation that short observation intervals are insufficient to capture meaningful trends in glacier dynamics using the current methodology (Piermattei et al., 2023).

The 2003 to 2007 series reveals a significant melt rate in the first time interval, but this result is undermined by a large confidence interval. The confidence interval, directly scaled from the NMAD, reflects reliable statistical calculations but may not fully capture the specific characteristics of the glacier's surface. In this case, the 2004 DEM shows increased snow coverage at higher elevations, which likely contributes to the higher NMAD and RMSE values in the corresponding dDEM (Hugonnet et al., 2022). Despite this limitation, the subsequent intervals in the 2003 to 2007 series demonstrate improved

alignment with expected patterns, particularly as observation intervals lengthen. The longer time series, represented by the Spring and Fall Series, provides more robust insights. Among the three glaciers studied, the Oberaletschgletscher shows the largest negative surface height change in both the Spring and Fall Series. This consistency across datasets reinforces the reliability of these results.

However, the same trend observed in the other glaciers is present here: the Fall Series consistently estimates a smaller negative surface height change compared to the Spring Series. This discrepancy, while falling within the calculated uncertainties, may be attributed to seasonal differences in snow coverage or the timing of DEM acquisition relative to the hydrological year (Berthier et al., 2023). Unexpectedly, the Spring Series shows a decrease in the rate of surface height change between the 2003–2021 and 2021–2024 intervals. Given the pronounced negative mass balance observed in 2022, this reduction in melt rate is counterintuitive. Possible explanations include variability in DEM quality or coverage, differences in snow or ice albedo during acquisition, or transient climatic anomalies during the study period (Bannwart et al., 2024). Such findings highlight the need for further investigation into short-term climatic events or additional datasets to better contextualize these results.

Overall, the Oberaletschgletscher exhibits trends that are consistent with those of the Grosser Aletschgletscher and Mittelaletschgletscher, despite its distinct topographical and surface characteristics. The sub-year series again fails to provide reliable results, while the longer time intervals in both the 2003–2007 and Spring and Fall Series offer meaningful insights into glacier dynamics. These results underscore the importance of long-term datasets for reducing uncertainty and capturing the complex interactions between seasonal, interannual, and long-term processes affecting glacier change (Hugonnet et al., 2021; Piermattei et al., 2023).

5.4 Comparing Time Series

Analysing the time series reveals that shorter intervals between DEM acquisitions are significantly more prone to higher uncertainties, highlighting the inherent limitations of the current pipeline and dataset configurations. For direct comparison, Figure 26 provides a direct overview of the glacier surface height changes through the different time series. Stable terrain metrics, such as NMAD and RMSE, served as critical indicators for co-registration quality, allowing a closer examination of the relationship between time series length and reliability.

Interestingly, the uncertainty in dDEMs does not scale linearly with the time elapsed between observations. Uncertainties tend to level off over longer periods, meaning that having more time between DEMs helps capture clearer changes while reducing noise from short-term events or small data issues. The algorithm used for co-registration performed consistently well across most time series, as evidenced by low mean differences over stable terrain, low NMAD, and low RMSE values. However, the results demonstrate that sub-year time series are particularly unreliable in this context. The inherent variability in glacier dynamics, coupled with the limited temporal signal, prevents the pipeline from detecting significant or meaningful changes in glacier surface elevation. This is consistent with findings by Zemp et al. (2023), who emphasised that seasonal or shorter-term glacier observations often face challenges due to variability and limited data coverage. Time series spanning one year begin to show more consistent and usable outputs, particularly when supplemented by high-resolution datasets and stringent co-registration protocols. However, the most reliable results emerge from a time series of two years or more, where uncertainties fall well within acceptable bounds for all three glaciers examined. Longer intervals allow the algorithm to overcome the noise introduced by seasonal snow cover, minor registration errors, or localised surface anomalies. For example, the increased time allows for a more substantial cumulative signal of glacier change, reducing the relative impact of measurement uncertainty (Hugonnet et al., 2021; Zemp & Welty, 2023).

One noteworthy limitation of the current dataset and pipeline configuration is its reliance on stable terrain metrics scaled to yearly values. While this approach ensures consistency across time series of varying lengths, it does not fully account for potential biases introduced by seasonal snow cover or

atmospheric effects present during DEM acquisition Bannwart et al. (2024). Future improvements could involve refining the uncertainty scaling to better reflect sub-annual variability or incorporating auxiliary datasets, such as seasonal snow masks or climatic indices, to adjust for short-term factors affecting surface elevation measurements.

In conclusion, as seen in Figure 26 this analysis underscores that the current pipeline performs best with a time series of two or more years, where the cumulative signal of glacier surface elevation change surpasses the uncertainties inherent to the method. Sub-year time series are not yet viable for deriving meaningful results, while single-year intervals represent the lower limit of reliability, contingent on favourable acquisition conditions and robust co-registration. This establishes a clear threshold for future studies: time series shorter than one year are unsuitable for meaningful glacier surface change analysis using this methodology, while intervals of two or more years yield the most reliable and interpretable results.
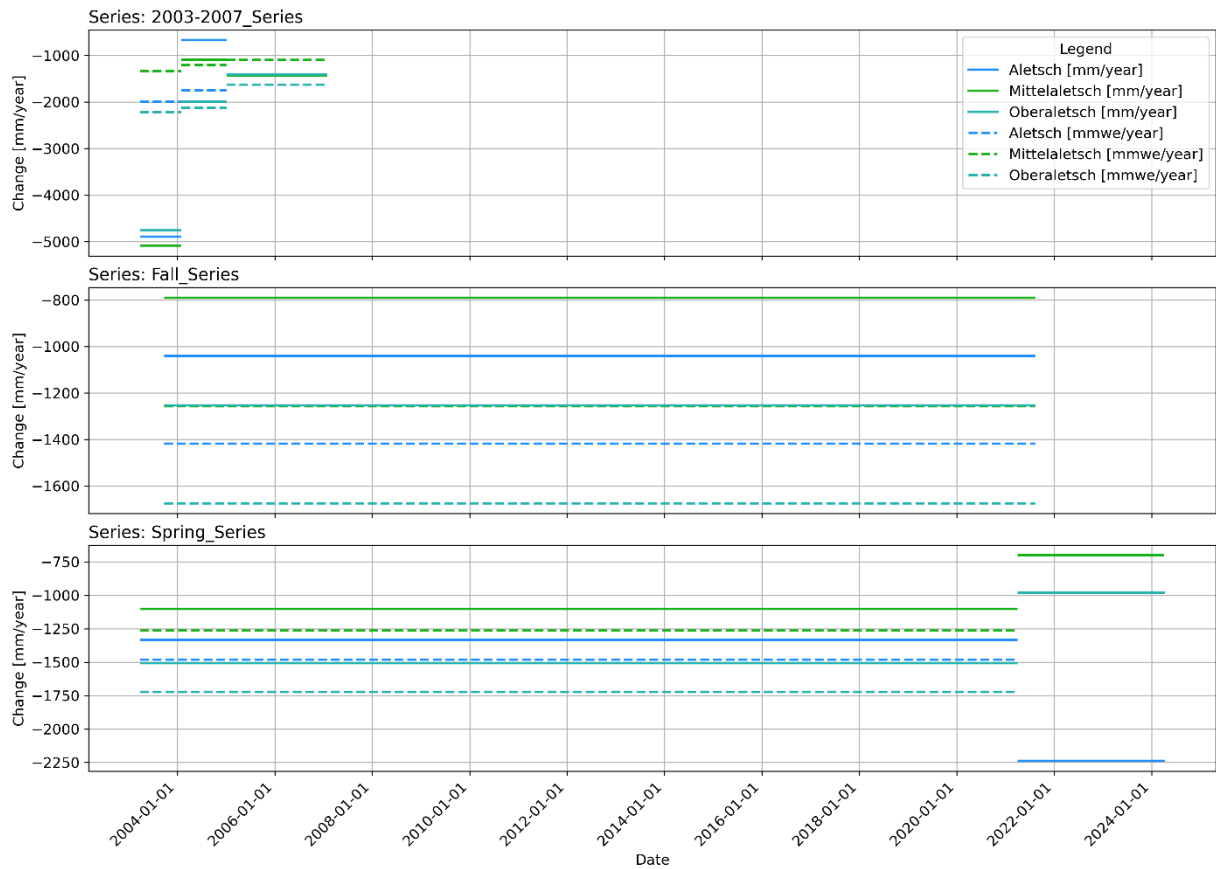

Figure 25: Plot of the spring series, fall series and 2003 to 2007 series. *Each series has its plot areas. The solid lines are the median values of the binned glaciers. The dotted lines are the Hugonnet et al 2021 values in millimetres water equivalent, whilst the surface change is in millimetre height per year. Because of a lack of information about snow and ice density at all points in time, a conversion for this graph has been decided against. The length of each line is determined by the start and end date. Hugonnets time series ends in the year 2020, explaining why there are no dotted lines after that.*

5.5 Comparing Glacier Areas

The glaciers processed for this thesis vary considerably in size, slope, and aspect, yet their shared regional context provides a unique opportunity for comparison. Because all three glaciers are located within the same stereo images, the results are inherently consistent across the time series, with each point in time derived from the same input DEMs. This ensures that uncertainties and errors affecting the glacier surface height change calculations are uniform across the datasets, enabling direct comparison of the results. However, glacier size introduces several key factors that affect the reliability and interpretation of the findings. Smaller glaciers, such as the Mittelaletsch- and Oberaletschgletscher, are more sensitive to errors introduced during processing. This sensitivity stems partly from the effect of slope, as steeper gradients can amplify uncertainties in elevation measurements, particularly over

glaciated terrain. This is compounded by the fact that smaller glaciers inherently cover less spatial area, reducing the number of bins created during the hypsometric binning process. In this study, binning was conducted in 100-metre elevation bands derived from the DEMs. While the Grosser Aletschgletscher, due to its larger vertical extent, was divided into 27 bins, the Mittelaletsch- and Oberaletschgletscher each had only 18 bins. The limited number of bins for smaller glaciers increases statistical noise and reduces the spatial resolution of the analysis, making localised anomalies or outliers more impactful (Maussion et al., 2019; Zemp et al., 2014).

Another consideration is the influence of edge effects and glacier boundary uncertainties. Smaller glaciers are more likely to experience disproportionate impacts from inaccuracies in delineation, especially when outlines are derived from older datasets, as was the case for the RGI 7.0 outlines used in this study. These boundaries, dating from 2003, may not accurately reflect current glacier extents, leading to potential inclusion or exclusion of areas affected by melt or accumulation processes. For larger glaciers, such discrepancies are diluted across their greater area, but for smaller glaciers, they can significantly influence results. Additionally, the robustness of the results depends on the relative scale of changes being measured. Smaller glaciers, with less absolute volume, often exhibit changes that are closer to the uncertainty thresholds of the processing pipeline, further complicating their interpretation (Nuth & Kääb, 2011). This is particularly evident in sub-year and one-year time series, where uncertainties often exceed the magnitude of detected changes. Conversely, larger glaciers benefit from the cumulative effect of changes over a larger area, making the signal more discernible even in shorter time series.

The findings from this thesis suggest that while the processing pipeline is effective across glaciers of varying sizes, smaller glaciers require careful consideration of these additional factors. For instance, the Mittelaletschgletscher and Oberaletschgletscher demonstrated higher sensitivity to slope-induced uncertainties and binning effects, particularly in the shorter time series. These effects were less pronounced for the Grosser Aletschgletscher, where its larger size and broader elevation range provided more stable and interpretable results. In addition, seasonal effects on snow and ice albedo disproportionately impact smaller glaciers, as their reduced area makes them more vulnerable to localised weather patterns and transient snow accumulation (Paul, 2020). This highlights the need for temporal and spatial consistency in DEM acquisition and careful interpretation when analysing smaller glaciers.

In conclusion, glacier size plays a critical role in the reliability of surface height change analyses. While the pipeline performs well across different glacier sizes, smaller glaciers are more susceptible to amplified uncertainties from slope, boundary delineation, and binning effects. For reliable and comparable results, it is recommended that future studies carefully assess these factors, especially when analysing small glaciers or those with steep slopes. Examples from this study highlight the importance of sufficient spatial coverage and the limitations imposed by fewer bins and smaller vertical extents, emphasising the need for refined methods to mitigate these challenges.

6 Conclusion and Outlook

This thesis set out to assess surface elevation changes of the Grosser Aletsch-, Mittelaletsch-, and Oberaletschgletscher using a newly developed processing pipeline that integrates SPOT5 and Pléiades-derived DEMs. By extending the temporal range of available datasets and applying robust co-registration techniques, this research contributes to understanding glacier dynamics in the context of ongoing climate change. The following paragraphs address the research findings, highlight the study's limitations, and propose directions for future research.

The integration of SPOT5 and Pléiades DEMs proved effective for glacier monitoring. The processing pipeline successfully aligned and analysed the datasets, yielding reliable surface elevation change estimates over long-term intervals. By incorporating Pléiades data, the timeline was extended to cover the period from 2003 to 2024, enabling insights into multi-year trends, particularly for the Spring Series, which highlighted an acceleration in melt rates. The combination of these datasets allowed for cross-validation of results, providing additional confidence in the observed trends and highlighting the potential for integrating multiple sensors to improve monitoring capabilities.

However, shorter time intervals between DEM acquisitions were associated with higher uncertainties, underlining the necessity of sufficient temporal gaps for reliable results. Sub-year time series failed to produce meaningful trends due to their high noise levels, while single-year intervals were only marginally reliable, with uncertainties occasionally obscuring the observed changes. The observed uncertainties in shorter time intervals suggest that the influence of seasonal snow cover and temporary surface fluctuations must be better accounted for in future research. The most robust results were derived from intervals of two years or more, where the cumulative glacier changes outweighed measurement noise, demonstrating the pipeline's strength in analysing longer temporal datasets. Comparing SPOT5 to ASTER, SPOT5 provided finer spatial resolution and better vertical accuracy, particularly in complex terrains, as demonstrated by Table 1. For the glaciers studied in this thesis, SPOT5 offered a potential advantage in temporal resolution around 2003 (Figure 9). However, ASTER's broader temporal coverage across the 2000–2024 period, when properly combined and temporally interpolated, remains significant. The use of Pléiades data alongside SPOT5 extended the time series into the present, demonstrating the potential for future extensions using SPOT6, SPOT7, and newer missions. Evaluations of normalised median absolute deviation and root mean square error over stable terrain supported the hypothesis of SPOT5's superior spatial and vertical accuracy.

Glacier size significantly influenced the reliability of the results. The larger Grosser Aletschgletscher yielded more stable and interpretable results due to its extensive spatial coverage and greater cumulative signal, which mitigated the impact of localised uncertainties. In contrast, smaller glaciers like Mittelaletschgletscher and Oberaletschgletscher were more susceptible to errors arising from steep slopes, fewer elevation bands, and greater sensitivity to edge effects. These factors amplified localised outliers and statistical noise, particularly in shorter time series, limiting the robustness of their results. Future studies should consider refining the analysis for smaller glaciers by incorporating higher-resolution datasets or employing advanced filtering techniques to mitigate edge effects. Nonetheless, when analysed over longer intervals, trends in surface elevation changes for smaller glaciers aligned with broader regional patterns, supporting the validity of the pipeline even for smaller glacier systems. Figure 26 reflects these results, showing that glacier size alone does not dictate the reliability of outcomes as long as sufficient temporal and seasonal considerations are maintained.

Modern open-source tools like xDEM were crucial for implementing the pipeline and ensuring reproducibility. The xDEM pipeline excelled in co-registering DEMs with precision, particularly when combined with other open-source tools. However, it was not a standalone solution and needed integration with complementary functionalities to fully meet the requirements of Piermattei et al. (2023)'s workflow. The flexibility of xDEM allowed for adaptation to different glacier environments, showcasing its potential for broader application in glaciological studies. Stable terrain played a pivotal

role in minimising vertical and horizontal misalignments during co-registration. Following Hugonnet's approach, a stable terrain mask was created using Copernicus land cover classes and RGI 7.0 glacier outlines, refined by removing three-sigma outliers to minimise void-induced distortions. This integration ensured effective alignment and robust outputs.

Seasonal variability significantly impacted the analysis. Snow cover in DEMs sourced during different seasons introduced uncertainties, particularly in the Fall Series, where snow accumulation distorted stable terrain and glacier surface heights. Surprising stability was observed in the Spring Series, where snow-covered acquisitions yielded consistent results, while sub-year time series like the 2003–2007 interval suffered from high noise due to snow effects. Hugonnet et al. (2021)'s interpolated datasets, less influenced by abrupt snow accumulation or ablation, provided a useful comparison. However, the inclusion of Pléiades data improved the long-term accuracy of the series, reinforcing the value of combining datasets for robust temporal coverage. The introduction of Pléiades data brought additional challenges due to resolution mismatches with SPOT5. To mitigate uncertainties, SPOT5's coarser pixel size was matched to that of Pléiades without pixel averaging. This adjustment constrained fine-scale measurements but ensured consistent analysis. Longer time series generated by this integration provided improved accuracy compared to shorter intervals. Direct comparisons of SPOT5 and Pléiades outputs remain an avenue for future research, as their combined use demonstrated robust results over extended timelines.

Several limitations were identified in this study. The temporal distribution of the data posed challenges, with SPOT5 DEMs clustered between 2003 and 2007 and large gaps until Pléiades acquisitions in 2021 and 2024. This limited the ability to capture short-term climatic variations and introduced potential biases due to temporal inconsistencies. These temporal gaps underscore the importance of developing strategies to interpolate or supplement data using alternative sources, such as UAV surveys or SAR data. Additionally, the resolution mismatch between SPOT5 and Pléiades required upscaling, which constrained the analysis to the coarser resolution of SPOT5 and may have reduced the precision of finer-scale measurements. The use of static RGI 7.0 glacier outlines from 2003 potentially overestimated glacier areas in more recent datasets, particularly for smaller glaciers that have retreated significantly since then. Furthermore, sub-annual analyses were unreliable due to high uncertainties, emphasising the need for improved temporal resolution and auxiliary datasets.

Future research should focus on addressing these limitations and expanding the applicability of the pipeline. The integration of time-varying glacier outlines would enhance the accuracy of area estimates, particularly for retreating glaciers. Additional datasets, such as SPOT6 or further Pléiades DEMs, could improve temporal resolution and fill gaps in the existing time series. Refining the uncertainty scaling to account for seasonal variability and incorporating auxiliary datasets like snow and meteorological models could mitigate biases introduced by seasonal snow cover and atmospheric effects. Machine learning techniques could be explored to enhance automated anomaly detection and uncertainty estimation within the processing pipeline. Moreover, automating the pipeline's key steps, such as co-registration and outlier filtering, would enhance scalability and applicability to other glacierised regions. Continued acquisitions from Pléiades or its successors are essential to building a consistent long-term time series, ensuring reliable monitoring of glacier dynamics in the face of accelerating climate change.

7 References

Abrams, M. (2000). The Advanced Spaceborne Thermal Emission and Reflection Radiometer (ASTER): Data products for the high spatial resolution imager on NASA's Terra platform. *International Journal of Remote Sensing*, *21*(5), 847–859. https://doi.org/10.1080/014311600210326

Abrams, M., Tsu, H., Hulley, G., Iwao, K., Pieri, D., Cudahy, T., & Kargel, J. (2015). The Advanced Spaceborne Thermal Emission and Reflection Radiometer (ASTER) after fifteen years: Review of global products. *International Journal of Applied Earth Observation and Geoinformation*, *38*, 292–301. https://doi.org/10.1016/j.jag.2015.01.013

Airbus. (2025). *Pléiades Very High-Resolution Satellites Imagery*. Airbus Defence and Space. https://space-solutions.airbus.com/imagery/our-optical-and-radar-satellite-imagery/pleiades/?utm_term=&utm_campaign=002000+-+G-ADS+-+VKS+-%E2%80%A61/9

Bannwart, J., Piermattei, L., Dussaillant, I., Krieger, L., Floricioiu, D., Berthier, E., Roeoesli, C., MacHguth, H., & Zemp, M. (2024). Elevation bias due to penetration of spaceborne radar signal on Grosser Aletschgletscher, Switzerland. *Journal of Glaciology*. https://doi.org/10.1017/jog.2024.37

Bernat, M., Belart, J. M. C., Berthier, E., Jóhannesson, T., Hugonnet, R., Dehecq, A., Magnússon, E., & Gunnarsson, A. (2023). Geodetic mass balance of Mýrdalsjökull ice cap, 1999-2021. *Jökull*, *73*(1), 35–53. https://doi.org/10.33799/jokull2023.73.035

Berthier, E., Arnaud, Y., Kumar, R., Ahmad, S., Wagnon, P., & Chevallier, P. (2007). Remote sensing estimates of glacier mass balances in the Himachal Pradesh (Western Himalaya, India). *Remote Sensing of Environment*, *108*(3), 327–338. https://doi.org/10.1016/j.rse.2006.11.017

Berthier, E., Floriciou, D., Gardner, A. S., Gourmelen, N., Jakob, L., Paul, F., Treichler, D., Wouters, B., Belart, J. M. C., Dehecq, A., Dussaillant, I., Hugonnet, R., Kääb, A., Krieger, L., Pálsson, F., & Zemp, M. (2023). Measuring glacier mass changes from space—a review. In *Reports on Progress in Physics* (Vol. 86, Issue 3). Institute of Physics. https://doi.org/10.1088/1361-6633/acaf8e

Berthier, E., Kargel, J. S., Raup, B., & Zemp, M. (2024). Earth surface monitoring is at risk. *Nature*, *630*, 563.

Berthier, E., Lebreton, J., Fontannaz, D., Hosford, S., Belart, J. M. C., Brun, F., Andreassen, L. M., Menounos, B., & Blondel, C. (2024). The Pléiades Glacier Observatory: high resolution digital elevation models and ortho-imagery to monitor glacier change. *EGUsphere*. https://doi.org/10.5194/egusphere-2024-250

Berthier, E., & Toutin, T. (2008). SPOT5-HRS digital elevation models and the monitoring of glacier elevation changes in North-West Canada and South-East Alaska. *Remote Sensing of Environment*, *112*(5), 2443–2454. https://doi.org/10.1016/j.rse.2007.11.004

Berthier, E., Vincent, C., Magnússon, E., Gunnlaugsson, P., Pitte, P., Le Meur, E., Masiokas, M., Ruiz, L., Pálsson, F., Belart, J. M. C., & Wagnon, P. (2014). Glacier topography and elevation changes derived from Pléiades sub-meter stereo images. *Cryosphere*, *8*(6), 2275–2291. https://doi.org/10.5194/tc-8-2275-2014

Beyer, R. A., Alexandrov, O., & McMichael, S. (2018). The Ames Stereo Pipeline: NASA's Open Source Software for Deriving and Processing Terrain Data. *Earth and Space Science*, *5*(9), 537–548. https://doi.org/10.1029/2018EA000409

Braun, M., Zemp, M., & Brun, F. (2022). *First results of the RAGMAC glacier elevation change intercomparison exercise*. https://doi.org/10.5194/egusphere-egu22-8606

CNES. (2024). *swh Data center*. REGARDS. https://regards.cnes.fr/user/swh/modules/60

Cogley, J. G., Hock, R., Rasmussen, L. A., Arendt, A. A., Bauder, A., Braithwaite, R. J., Jahnsson, P., Kaser, G., Möller, M., Nicholson, L., & Zemp, M. (2011). Glossary of glacier mass balance and related terms. *IHP-VII Technical Documents in Hydrology*, *2*(86). http://www.unesco.org/water/ihp/

Copernicus. (2020). *Land Cover 2015-2019 (raster 100 m)*. European Commission Directorate-General Joint Research Centre. https://land.copernicus.eu/en/data-policy

ESA. (2024). *SPOT5*. https://earth.esa.int/eogateway/missions/spot-5#instruments-section

Filchev, L., Pashova, L., Kolev, V., & Frye, S. (2020). Surveys, Catalogues, Databases/Archives, and State-of-the-Art Methods for Geoscience Data Processing. *Knowledge Discovery in Big Data from Astronomy and Earth Observation: Astrogeoinformatics*, 103–136. https://doi.org/10.1016/B978-0-12-819154-5.00016-3

Gärtner-Roer, I., Nussbaumer, S. U., Hüsler, F., & Zemp, M. (2019). Worldwide assessment of national glacier monitoring and future perspectives. *Mountain Research and Development*, *39*(2), A1–A11. https://doi.org/10.1659/MRD-JOURNAL-D-19-00021.1

GLAMOS. (2022). *Swiss Glacier Mass Balance, release 2022*.

GLAMOS. (2024). *The Swiss Glaciers 1881-2020/21, Glaciological Reports No 1-142*.

Huber, J., McNabb, R., & Zemp, M. (2020). Elevation Changes of West-Central Greenland Glaciers From 1985 to 2012 From Remote Sensing. *Frontiers in Earth Science*, *8*. https://doi.org/10.3389/feart.2020.00035

Hugonnet, R., Brun, F., Berthier, E., Dehecq, A., Mannerfelt, E. S., Eckert, N., & Farinotti, D. (2022). Uncertainty Analysis of Digital Elevation Models by Spatial Inference From Stable Terrain. *IEEE Journal of Selected Topics in Applied Earth Observations and Remote Sensing*, *15*, 6456–6472. https://doi.org/10.1109/JSTARS.2022.3188922

Hugonnet, R., Mannerfelt, E., Dehecq, A., Knuth, F., & Tedstone, A. (2023). *xDEM*. GlacioHack. https://doi.org/10.5281/ZENODO.11204531

Hugonnet, R., McNabb, R., Berthier, E., Menounos, B., Nuth, C., Girod, L., Farinotti, D., Huss, M., Dussaillant, I., Brun, F., & Kääb, A. (2021). Accelerated global glacier mass loss in the early twenty-first century. *Nature*, *592*(7856), 726–731. https://doi.org/10.1038/s41586-021-03436-z

Huss, M., Bauder, A., & Linsbauer, A. (2024). *Winter snow accumulation on Swiss glaciers in 2024*.

Jouvet, G., & Huss, M. (2019). Future retreat of Great Aletsch Glacier. In *Journal of Glaciology* (Vol. 65, Issue 253, pp. 869–872). Cambridge University Press. https://doi.org/10.1017/jog.2019.52

Kääb, A. (2002). *Monitoring high-mountain terrain deformation from repeated air-and spaceborne optical data: examples using digital aerial imagery and ASTER data*. www.elsevier.com/locate/isprsjprs

Kennedy, J., Trewin, B., Betts, R., Thorne, P., Forster, P., Siegmund, P., Ziese, M., Alvar-Beltran, J., Gialetti, A., Birner, J., Reusing, R.-S., du Parc, E., Anzellini, V., Ponserre, S., Grasso, V., Msemo, N., Cuellar Vargas, D., Bastani, H., Boscolo, R., & Naran, B. (2024). State of the Climate 2024 Update for COP29. In *World Meteorological Organization*.

https://library.wmo.int/viewer/69075/download?file=State-Climate-2024-Update-COP29_en.pdf&type=pdf&navigator=1

Korona, J., Berthier, E., Bernard, M., Rémy, F., & Thouvenot, E. (2009). SPIRIT. SPOT 5 stereoscopic survey of Polar Ice: Reference Images and Topographies during the fourth International Polar Year (2007-2009). *ISPRS Journal of Photogrammetry and Remote Sensing*, *64*(2), 204–212. https://doi.org/10.1016/j.isprsjprs.2008.10.005

Kos, A., Amann, F., Strozzi, T., Delaloye, R., von Ruette, J., & Springman, S. (2016). Contemporary glacier retreat triggers a rapid landslide response, Great Aletsch Glacier, Switzerland. *Geophysical Research Letters*, *43*(24), 12,466-12,474. https://doi.org/10.1002/2016GL071708

LEGOS. (2025). *FormaTerre/THEIA - Pléiades Glacier Observatory data products*. Laboratory of Space Geophysical and Oceanographic Studies. https://doi.theia.data-terra.org/pgo/

Mesa-Mingorance, J. L., & Ariza-López, F. J. (2020). Accuracy assessment of digital elevation models (DEMs): A critical review of practices of the past three decades. *Remote Sensing*, *12*(16). https://doi.org/10.3390/RS12162630

NASA. (2004). *Advanced Spaceborne Thermal Emission and Reflection Radiometer*. Jet Propulsion Laboratory. https://asterweb.jpl.nasa.gov/instrument.asp

Nuth, C., & Kääb. (2011). Co-registration and bias corrections of satellite elevation data sets for quantifying glacier thickness change. *Cryosphere*, *5*(1), 271–290. https://doi.org/10.5194/tc-5-271-2011

Paul, F. (2020). A 60-year chronology of glacier surges in the central Karakoram from the analysis of satellite image time-series. *Geomorphology*, *352*. https://doi.org/10.1016/j.geomorph.2019.106993

Piermattei, L., Zemp, M., Sommer, C., Brun, F., Braun, M. H., Andreassen, L. M., Belart, J. M. C., Berthier, E., Bhattacharya, A., Boehm Vock, L., Bolch, T., Dehecq, A., Dussaillant, I., Falaschi, D., Florentine, C., Floricioiu, D., Ginzler, C., Guillet, G., Hugonnet, R., … Yang, R. (2023). *Observing glacier elevation changes from spaceborne optical and radar sensors – an inter-comparison experiment using ASTER and TanDEM-X data*. https://doi.org/10.5194/egusphere-2023-2309

Racoviteanu, A. E., Paul, F., Raup, B., Jodha, S., Khalsa, S., & Armstrong, R. (2009). *Challenges and recommendations in mapping of glacier parameters from space: results of the 2008 Global Land Ice Measurements from Space (GLIMS) workshop, Boulder, Colorado, USA*. http://www.gdem.

RGI 7.0 Consortium. (2023). *Randolph Glacier Inventory - A Dataset of Global Glacier Outlines, Version 7.0*.

Swisstopo. (2024). *Maps of Switzerland*. Geo.Admin.Ch. https://map.geo.admin.ch/#/map?lang=en&center=2660000,1190000&z=1&topic=ech&layers=ch.swisstopo.zeitreihen@year=1864,f;ch.bfs.gebaeude_wohnungs_register,f;ch.bav.haltestellen-oev,f;ch.swisstopo.swisstlm3d-wanderwege,f;ch.vbs.schiessanzeigen,f;ch.astra.wanderland-sperrungen_umleitungen,f&bgLayer=ch.swisstopo.pixelkarte-farbe

Toutin, T. (2001). Elevation modelling from satellite visible and infrared (VIR) data. *International Journal of Remote Sensing*, *22*(6), 1097–1125. https://doi.org/10.1080/01431160117862

Zemp, M., Armstrong, R., Gärtner-Roer, I., Haeberli, W., Hoelzle, M., Kääb, A., Kargel, J. S., Khalsa, S. J. S., Leonard, G. J., Paul, F., & Raup, B. H. (2014). Introduction: Global Glacier Monitoring—a Long-Term Task Integrating in Situ Observations and Remote Sensing. In *Global*

Land Ice Measurements from Space (pp. 1–21). Springer Berlin Heidelberg. https://doi.org/10.1007/978-3-540-79818-7_1

Zemp, M., Thibert, E., Huss, M., Stumm, D., Rolstad Denby, C., Nuth, C., Nussbaumer, S. U., Moholdt, G., Mercer, A., Mayer, C., Joerg, P. C., Jansson, P., Hynek, B., Fischer, A., Escher-Vetter, H., Elvehøy, H., & Andreassen, L. M. (2013). Reanalysing glacier mass balance measurement series. *Cryosphere*, *7*(4), 1227–1245. https://doi.org/10.5194/tc-7-1227-2013

Zemp, M., & Welty, E. (2023). Temporal downscaling of glaciological mass balance using seasonal observations. *Journal of Glaciology*. https://doi.org/10.1017/jog.2023.66

8 Appendix

In the Figures listed in the appendix, part of the output in the form of three graphs per time series generated by the Analysis Code (Script 3) can be seen. They give an overview of the surface height change and how it is distributed over time and space in between the three glaciers. They are sorted by time series, followed by sorting by glacier and then by the time frame. The time series contained in the appendix are the Spring Series, the Fall Series and the 2003-2007 Series. If graphs share the same time frame, they also share the same difference DEM that is the basis for the analysis. Therefore, some of the stable terrain hypsometry are the same. The areas were divided by use of the stable terrain masks as well as glacier masks for each of the three study glaciers.

8.1 Graphs

Spring Series - Grosser Aletschgletscher - 26.03.2003 – 31.03.2021
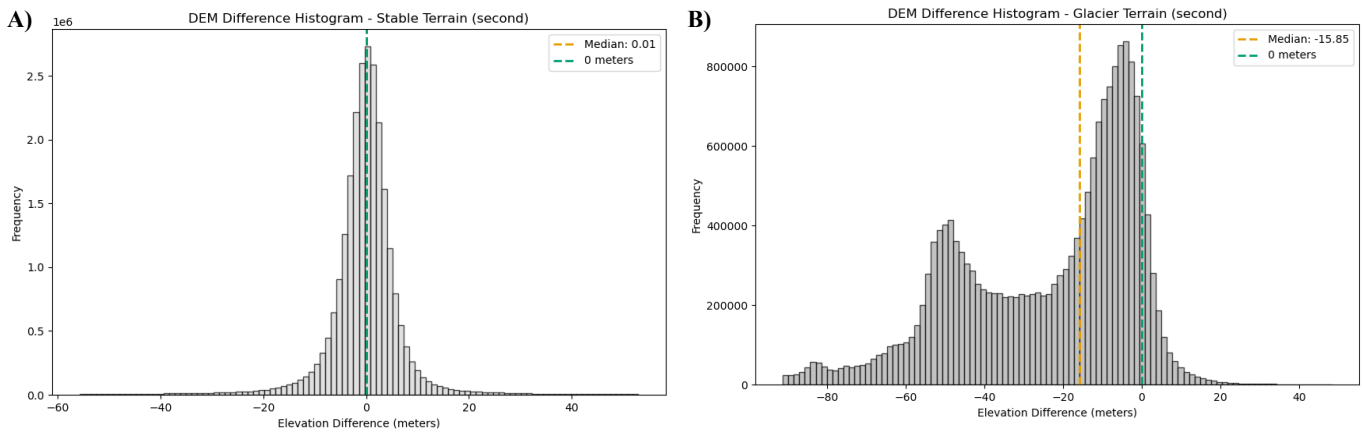
Figure 27: A) Code output of stable terrain hypsometry calculated from the dDEM for the Grosser Aletschgletscher. The graph includes median and a dashed 0-metre line with dynamically generated axis labelling. B) Code output of glacier terrain hypsometry calculated from the dDEM for the Grosser Aletschgletscher. The graph includes median and a dashed 0-metre line with dynamically generated axis labelling. The x-axes show the elevation difference in metres, whilst the y-axes show the frequency.
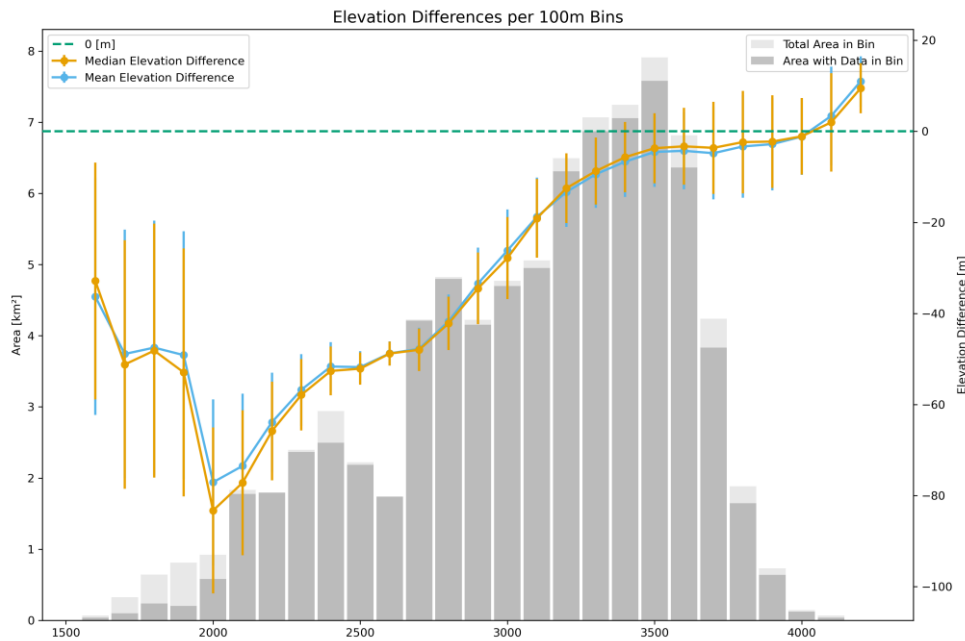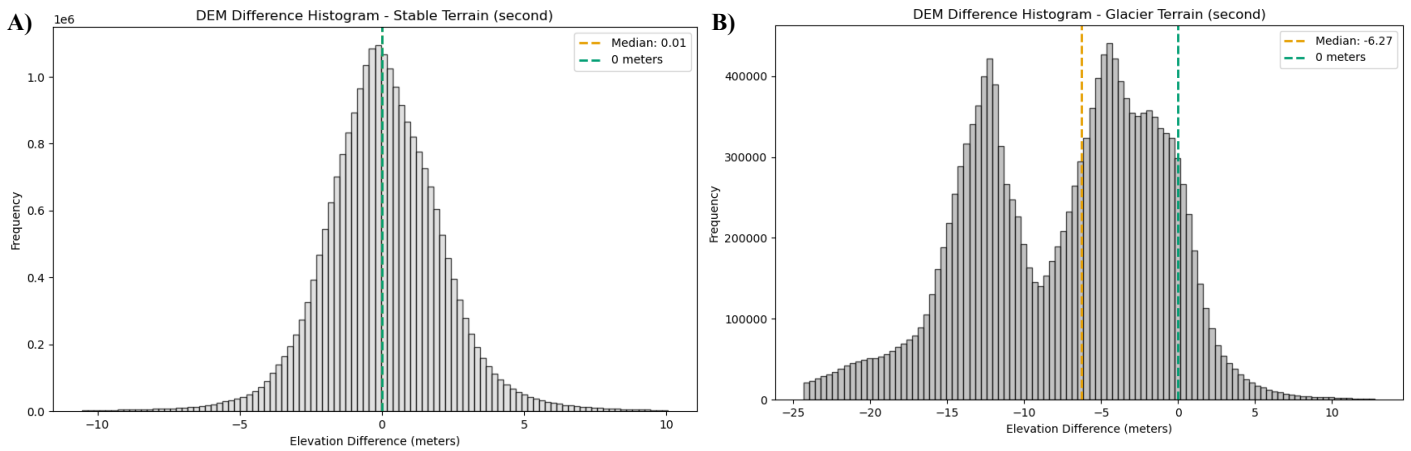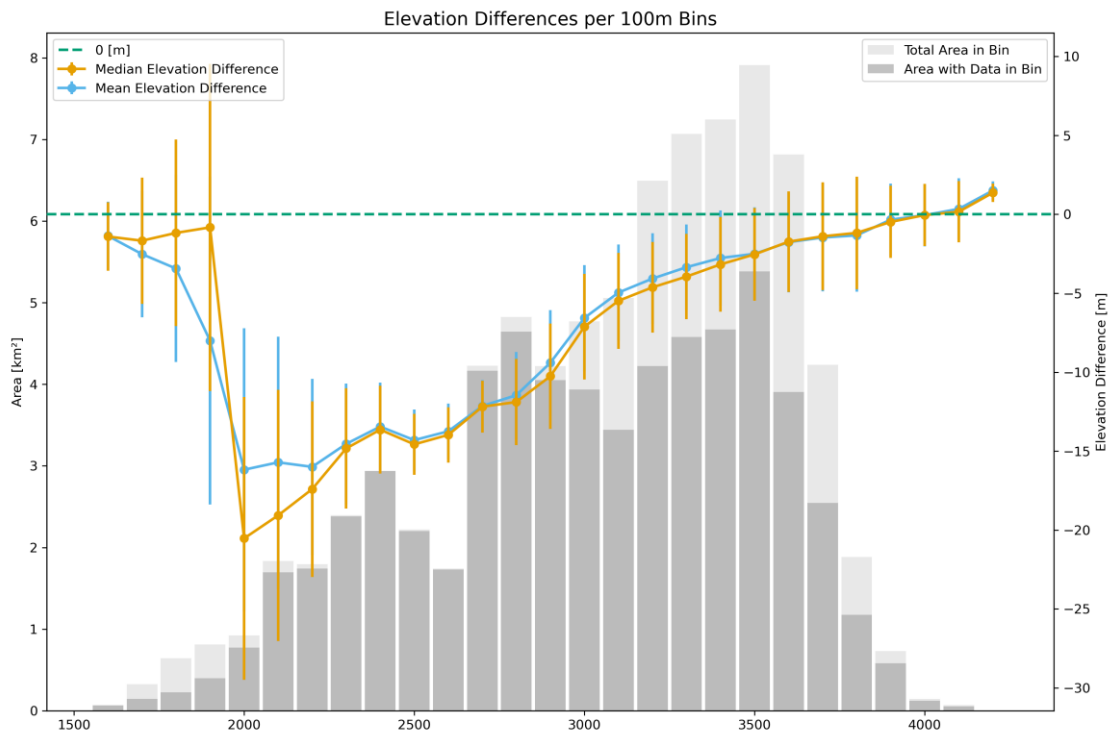

Figure 28: Elevation difference hypsometry plot showing the glacier area in bins for each 100-metre height band of the Grosser Aletschgletscher. The x-axis shows the metres above sea level. The first y-axis shows the area each hypsometric bin contains. The bins are separated into light grey for the total area available in that bin, the dark grey shows the area with valid

data in that bin. The second y-axis shows the elevation difference calculated in each bin that can be seen as points with one standard deviation whiskers. The elevation difference is displayed for both the median and the mean elevation difference calculated in each bin with a dashed line indicating an elevation difference of zero.

Spring Series - Grosser Aletschgletscher - 31.03.2021 – 11.04.2024

Figure 29: A) Code output of stable terrain hypsometry calculated from the dDEM for the Grosser Aletschgletscher. The graph includes median and a dashed 0-metre line with dynamically generated axis labelling. The x-axis shows the elevation difference in metres, whilst the y-axis shows the pixel frequency. B) Code output of glacier terrain hypsometry calculated from the dDEM for the Grosser Aletschgletscher. The graph includes median and a dashed 0-metre line with dynamically generated axis labelling. The x-axis shows the elevation difference in metres, whilst the y-axis shows the frequency.

Figure 30: Elevation difference hypsometry plot showing the glacier area in bins for each 100-metre height band of the Grosser Aletschgletscher. The x-axis shows the metres above sea level. The first y-axis shows the area each hypsometric bin contains. The bins are separated into light grey for the total area available in that bin, the dark grey shows the area with valid data in that bin. The second y-axis shows the elevation difference calculated in each bin that can be seen as points with one standard deviation whiskers. The elevation difference is displayed for both the median and the mean elevation difference calculated in each bin with a dashed line indicating an elevation difference of zero.

Spring Series – Mittelaletschgletscher - 26.03.2003 – 31.03.2021
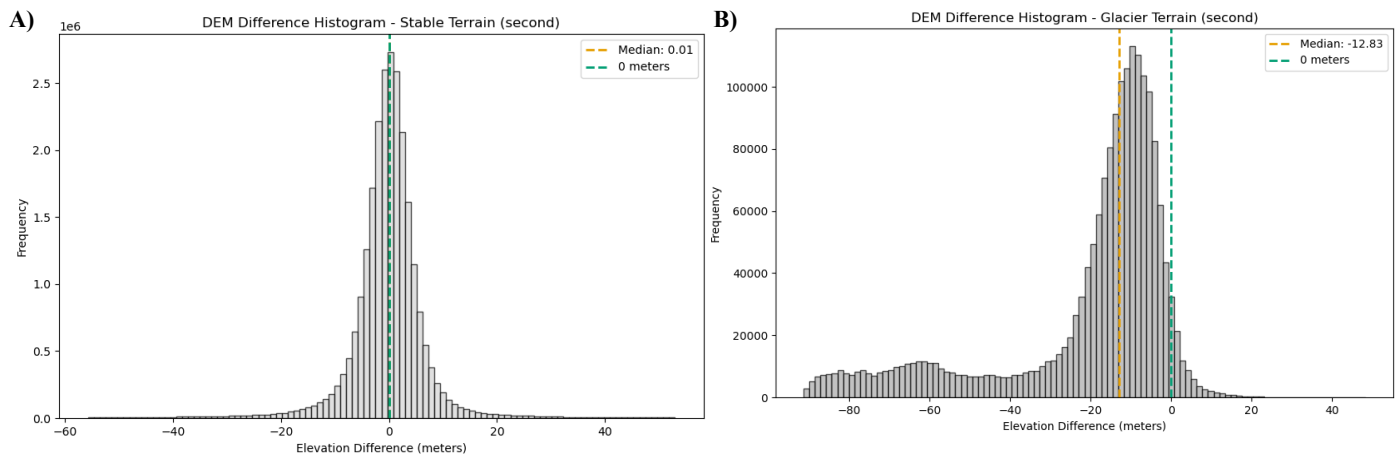

Figure 3126: A) Code output of stable terrain hypsometry calculated from the dDEM for the Mittelaletschgletscher, The graph includes median and a dashed 0-metre line with dynamically generated axis labelling. The x-axis shows the elevation difference in metres, whi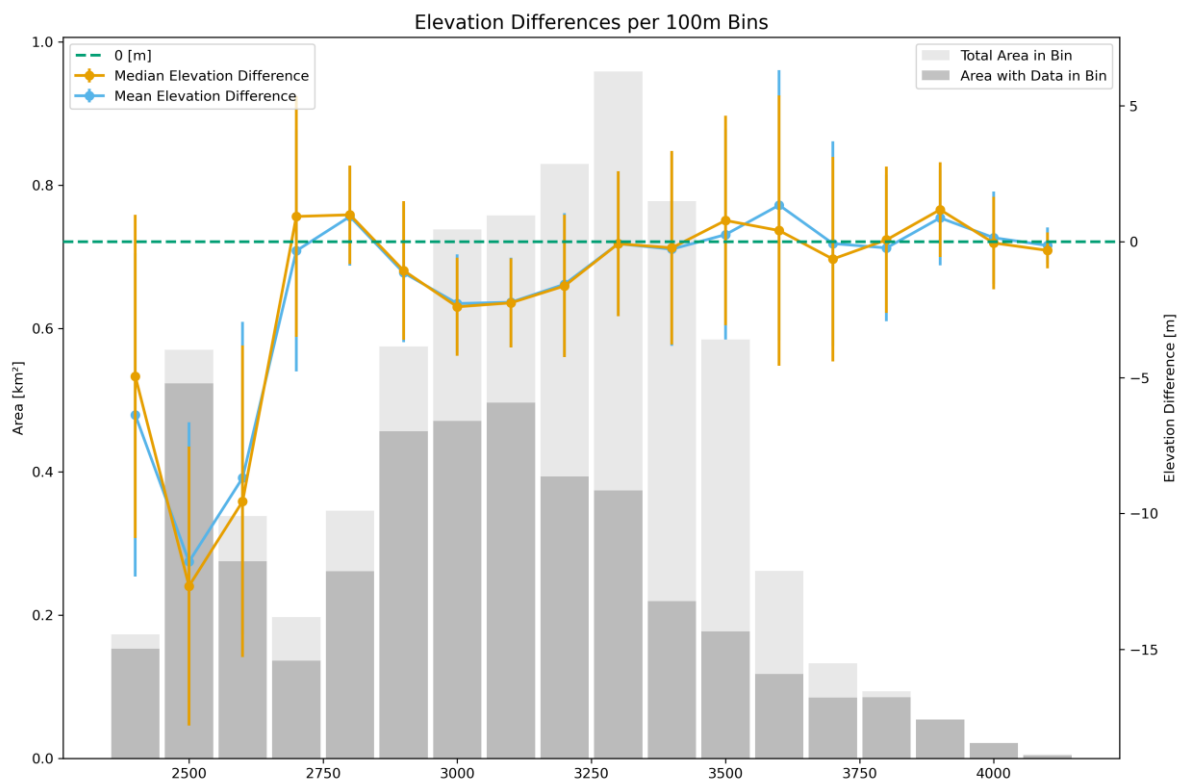lst the y-axis shows the pixel frequency. **B) Code output of glacier terrain hypsometry calculated from the dDEM for the Mittelaletschgletscher.** *The graph includes median and a dashed 0-metre line with dynamically generated axis labelling. The x-axis shows the elevation difference in metres, whilst the y-axis shows the frequency.*

Figure 32: Elevation difference hypsometry plot showing the glacier area in bins for each 100-metre height band of the Mittelaletschgletscher. The x-axis shows the metres above sea level. The first y-axis shows the area each hypsometric bin contains. The bins are separated into light grey for the total area available in that bin, the dark grey shows the area with valid data in that bin. The second y-axis shows the elevation difference calculated in each bin that can be seen as points with one standard deviation whiskers. The elevation difference is displayed for both the median and the mean elevation difference calculated in each bin with a dashed line indicating an elevation difference of zero.

Spring Series – Mittelaletschgletscher - 31.03.2021 – 11.04.2024
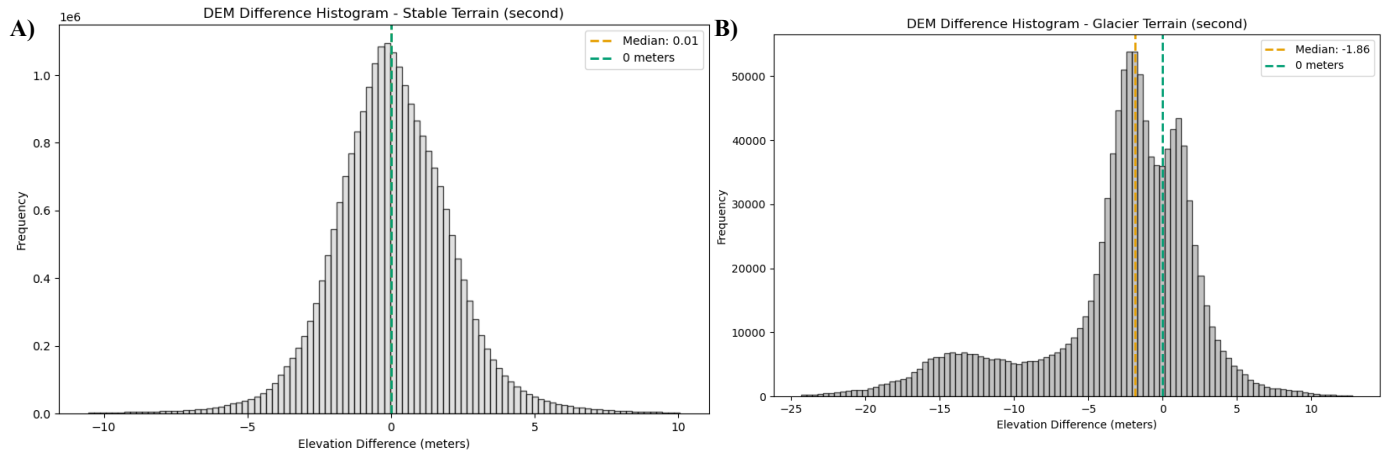

A)

B)

Figure 33: A) Code output of stable terrain hypsometry calculated from the dDEM for the Mittelaletschgletscher. Including median and a dashed 0-metre line with dynamically generated axis labelling. The x-axis shows the elevation difference in metres, whilst the y-axis shows the pixel frequency. B) Code output of glacier terrain hypsometry calculated from the dDEM for the Mittelaletschgletscher. Including median and a dashed 0-metre line with dynamically generated axis labelling. The x-axis shows the elevation difference in metres, whilst the y-axis shows the frequency.
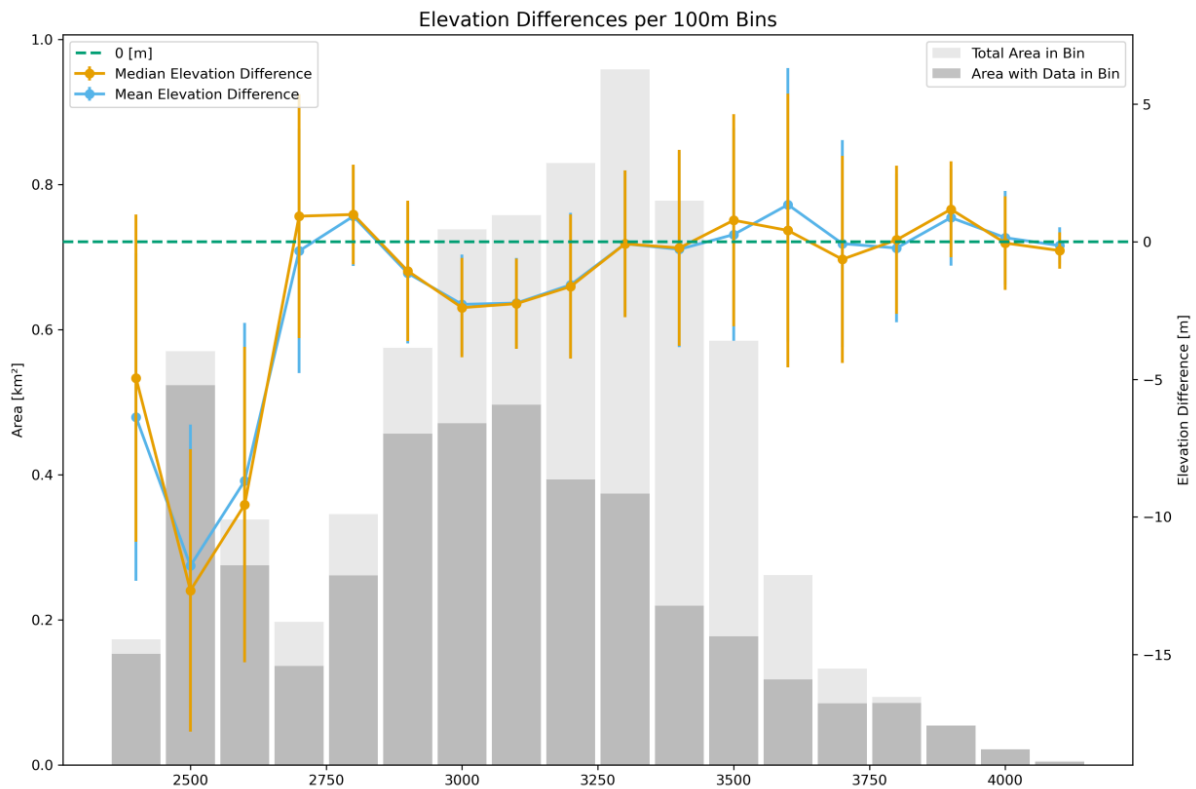

Figure 34: Elevation difference hypsometry plot showing the glacier area in bins for each 100-metre height band of the Mittelaletschgletscher. The x-axis shows the metres above sea level. The first y-axis shows the area each hypsometric bin contains. The bins are separated into light grey for the total area available in that bin, the dark grey shows the area with valid data in that bin. The second y-axis shows the elevation difference calculated in each bin that can be seen as points with one standard deviation whiskers. The elevation difference is displayed for both the median and the mean elevation difference calculated in each bin with a dashed line indicating an elevation difference of zero.
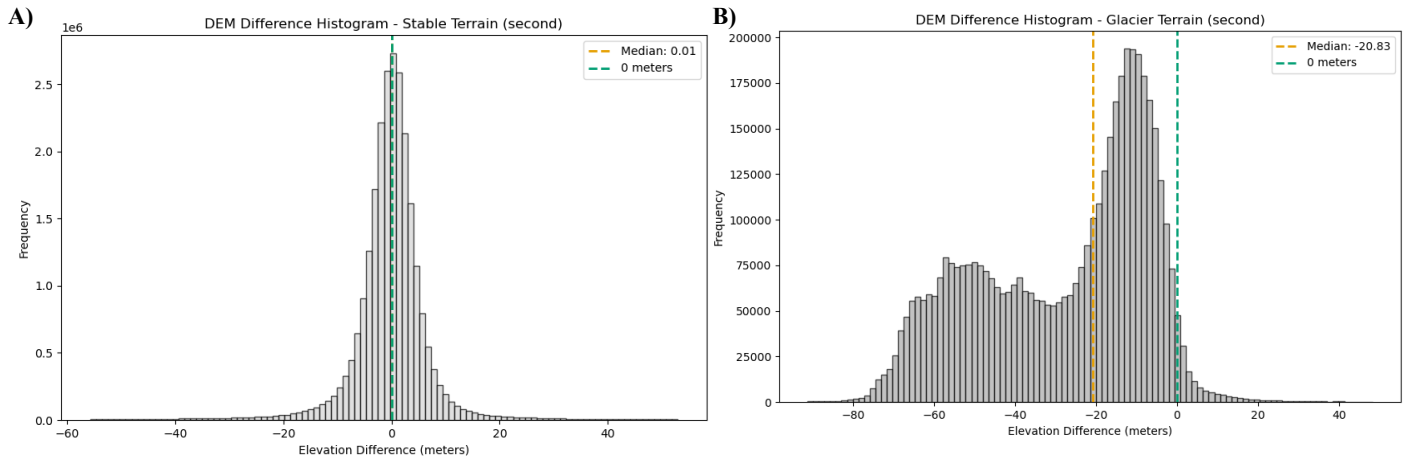
A)

B)

Figure 35: A) Code output of stable terrain hypsometry calculated from the dDEM for the Oberaletschgletscher. Including median and a dashed 0-metre line with dynamically generated axis labelling. The x-axis shows the elevation difference in metres, whilst the y-axis shows the pixel frequency. B) Code output of glacier terrain hypsometry calculated from the dDEM for the Oberaletschgletscher. Including median and a dashed 0-metre line with dynamically generated axis labelling. The x-axis shows the elevation difference in metres, whilst the y-axis shows the frequency.
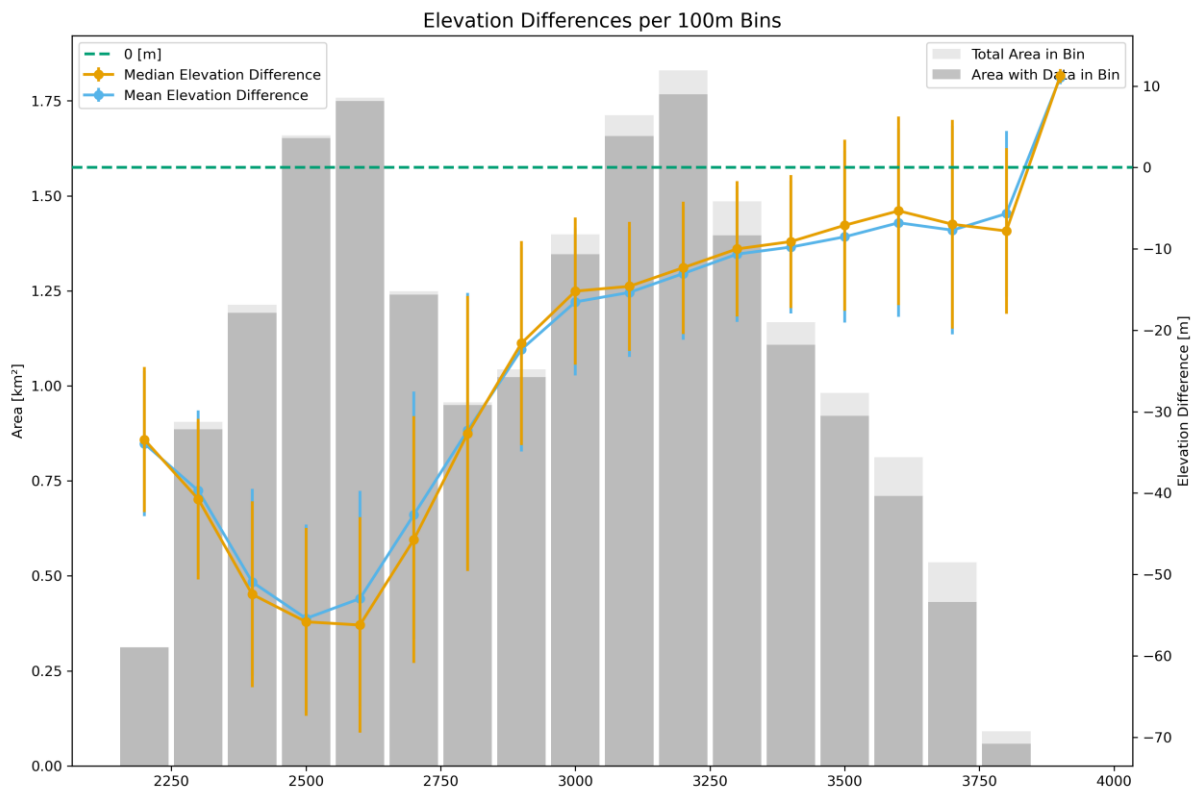

Figure 36: Elevation difference hypsometry plot showing the glacier area in bins for each 100-metre height band of the Oberaletschgletscher. The x-axis shows the metres above sea level. The first y-axis shows the area each hypsometric bin contains. The bins are separated into light grey for the total area available in that bin, the dark grey shows the area with valid data in that bin. The second y-axis shows the elevation difference calculated in each bin that can be seen as points with one standard deviation whiskers. The elevation difference is displayed for both the median and the mean elevation difference calculated in each bin with a dashed line indicating an elevation difference of zero.

Spring Series - Oberaletschgletscher - 31.03.2021 – 11.04.2024
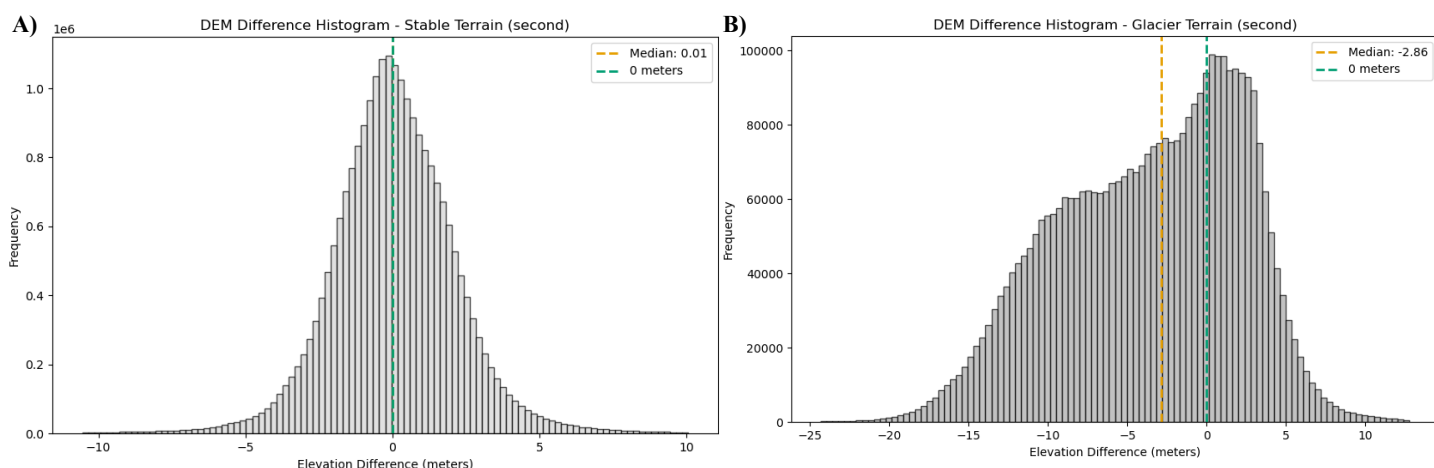
A)

B)

Figure 37: A) Code output of stable terrain hypsometry calculated from the dDEM for the Oberaletschgletscher. Including median and a dashed 0-metre line with dynamically generated axis labelling. The x-axis shows the elevation difference in metres, whilst the y-axis shows the pixel frequency. B) Code output of glacier terrain hypsometry calculated from the dDEM for the Oberaletschgletscher. Including median and a dashed 0-metre line with dynamically generated axis labelling. The x-axis shows the elevation difference in metres, whilst the y-axis shows the frequency.
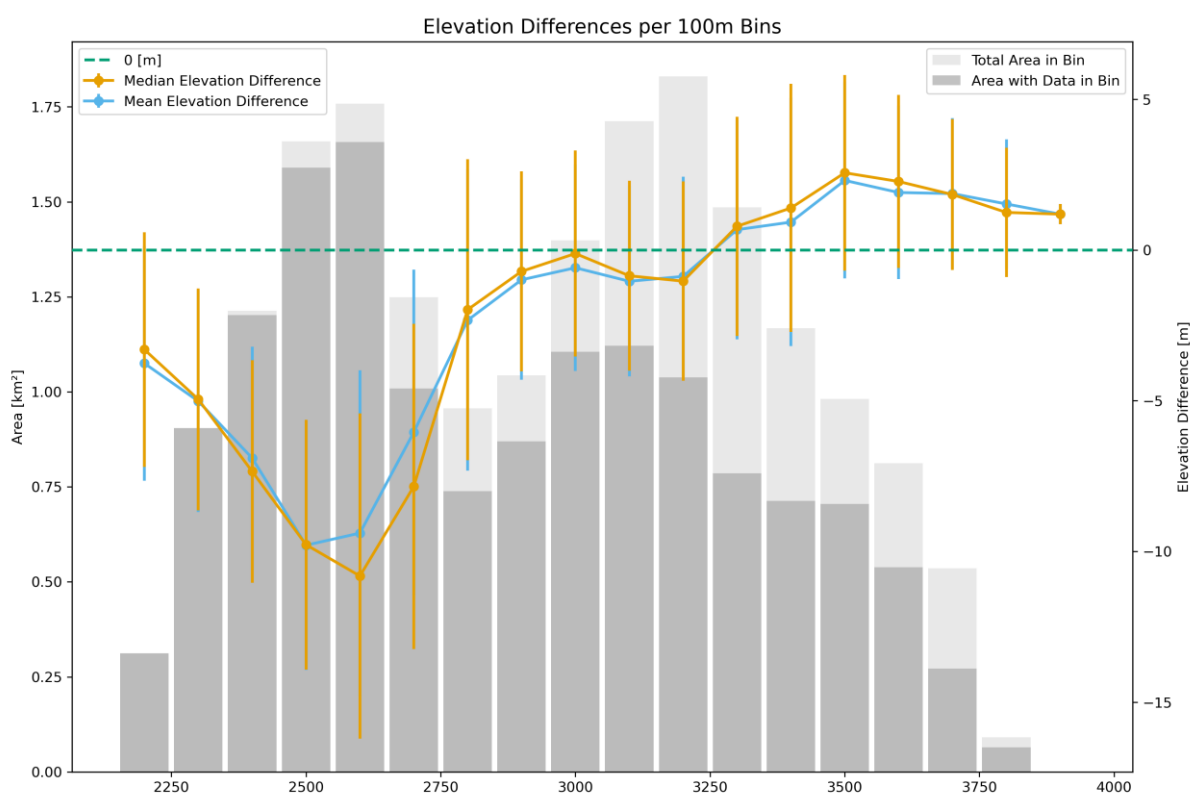

Figure 38: Elevation difference hypsometry plot showing the glacier area in bins for each 100-metre height band of the Oberaletschgletscher. The x-axis shows the metres above sea level. The first y-axis shows the area each hypsometric bin contains. The bins are separated into light grey for the total area available in that bin, the dark grey shows the area with valid data in that bin. The second y-axis shows the elevation difference calculated in each bin that can be seen as points with one standard deviation whiskers. The elevation difference is displayed for both the median and the mean elevation difference calculated in each bin with a dashed line indicating an elevation difference of zero.

Fall Series - Grosser Aletschgletscher - 24.09.2003 – 10.08.2021
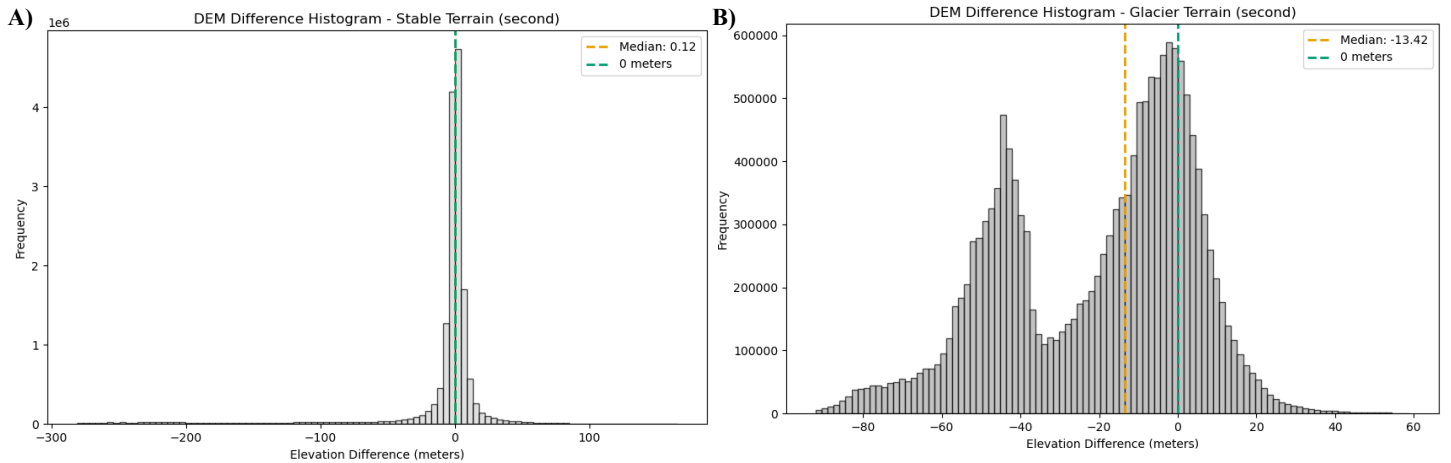
A)

B)

*Figure 39: Code output of stable terrain hypsometry calculated from the dDEM for the Grosser Aletschgletscher. Including median and a dashed 0-metre line with dynamically generated axis labelling. The x-axis shows the elevation difference in metres, whilst the y-axis shows the pixel frequency. **B) Code output of glacier terrain hypsometry calculated from the dDEM for the Grosser Aletschgletscher.** Including median and a dashed 0-metre line with dynamically generated axis labelling. The x-axis shows the elevation difference in metres, whilst the y-axis shows the frequency.*
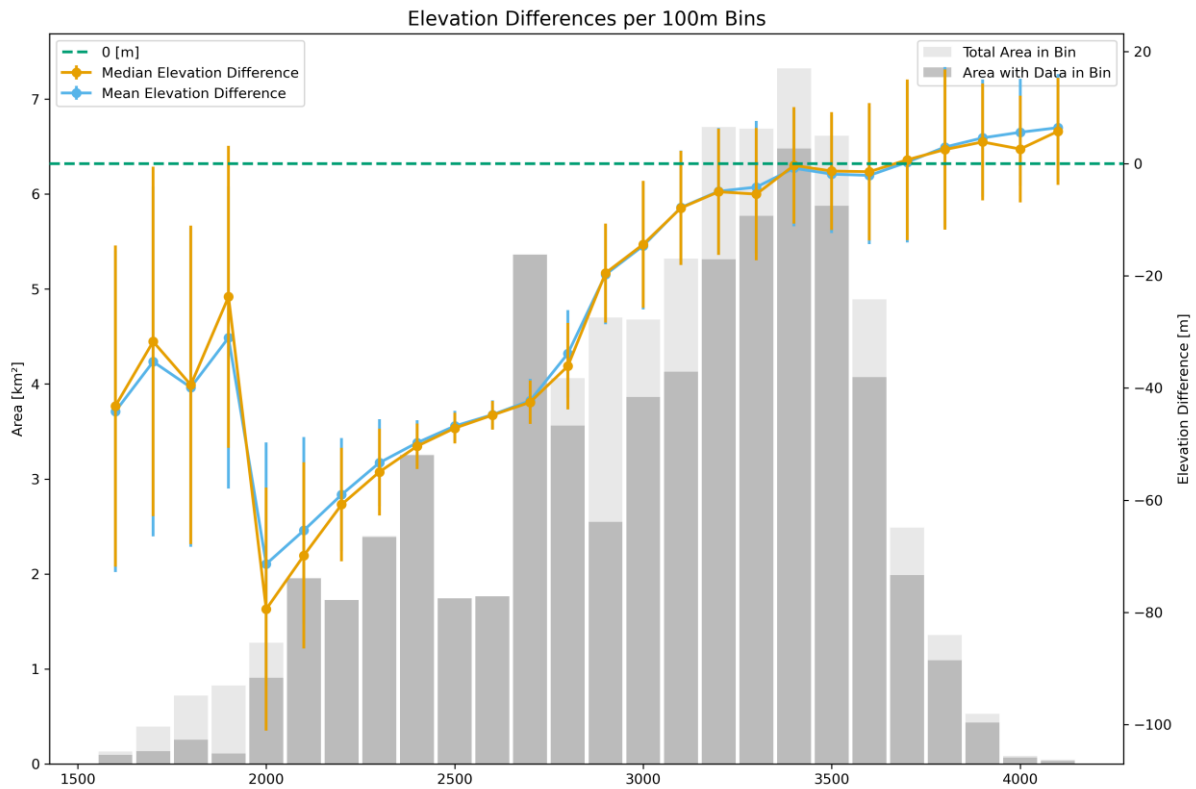

Figure 40: Elevation difference hypsometry plot showing the glacier area in bins for each 100-metre height band of the Grosser Aletschgletscher. The x-axis shows the metres above sea level. The first y-axis shows the area each hypsometric bin contains. The bins are separated into light grey for the total area available in that bin, the dark grey shows the area with valid data in that bin. The second y-axis shows the elevation difference calculated in each bin that can be seen as points with one standard deviation whiskers. The elevation difference is displayed for both the median and the mean elevation difference calculated in each bin with a dashed line indicating an elevation difference of zero.

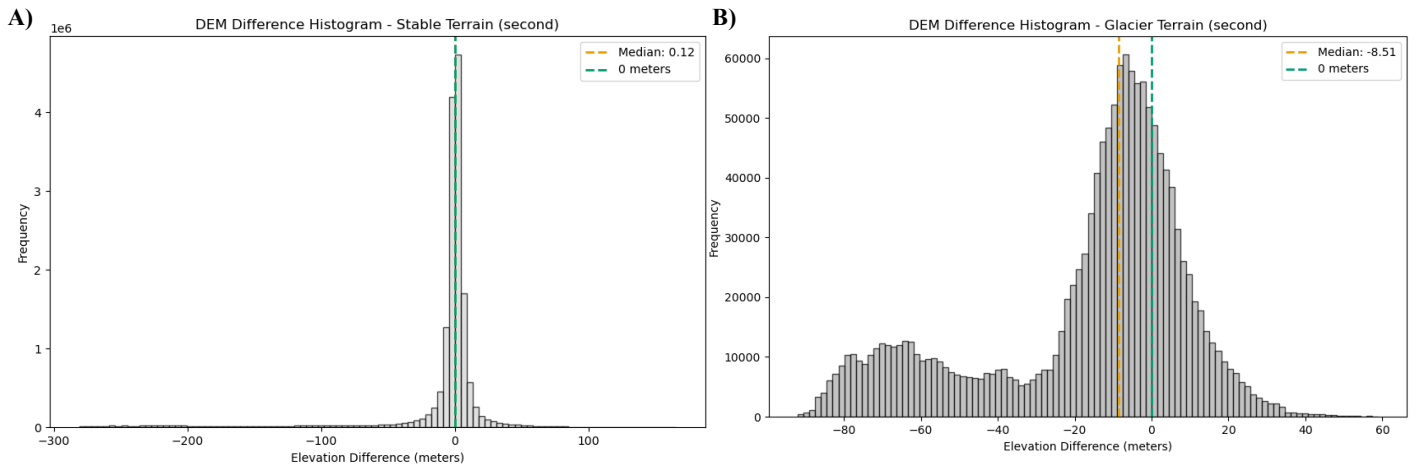**Fall Series - Mittelaletschgletscher - 24.09.2003 – 10.08.2021**

A)

B)

Figure 41: A) Code output of stable terrain hypsometry calculated from the dDEM for the Mittelaletschgletscher. Including median and a dashed 0-metre line with dynamically generated axis labelling. The x-axis shows the elevation difference in metres, whilst the y-axis shows the pixel frequency. B) Code output of glacier terrain hypsometry calculated from the dDEM for the Mittelaletschgletscher. Including median and a dashed 0-metre line with dynamically generated axis labelling. The x-axis shows the elevation difference in metres, whilst the y-axis shows the frequency.
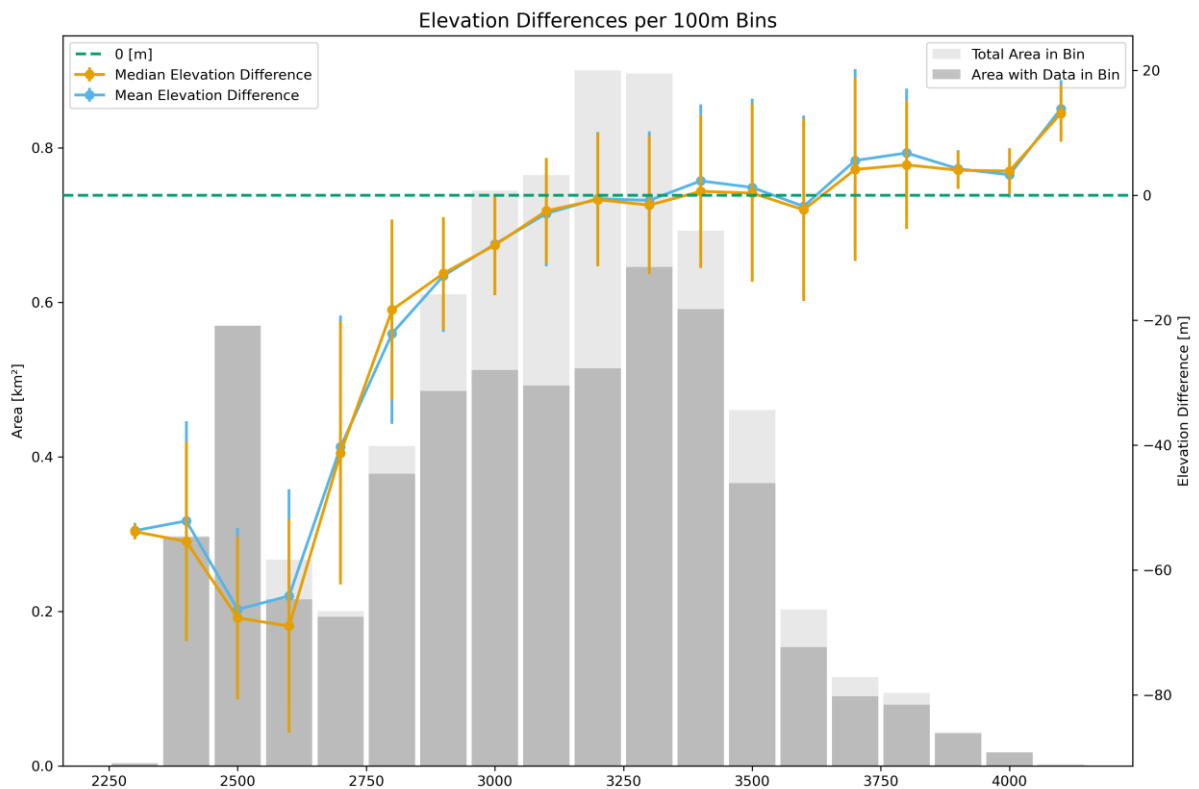

Figure 42: Elevation difference hypsometry plot showing the glacier area in bins for each 100-metre height band of the Mittelaletschgletscher. The x-axis shows the metres above sea level. The first y-axis shows the area each hypsometric bin contains. The bins are separated into light grey for the total area available in that bin, the dark grey shows the area with valid data in that bin. The second y-axis shows the elevation difference calculated in each bin that can be seen as points with one standard deviation whiskers. The elevation difference is displayed for both the median and the mean elevation difference calculated in each bin with a dashed line indicating an elevation difference of zero.
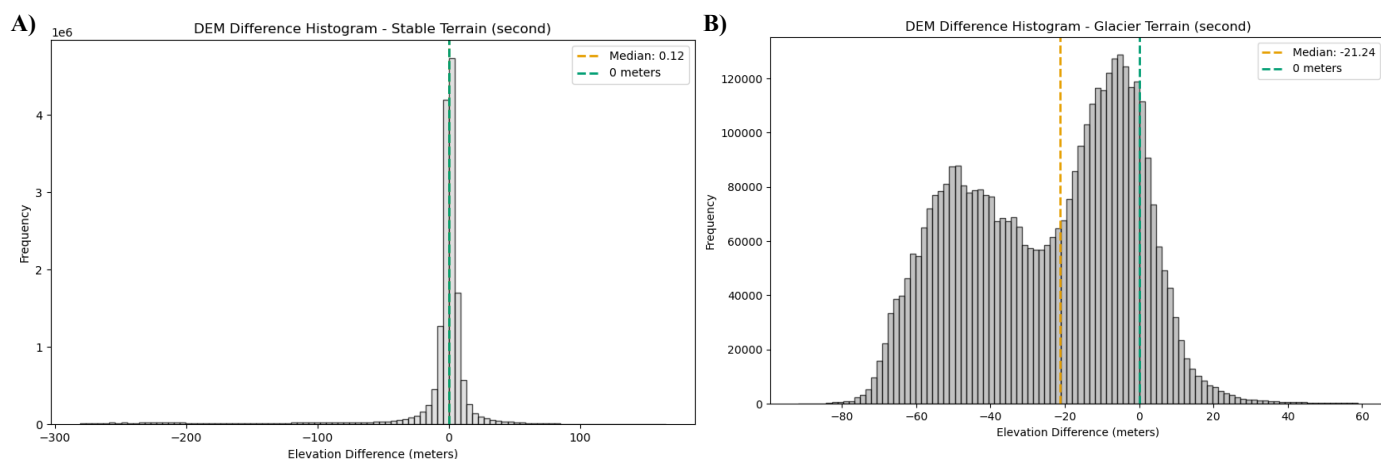
A)

B)

Figure 43: A) Code output of stable terrain hypsometry calculated from the dDEM for the Oberaletschgletscher. Including median and a dashed 0-metre line with dynamically generated axis labelling. The x-axis shows the elevation difference in metres, whilst the y-axis shows the pixel frequency. B) Code output of glacier terrain hypsometry calculated from the dDEM for the Oberaletschgletscher, including median and a dashed 0-metre line with dynamically generated axis labelling. The x-axis shows the elevation difference in metres, whilst the y-axis shows the frequency.
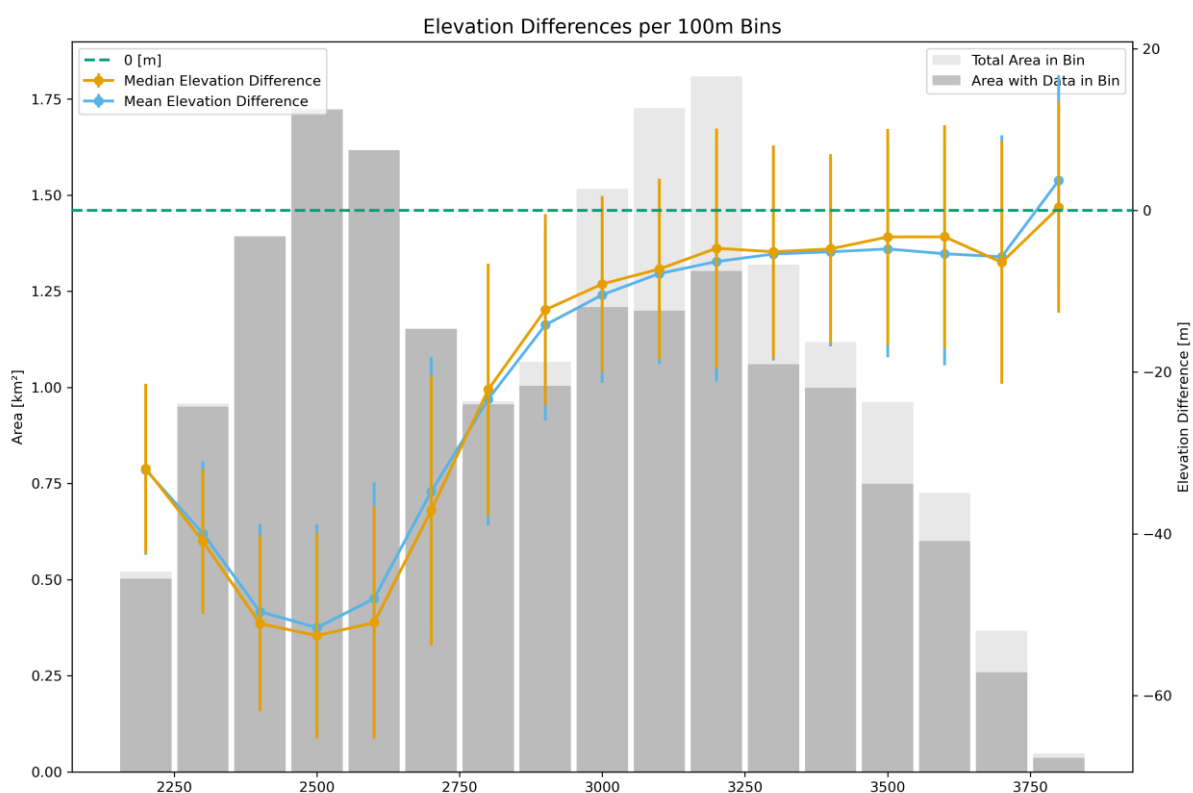
Figure 44: Elevation difference hypsometry plot showing the glacier area in bins for each 100-metre height band of the Oberaletschgletscher. The x-axis shows the metres above sea level. The first y-axis shows the area each hypsometric bin contains. The bins are separated into light grey for the total area available in that bin, the dark grey shows the area with valid data in that bin. The second y-axis shows the elevation difference calculated in each bin that can be seen as points with one standard deviation whiskers. The elevation difference is displayed for both the median and the mean elevation difference calculated in each bin with a dashed line indicating an elevation difference of zero.

A)

B)

Figure 45: A) Code output of stable terrain hypsometry calculated from the dDEM for the Grosser Aletschgletscher, including median and a dashed 0-metre line with dynamically generated axis labelling. The x-axis shows the elevation difference in metres, whilst the y-axis shows the pixel frequency. B) Code output of glacier terrain hypsometry calculated from the dDEM for the Grosser Aletschgletscher, including median and a dashed 0-metre line with dynamically generated axis labelling. The x-axis shows the elevation difference in metres, whilst the y-axis shows the frequency.

Figure 46: Elevation difference hypsometry plot showing the glacier area in bins for each 100-metre height band of the Grosser Aletschgletscher. The x-axis shows the metres above sea level. The first y-axis shows the area each hypsometric bin contains. The bins are separated into light grey for the total area available in that bin, the dark grey shows the area with valid data in that bin. The second y-axis shows the elevation difference calculated in each bin that can be seen as points with one standard deviation whiskers. The elevation difference is displayed for both the median and the mean elevation difference calculated in each bin with a dashed line indicating an elevation difference of zero.

2003-2007 Series - Grosser Aletschgletscher - 01.02.2004 – 04.01.2005
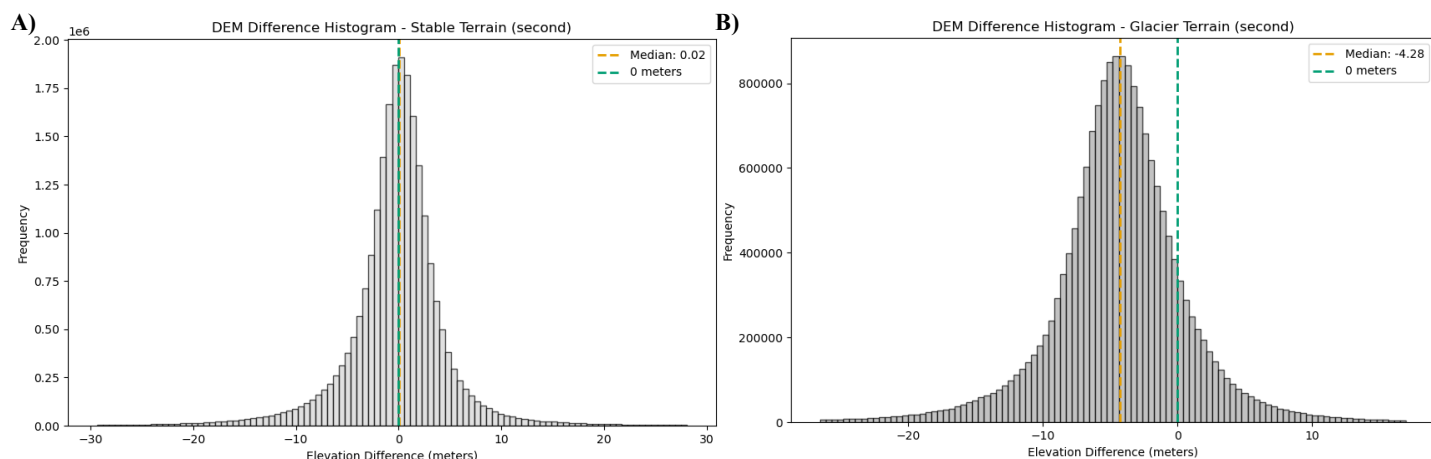
A)

B)

Figure 47: A) Code output of stable terrain hypsometry calculated from the dDEM for the Grosser Aletschgletscher, including median and a dashed 0-metre line with dynamically generated axis labelling. The x-axis shows the elevation difference in metres, whilst the y-axis shows the pixel frequency. B) Code output of glacier terrain hypsometry calculated from the dDEM for the Grosser Aletschgletscher, including median and a dashed 0-metre line with dynamically generated axis labelling. The x-axis shows the elevation difference in metres, whilst the y-axis shows the frequency.
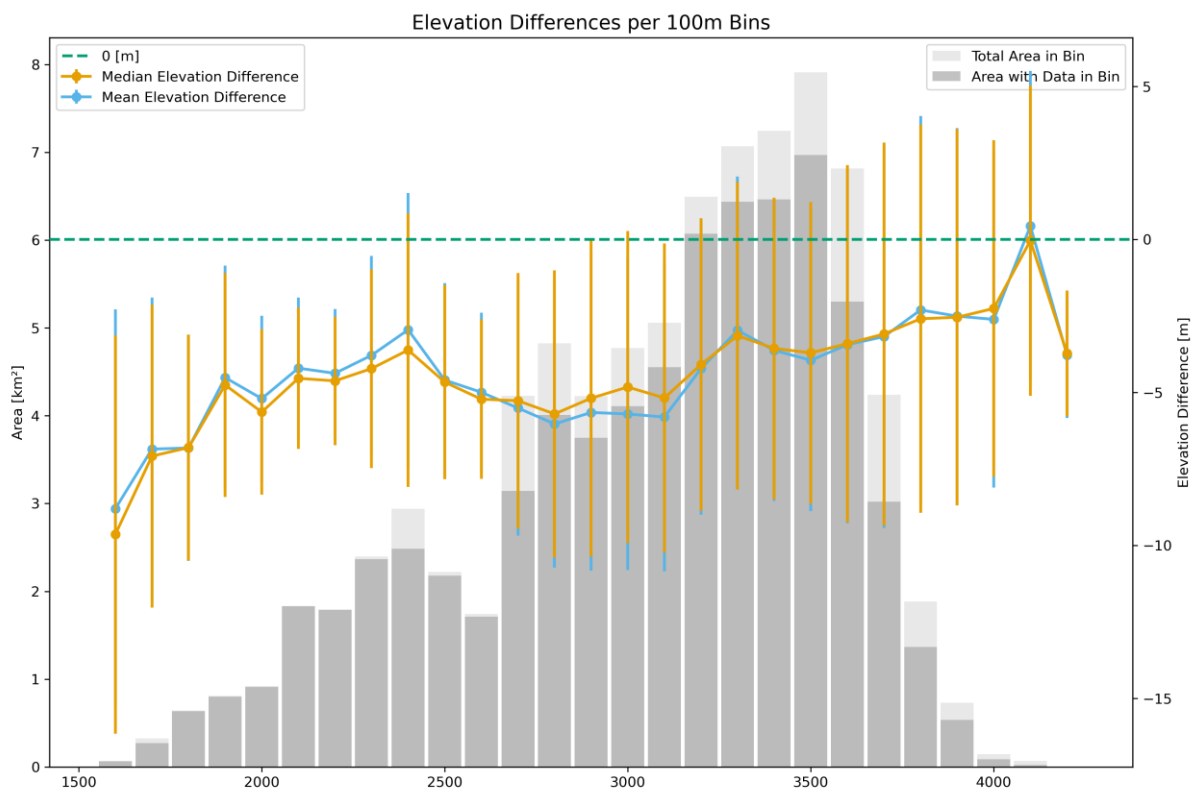

Figure 48: Elevation difference hypsometry plot showing the glacier area in bins for each 100-metre height band of the Grosser Aletschgletscher. The x-axis shows the metres above sea level. The first y-axis shows the area each hypsometric bin contains. The bins are separated into light grey for the total area available in that bin, the dark grey shows the area with valid data in that bin. The second y-axis shows the elevation difference calculated in each bin that can be seen as points with one standard deviation whiskers. The elevation difference is displayed for both the median and the mean elevation difference calculated in each bin with a dashed line indicating an elevation difference of zero.

61

2003-2007 Series - Grosser Aletschgletscher - 04.01.2005 – 28.01.2007
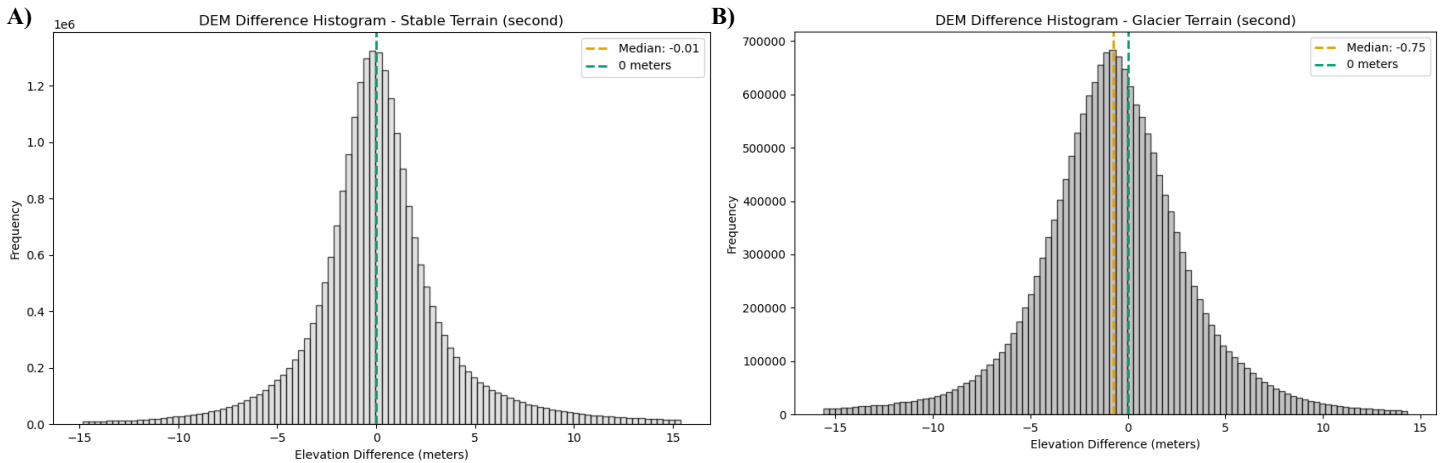
A)

B)

Figure 49: A) Code output of stable terrain hypsometry calculated from the dDEM for the Grosser Aletschgletscher, including median and a dashed 0-metre line with dynamically generated axis labelling. The x-axis shows the elevation difference in metres, whilst the y-axis shows the pixel frequency. B) Code output of glacier terrain hypsometry calculated from the dDEM for the Grosser Aletschgletscher, including median and a dashed 0-metre line with dynamically generated axis labelling. The x-axis shows the elevation difference in metres, whilst the y-axis shows the frequency.
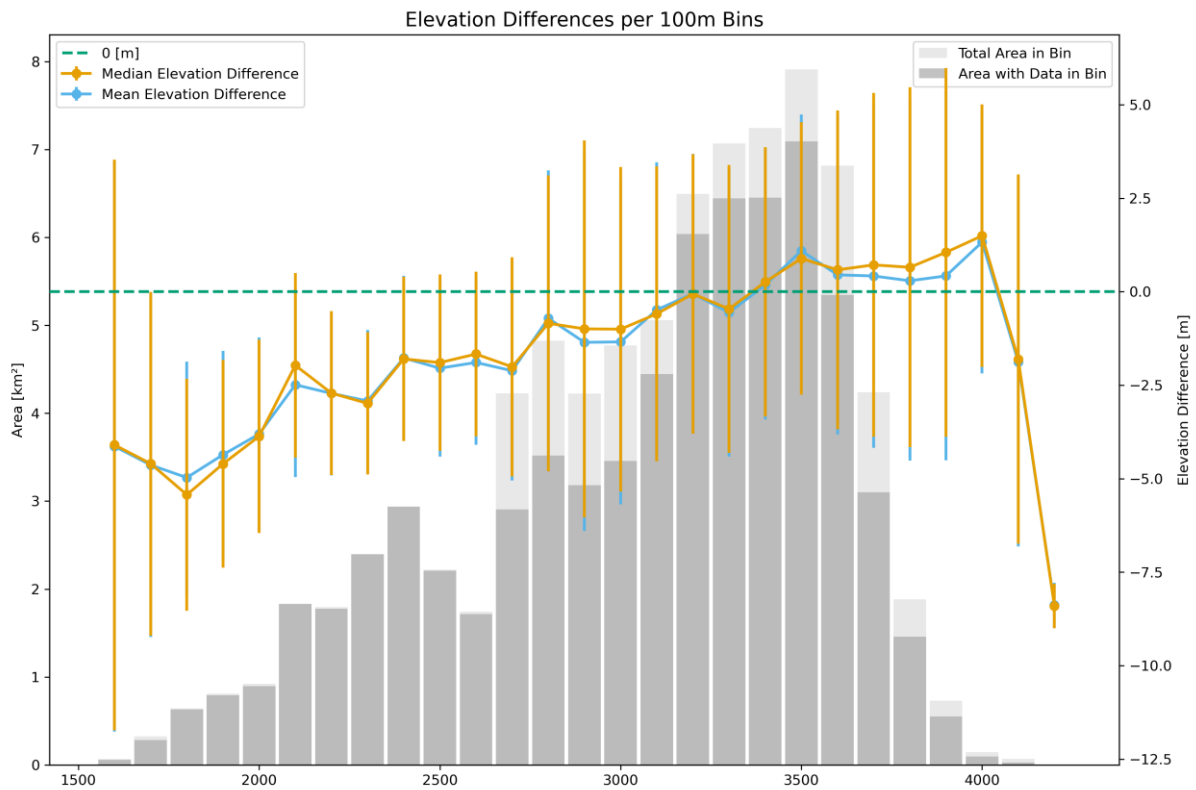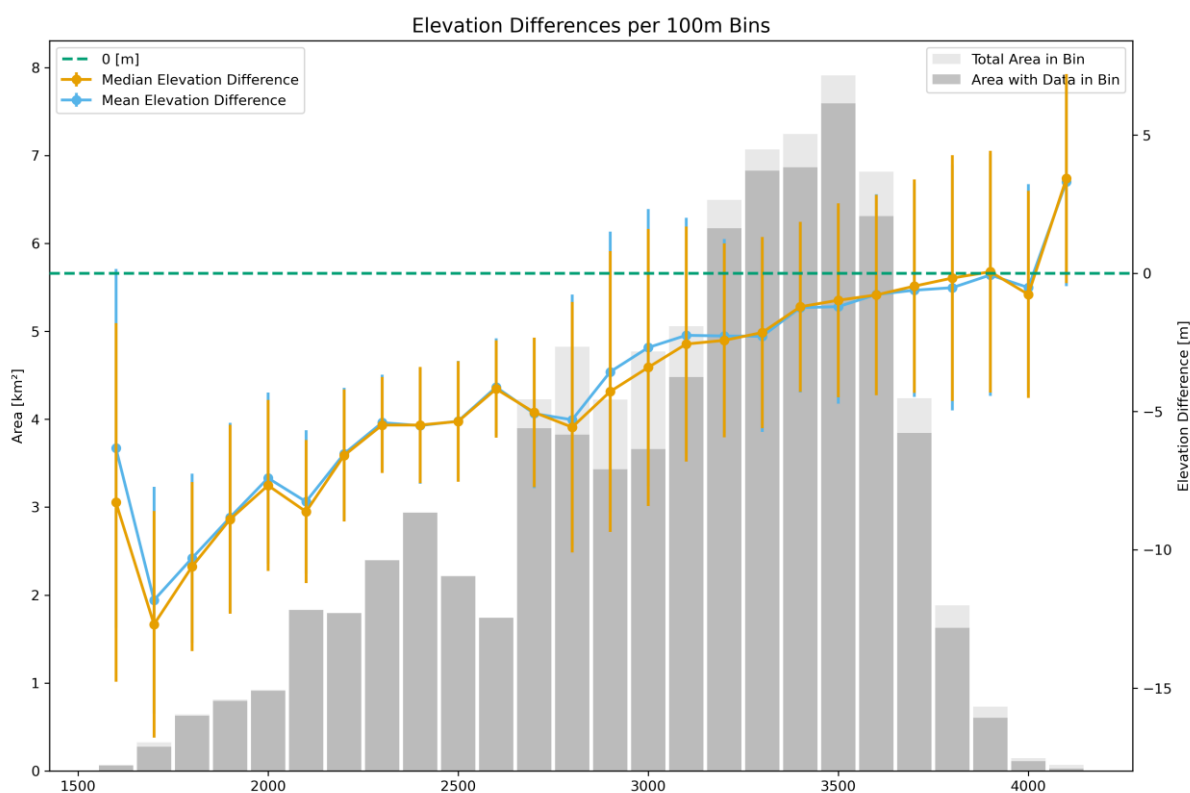

Figure 50: Elevation difference hypsometry plot showing the glacier area in bins for each 100-metre height band of the Grosser Aletschgletscher. The x-axis shows the metres above sea level. The first y-axis shows the area each hypsometric bin contains. The bins are separated into light grey for the total area available in that bin, the dark grey shows the area with valid data in that bin. The second y-axis shows the elevation difference calculated in each bin that can be seen as points with one standard deviation whiskers. The elevation difference is displayed for both the median and the mean elevation difference calculated in each bin with a dashed line indicating an elevation difference of zero.
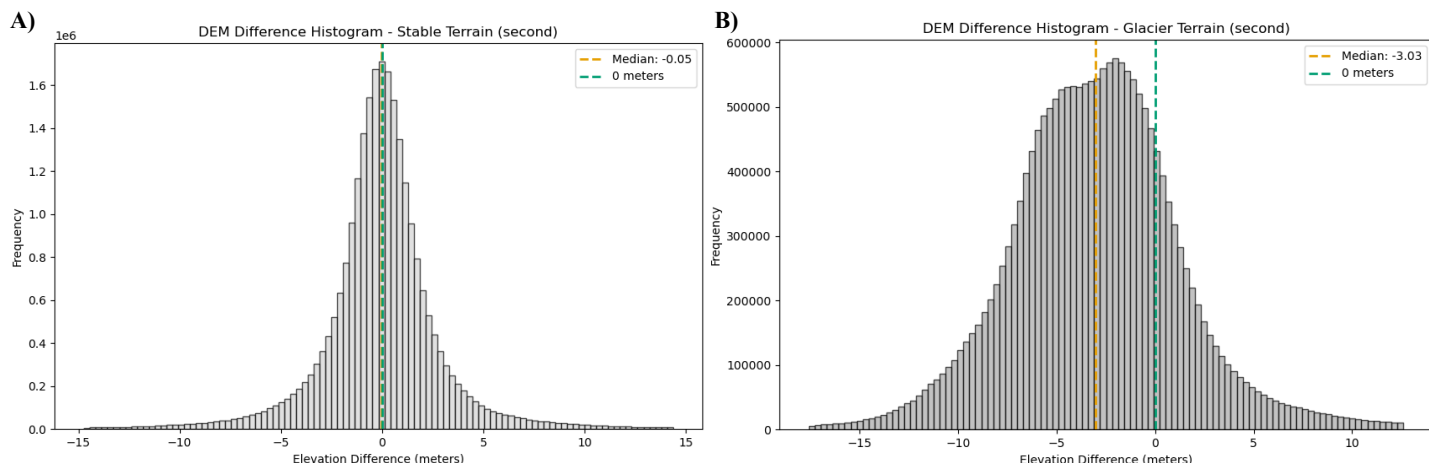
***Figure 51: A) Code output of stable terrain hypsometry calculated from the dDEM for the Mittelaletschgletscher**, including median and a dashed 0-metre line with dynamically generated axis labelling. The x-axis shows the elevation difference in metres, whilst the y-axis shows the pixel frequency. **B) Code output of glacier terrain hypsometry calculated from the dDEM for the Mittelaletschgletscher**, including median and a dashed 0-metre line with dynamically generated axis labelling. The x-axis shows the elevation difference in metres, whilst the y-axis shows the frequency.*

***Figure 52: Elevation difference hypsometry plot showing the glacier area in bins for each 100-metre height band of the Mittelaletschgletscher**. The x-axis shows the metres above sea level. The first y-axis shows the area each hypsometric bin contains. The bins are separated into light grey for the total area available in that bin, the dark grey shows the area with valid data in that bin. The second y-axis shows the elevation difference calculated in each bin that can be seen as points with one standard deviation whiskers. The elevation difference is displayed for both the median and the mean elevation difference calculated in each bin with a dashed line indicating an elevation difference of zero.*

2003-2007 Series – Mittelaletschgletscher - 01.02.2004 – 04.01.2005

A)

B)

Figure 53: A) Code output of stable terrain hypsometry calculated from the dDEM for the Mittelaletschgletscher, *including median and a dashed 0-metre line with dynamically generated axis labelling. The x-axis shows the e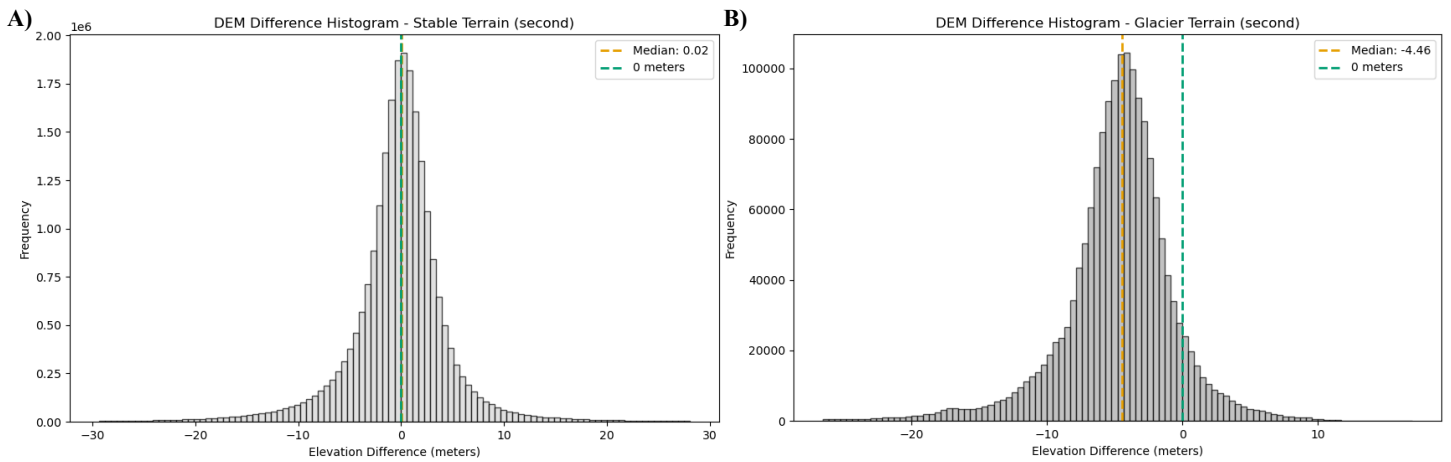levation difference in metres, whilst the y-axis shows the pixel frequency.* ***B) Code output of glacier terrain hypsometry calculated from the dDEM for the Mittelaletschgletscher***, *including median and a dashed 0-metre line with dynamically generated axis labelling. The x-axis shows the elevation difference in metres, whilst the y-axis shows the frequency.*
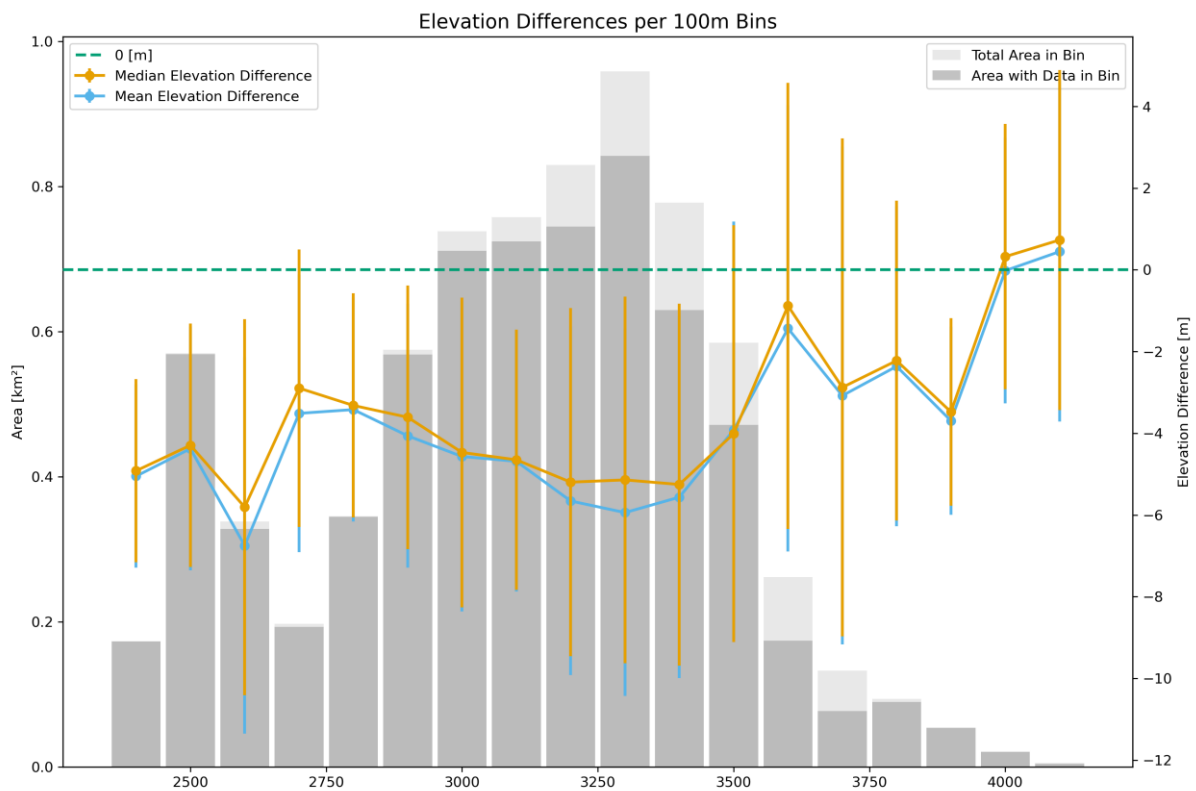

Figure 54: Elevation difference hypsometry plot showing the glacier area in bins for each 100-metre height band of the Mittelaletschgletscher. *The x-axis shows the metres above sea level. The first y-axis shows the area each hypsometric bin contains. The bins are separated into light grey for the total area available in that bin, the dark grey shows the area with valid data in that bin. The second y-axis shows the elevation difference calculated in each bin that can be seen as points with one standard deviation whiskers. The elevation difference is displayed for both the median and the mean elevation difference calculated in each bin with a dashed line indicating an elevation difference of zero.*

A)

B)

Figure 55: A) Code output of stable terrain hypsometry calculated from the dDEM for the Mittelaletschgletscher, including median and a dashed 0-metre line with dynamically generated axis labelling. The x-axis shows the elevation difference in metres, whilst the y-axis shows the pixel frequency. B) Code output of glacier terrain hypsometry calculated from the dDEM for the Mittelaletschgletscher, including median and a dashed 0-metre line with dynamically generated axis labelling. The x-axis shows the elevation difference in metres, whilst the y-axis shows the frequency.

Figure 56: Elevation difference hypsometry plot showing the glacier area in bins for each 100-metre height band of the Mittelaletschgletscher. The x-axis shows the metres above sea level. The first y-axis shows the area each hypsometric bin contains. The bins are separated into light grey for the total area available in that bin, the dark grey shows the area with valid data in that bin. The second y-axis shows the elevation difference calculated in each bin that can be seen as points with one standard deviation whiskers. The elevation difference is displayed for both the median and the mean elevation difference calculated in each bin with a dashed line indicating an elevation difference of zero.

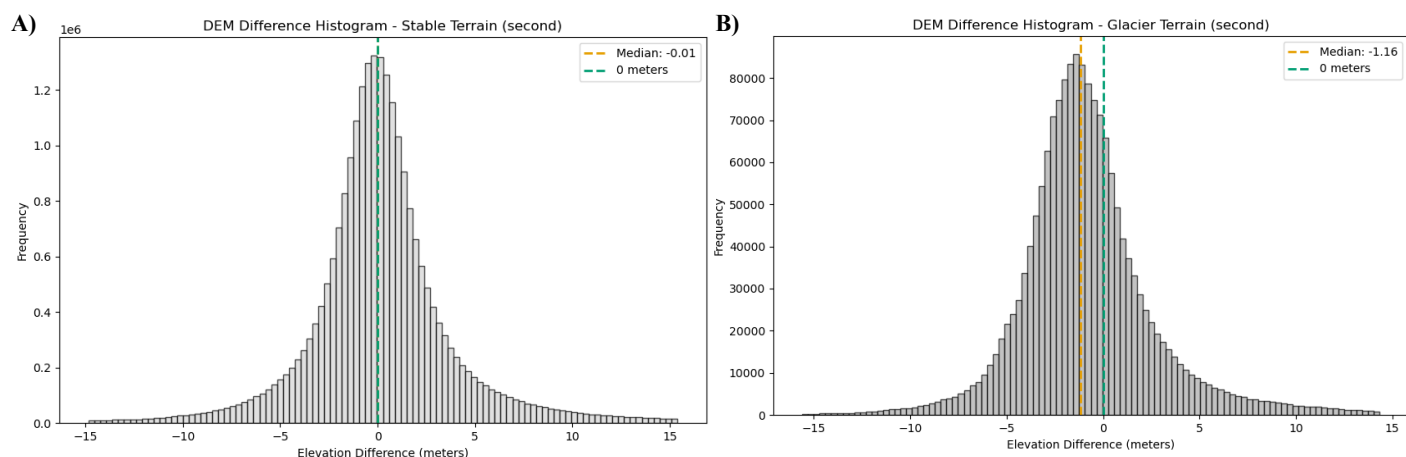**2003-2007 Series - Oberaletschgletscher - 26.03.2003 – 01.02.2004**

Figure 57: A) Code output of stable terrain hypsometry calculated from the dDEM for the Oberaletschgletscher, including median and a dashed 0-metre line with dynamically generated axis labelling. The x-axis shows the elevation difference in metres, whilst the y-axis shows the pixel frequency. B) Code output of glacier terrain hypsometry calculated from the dDEM for the Oberaletschgletscher, including median and a dashed 0-metre line with dynamically generated axis labelling. The x-axis shows the elevation difference in metres, whilst the y-axis shows the frequency.
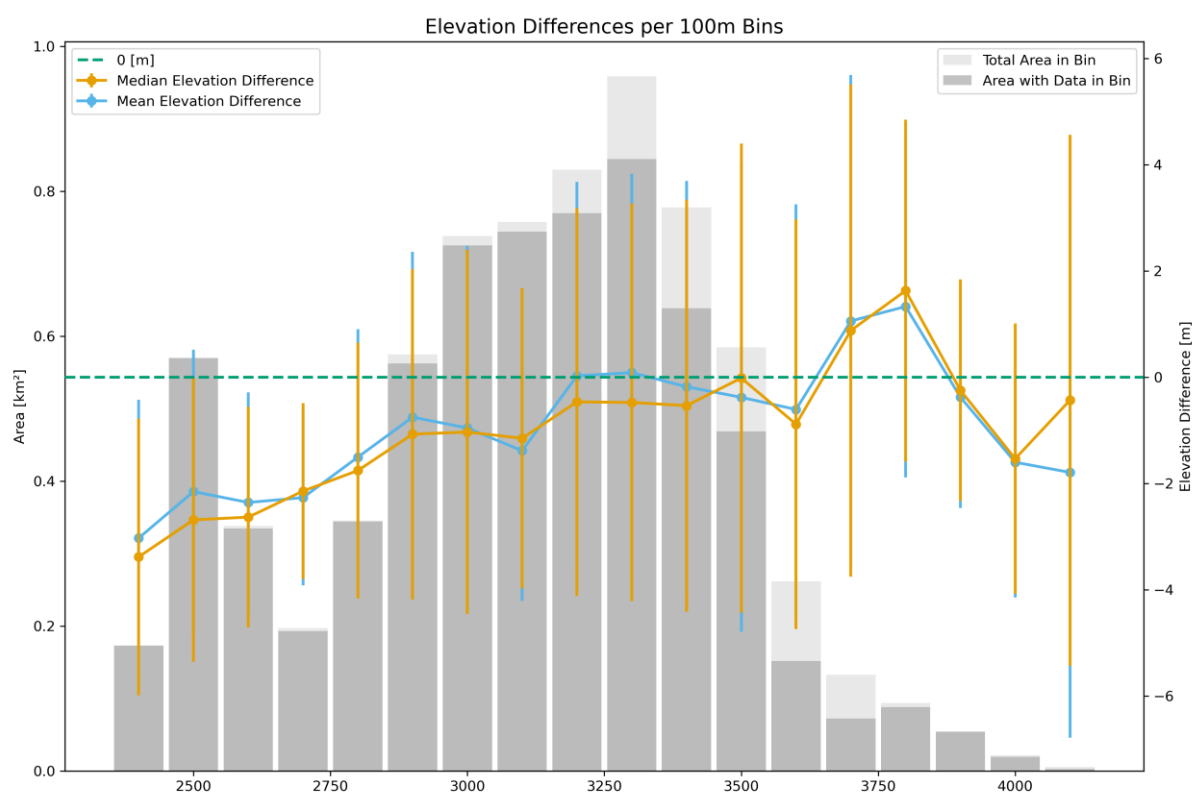

Figure 58: Elevation difference hypsometry plot showing the glacier area in bins for each 100-metre height band of the Oberaletschgletscher. The x-axis shows the metres above sea level. The first y-axis shows the area each hypsometric bin contains. The bins are separated into light grey for the total area available in that bin, the dark grey shows the area with valid data in that bin. The second y-axis shows the elevation difference calculated in each bin that can be seen as points with one standard deviation whiskers. The elevation difference is displayed for both the median and the mean elevation difference calculated in each bin with a dashed line indicating an elevation difference of zero.

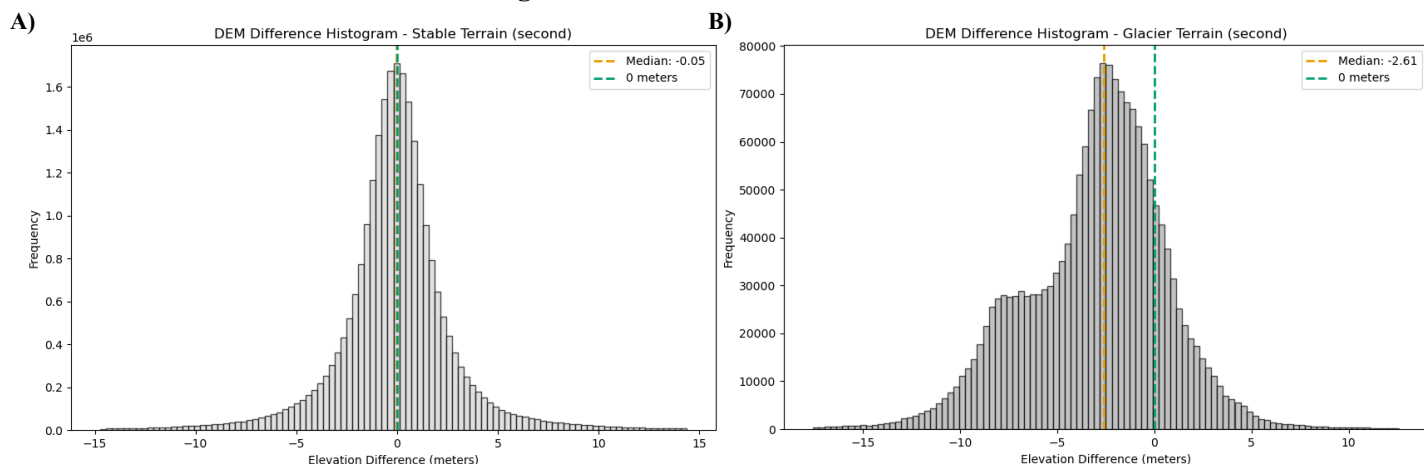**2003-2007 Series - Oberaletschgletscher - 01.02.2004 – 04.01.2005**

A)

B)

Figure 59: A) Code output of stable terrain hypsometry calculated from the dDEM for the Oberaletschgletscher, including median and a dashed 0-metre line with dynamically generated axis labelling. The x-axis shows the elevation difference in metres, whilst the y-axis shows the pixel frequency. B) Code output of glacier terrain hypsometry calculated from the dDEM for the Oberaletschgletscher, including median and a dashed 0-metre line with dynamically generated axis labelling. The x-axis shows the elevation difference in metres, whilst the y-axis shows the frequency.
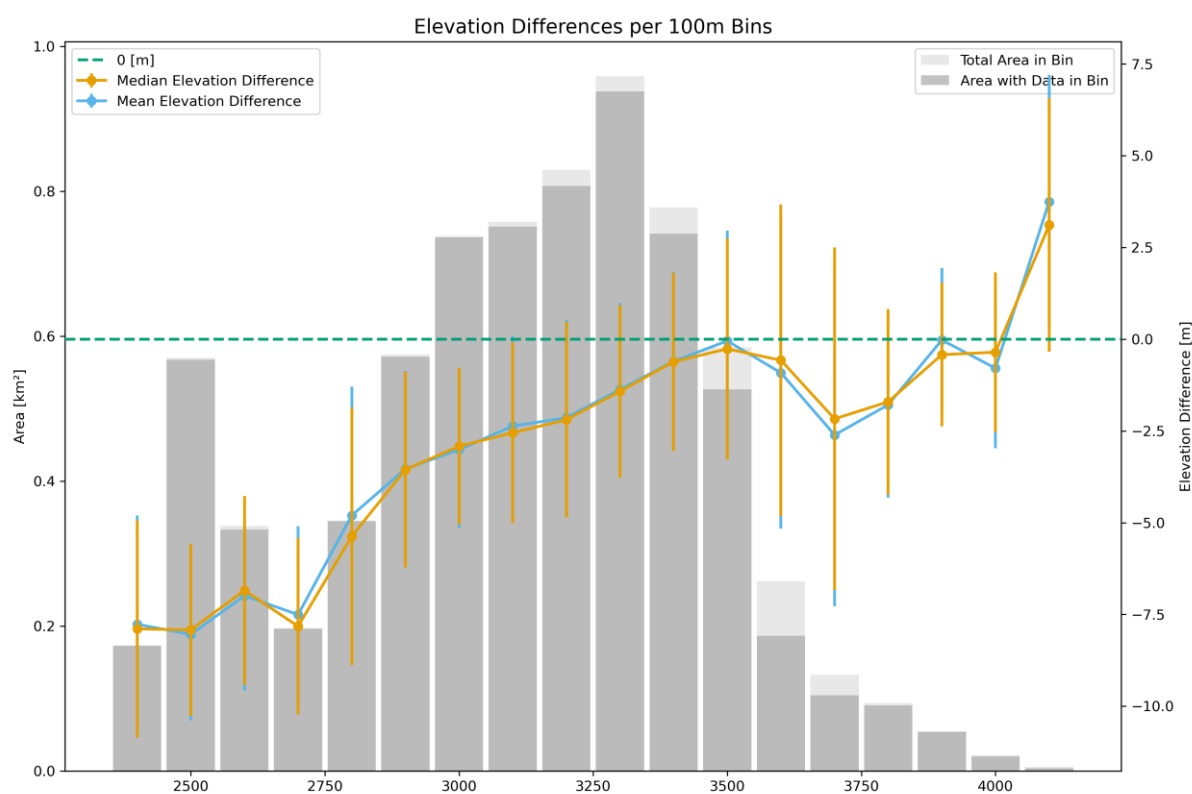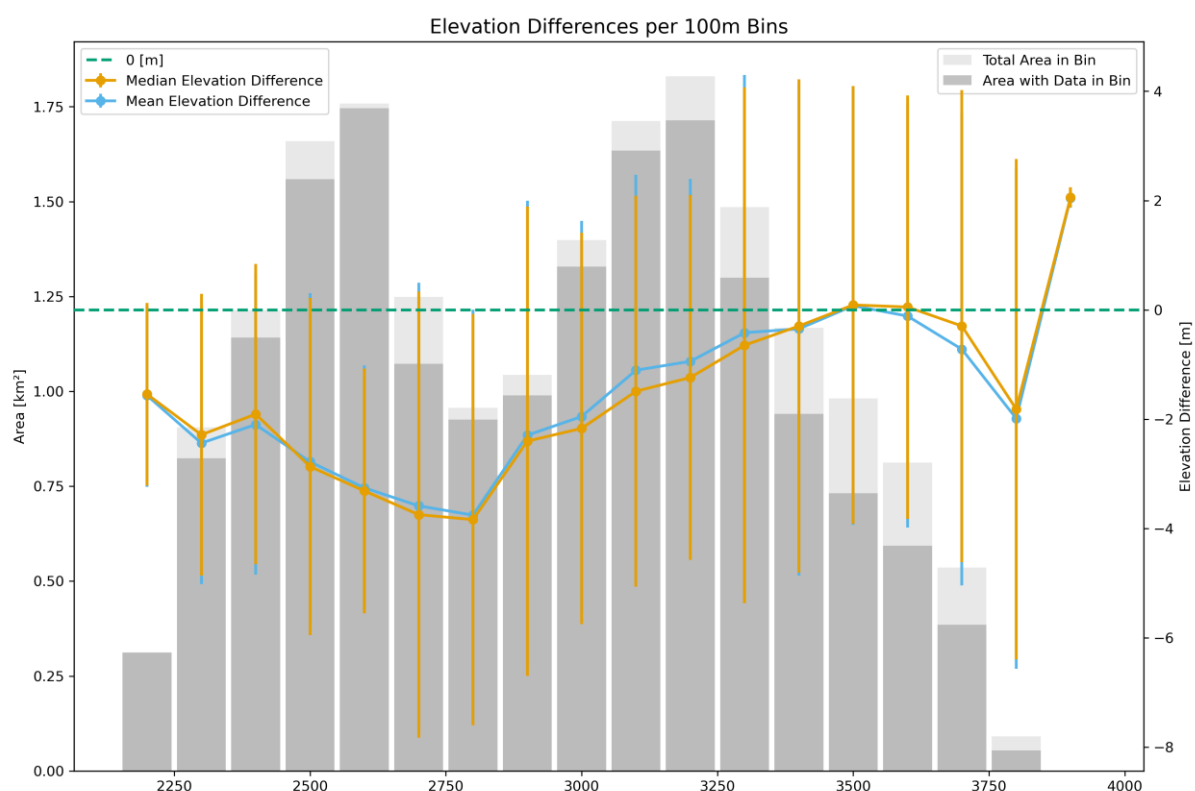

Figure 60: Elevation difference hypsometry plot showing the glacier area in bins for each 100-metre height band of the Oberaletschgletscher. The x-axis shows the metres above sea level. The first y-axis shows the area each hypsometric bin contains. The bins are separated into light grey for the total area available in that bin, the dark grey shows the area with valid data in that bin. The second y-axis shows the elevation difference calculated in each bin that can be seen as points with one standard deviation whiskers. The elevation difference is displayed for both the median and the mean elevation difference calculated in each bin with a dashed line indicating an elevation difference of zero.
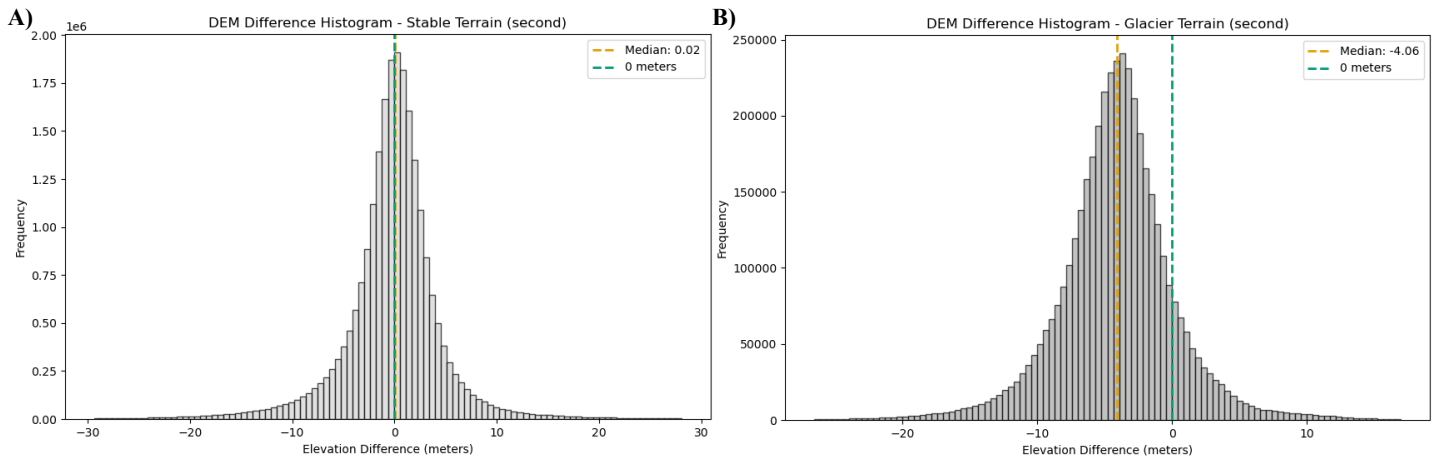
A)

B)

Figure 61: A) Code output of stable terrain hypsometry calculated from the dDEM for the Oberaletschgletscher, including median and a dashed 0-metre line with dynamically generated axis labelling. The x-axis shows the elevation difference in metres, whilst the y-axis shows the pixel frequency. B) Code output of glacier terrain hypsometry calculated from the dDEM for the Oberaletschgletscher, including median and a dashed 0-metre line with dynamically generated axis labelling. The x-axis shows the elevation difference in metres, whilst the y-axis shows the frequency.
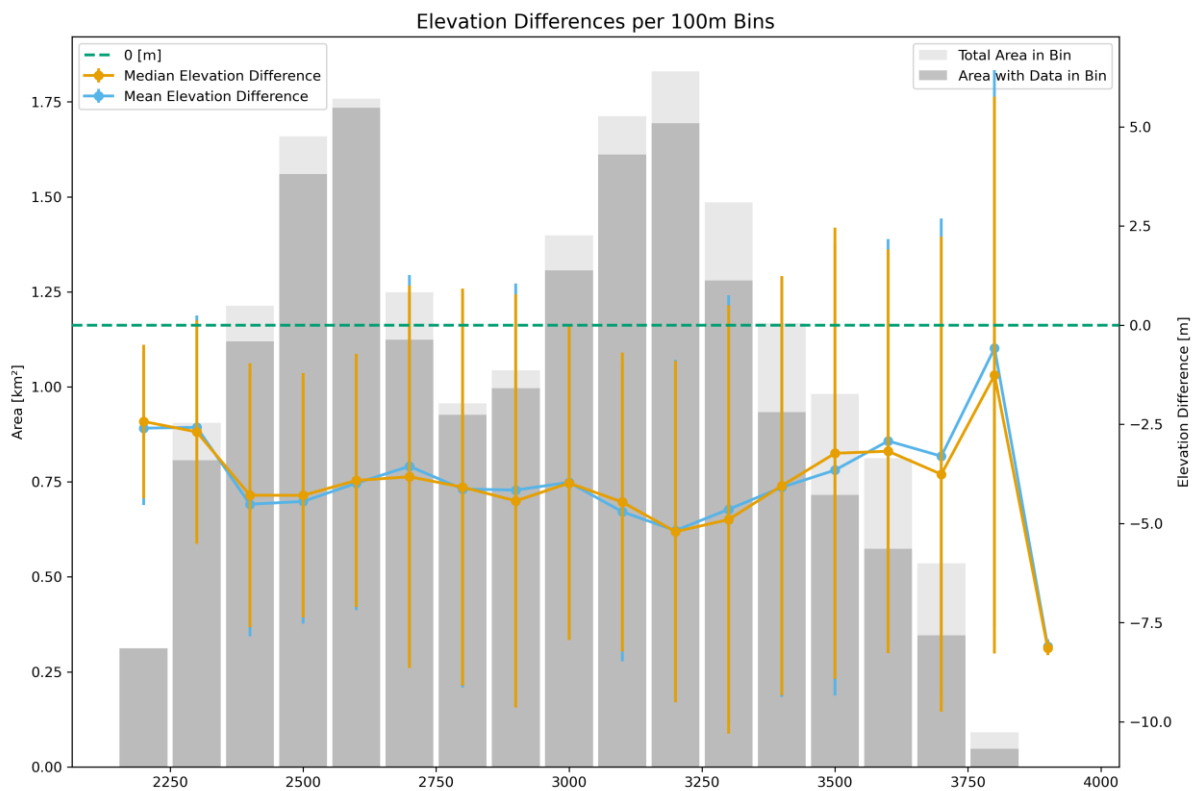

Figure 62: Elevation difference hypsometry plot showing the glacier area in bins for each 100-metre height band of the Oberaletschgletscher. The x-axis shows the metres above sea level. The first y-axis shows the area each hypsometric bin contains. The bins are separated into light grey for the total area available in that bin, the dark grey shows the area with valid data in that bin. The second y-axis shows the elevation difference calculated in each bin that can be seen as points with one standard deviation whiskers. The elevation difference is displayed for both the median and the mean elevation difference calculated in each bin with a dashed line indicating an elevation difference of zero.

8.2 Pictures

8.2.1 Spring Series

Image 3: Display of single stereo images that were used to produce the Spring Series DEMs. *(A) SPOT5 HRS image from 26.03.2003, (B) Pléiades HiRI image from 31.03.2021, (C) Pléiades Image from 11.04.2024.*

8.2.2 Fall Series
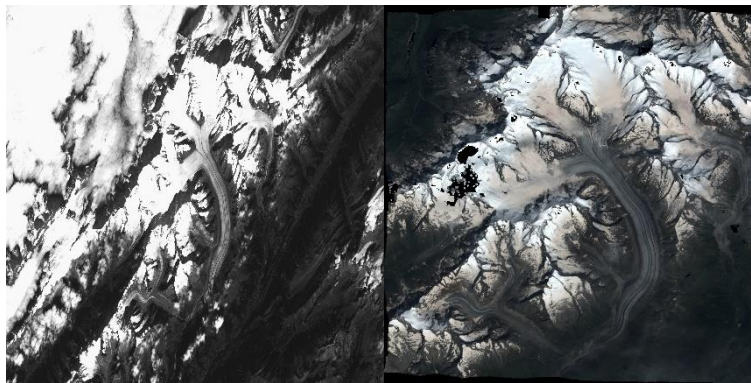
Image 4: Display of single stereo images that were used to produce the Fall Series DEMs. *(A) SPOT 5 HRS image from 24.09.2003, (B) Pléiades image from 10.08.2021.*

8.2.3 2003-2007 Series

Image 5: Display of single stereo images that were used to produce the Fall Series DEMs. *(A) SPOT5 HRS image from 26.03.2003, (B) SPOT5 HRS image from 01.02.2004, (C) SPOT5 HRS image from 04.01.2005, (D) SPOT5 HRS image from 28.01.2007.*

9 Data Availability

9.1 Input Data

Berthier, E., Lebreton, J., Fontannaz, D., Hosford, S., Belart, J.M.C., Brun, F., Andreassen, L.M., Menounos, B. and Blondel, C., 2024. The Pléiades Glacier Observatory: high-resolution digital elevation models and ortho-imagery to monitor glacier change. The Cryosphere, 18(12), pp.5551-5571.https://doi.org/10.5194/tc-18-5551-2024

Beyer, R. A., Alexandrov, O., and McMichael, S.: The Ames Stereo Pipeline: NASA's Open Source Software for Deriving and Processing Terrain Data, Earth and Space Science, 5, 537–548, https://doi.org/10.1029/2018EA000409, 2018

Copernicus. (2020). Land Cover 2015-2019 (raster 100 m). European Commission Directorate-General Joint Research Centre. https://land.copernicus.eu/en/data-policy

CNES, 2025. https://regards.cnes.fr/user/swh/modules/60. Last access 12 January 2025.

GLAMOS. (2022). Swiss Glacier Mass Balance, release 2022.

GLAMOS. (2024). The Swiss Glaciers 1881-2020/21, Glaciological Reports No 1-142.

Hugonnet, R., McNabb, R., Berthier, E., Menounos, B., Nuth, C., Girod, L., Farinotti, D., Huss, M., Dussaillant, I., Brun, F., & Kääb, A. (2021). Accelerated global glacier mass loss in the early twenty-first century. Nature, 592(7856), 726–731. https://doi.org/10.1038/s41586-021-03436-z

Huss, M., Bauder, A., & Linsbauer, A. (2024). Winter snow accumulation on Swiss glaciers in 2024.

RGI 7.0 Consortium. (2023). Randolph Glacier Inventory - A Dataset of Global Glacier Outlines, Version 7.0.

9.2 Pipeline Products

The output data is available from the author upon request. To get in contact, please use the following e-mail address:

andrin.schmidli@uzh.ch

For contact after the 31.07.2025, please use the following e-mail:

andrin.schmidli@outlook.com

10 Code

In the following three sections are the scripts written to process spatial data. The data was coded in Spyder. The Anaconda version is 3.12.3.

10.1 Co-Registration

```python
# -----------------------------------------------------------------------------
# DEM Coregistration Script
# Author: Andrin Schmidli
# Date: 31.01.2025
# Purpose: This script performs coregistration of DEMs using Nuth & Kääb's method,
#          generates stable terrain masks, handles landcover reclassification,
#          and outputs the coregistered DEM alongside relevant masks and metadata.
# -----------------------------------------------------------------------------

import os
import shutil
import numpy as np
import rasterio
from rasterio.warp import reproject, Resampling
import datetime
import xdem
import geopandas as gpd
from shapely.ops import unary_union
from fpdf import FPDF

# Libraries used in this script:
# - os: For file and directory management.
# - shutil: For folder management, such as clearing the output directory.
# - numpy: For numerical computations and array handling.
# - rasterio: For raster data manipulation and reprojection.
# - geopandas: For handling vector data such as shapefiles.
# - shapely: For geometric operations on vector data.
# - fpdf: For generating PDF files to document options and outputs.
# - xdem: For DEM-specific operations like coregistration using Nuth & Kääb's method.


# Options
coregistration_iterations = 10
buffer_distance_m = 200  # Buffer distance in meters
output_epsg = 32632

# Define paths for easy modification
ref_dem_path = r"W:\Desktop\GIS_Selection\Ref_DEM\2021-03-31_Aletsch_DEM_SGM_2m.tif"
tba_dem_path = r"W:\Desktop\GIS_Selection\1_Spring_20Y_Ale\2024-04-11_Aletsch_DEM_SGM_2m.tif"
landcover_path =
r"\\geofiles.d.uzh.ch\private\aschmidl\windows\Desktop\Data\PROBAV_LC100_global_v3.0.1_2019-
nrt_Discrete-Classification-map_EPSG-4326.tif"
outlines_path = r"\\geofiles.d.uzh.ch\private\aschmidl\windows\Desktop\Data\RGI2000-v7.0-G-
11_central_europe\RGI2000-v7.0-G-11_central_europe.shp"
output_base_folder = r"W:\Desktop\GIS_Selection\1_Spring_20Y_Ale\output_0"

# Create output folder with the name of the tba_dem
output_folder_name = os.path.splitext(os.path.basename(tba_dem_path))[0]
output_folder = os.path.join(output_base_folder, output_folder_name)
os.makedirs(output_folder, exist_ok=True)

# Function to clear output folder
def clear_output_folder(output_folder):
    if os.path.exists(output_folder):
        shutil.rmtree(output_folder)
    os.makedirs(output_folder)
```

```python
# Function to reproject raster
def reproject_raster_to_epsg(src_path, dst_path, dst_epsg):
    with rasterio.open(src_path) as src:
        if src.crs.to_epsg() == dst_epsg:
            print("{}: No reproject needed for {}".format(datetime.datetime.now(), src_path))
            return src_path

        dst_transform, dst_width, dst_height = rasterio.warp.calculate_default_transform(
            src.crs, "EPSG:{}".format(dst_epsg), src.width, src.height, *src.bounds)
        dst_meta = src.meta.copy()
        dst_meta.update({
            "crs": "EPSG:{}".format(dst_epsg),
            "transform": dst_transform,
            "width": dst_width,
            "height": dst_height
        })

        with rasterio.open(dst_path, "w", **dst_meta) as dst:
            for i in range(1, src.count + 1):
                reproject(
                    source=rasterio.band(src, i),
                    destination=rasterio.band(dst, i),
                    src_transform=src.transform,
                    src_crs=src.crs,
                    dst_transform=dst_transform,
                    dst_crs="EPSG:{}".format(dst_epsg),
                    resampling=Resampling.nearest
                )
        print("{}: Reprojected and saved {}".format(datetime.datetime.now(), dst_path))
        return dst_path

# Function to align DEMs
def align_dem(ref_dem_path, tba_dem_path):
    with rasterio.open(ref_dem_path) as ref:
        ref_data = ref.read(1)
        ref_transform = ref.transform
        ref_meta = ref.meta.copy()

        with rasterio.open(tba_dem_path) as tba:
            tba_data = tba.read(1)
            tba_transform = tba.transform

            aligned_tba_data = np.empty_like(ref_data, dtype=np.float32)

            reproject(
                source=tba_data,
                destination=aligned_tba_data,
                src_transform=tba_transform,
                src_crs=tba.crs,
                dst_transform=ref_transform,
                dst_crs=ref.crs,
                resampling=Resampling.bilinear,
                src_nodata=tba.meta['nodata'],
                dst_nodata=ref_meta['nodata']
            )

            print("{}: Aligned TBA DEM to reference DEM".format(datetime.datetime.now()))
            return ref_data, aligned_tba_data, ref_meta

# Function to create overlap mask
def create_overlap_mask(ref_dem, tba_dem, nodata):
    valid_ref_dem = (ref_dem != nodata) & ~np.isnan(ref_dem)
    valid_tba_dem = (tba_dem != nodata) & ~np.isnan(tba_dem)
    return valid_ref_dem & valid_tba_dem

# Function to save masks
```

```python
def save_mask(mask, temp_path, meta):
    mask_data = mask.astype(np.uint8) * 255
    mask_meta = meta.copy()
    mask_meta.update(dtype='uint8', count=1, nodata=None)
    with rasterio.open(temp_path, 'w', **mask_meta) as dst:
        dst.write(mask_data, 1)
    print("{}: Saved mask to {}".format(datetime.datetime.now(), temp_path))


# Function to reproject landcover
def reproject_landcover_to_dem(landcover_path, ref_meta, output_folder):
    reprojected_landcover_path = os.path.join(output_folder, "reprojected_landcover.tif")
    return reproject_raster_to_epsg(landcover_path, reprojected_landcover_path,
ref_meta['crs'].to_epsg())


# Function to create stable terrain mask
def create_and_save_stable_terrain_mask(landcover_path, ref_meta, output_folder, outlines_mask):
    with rasterio.open(landcover_path) as landcover:
        landcover_data = landcover.read(1)
        landcover_transform = landcover.transform
        stable_mask = np.isin(landcover_data, [30, 60])

    aligned_stable_mask = np.empty((ref_meta['height'], ref_meta['width']), dtype=np.uint8)
    reproject(
        source=stable_mask.astype(np.uint8),
        destination=aligned_stable_mask,
        src_transform=landcover_transform,
        src_crs=landcover.crs,
        dst_transform=ref_meta['transform'],
        dst_crs=ref_meta['crs'],
        resampling=Resampling.nearest
    )
    aligned_stable_mask[outlines_mask] = 0

    stable_mask_path = os.path.join(output_folder, "stable_terrain_mask.tif")
    save_mask(aligned_stable_mask.astype(np.uint8), stable_mask_path, ref_meta)
    return aligned_stable_mask, stable_mask_path


# Function to rasterize glacier outlines
def rasterize_glacier_outlines(outlines_path, buffer_distance_m, ref_dem_path, ref_meta,
output_folder):
    glacier_gdf = gpd.read_file(outlines_path)
    glacier_gdf = glacier_gdf.to_crs(epsg=output_epsg)  # Reproject to desired EPSG
    glacier_gdf['geometry'] = glacier_gdf.buffer(buffer_distance_m)
    buffered_glaciers = unary_union(glacier_gdf.geometry)  # Merge all geometries into a single
shape

    rasterized_outlines_path = os.path.join(output_folder, "rasterized_outlines.tif")

    with rasterio.open(ref_dem_path) as ref:
        meta = ref.meta.copy()
        meta.update(count=1, dtype=rasterio.uint8, nodata=0)
        with rasterio.open(rasterized_outlines_path, 'w+', **meta) as out:
            out_arr = out.read(1)
            shapes = ((geom, 1) for geom in [buffered_glaciers])
            burned = rasterio.features.rasterize(shapes=shapes, fill=0, out=out_arr,
transform=out.transform)
            out.write_band(1, burned)

    with rasterio.open(rasterized_outlines_path) as outlines_src:
        outlines_mask = outlines_src.read(1).astype(bool)

    outlines_mask_path = os.path.join(output_folder, "outlines_mask.tif")
    save_mask(outlines_mask, outlines_mask_path, ref_meta)
    return outlines_mask, outlines_mask_path


# Function to perform coregistration
```

```python
def perform_coregistration(ref_dem_filled_array, aligned_tba_dem_filled_array, stable_mask,
ref_meta, iterations):
    stable_mask = stable_mask.astype(bool)
    nuth_kaab = xdem.coreg.NuthKaab(max_iterations=iterations)
    nuth_kaab.fit(
        xdem.DEM.from_array(ref_dem_filled_array, ref_meta['transform'], ref_meta['crs']),
        xdem.DEM.from_array(aligned_tba_dem_filled_array, ref_meta['transform'], ref_meta['crs']),
        inlier_mask=stable_mask
    )
    coreg_dem = nuth_kaab.apply(xdem.DEM.from_array(aligned_tba_dem_filled_array,
ref_meta['transform'], ref_meta['crs']))

    return coreg_dem.data

# Function to save DEM
def save_dem(data, path, meta):
    with rasterio.open(path, 'w', **meta) as dst:
        dst.write(data, 1)
    print("{}: Saved DEM to {}".format(datetime.datetime.now(), path))

# Function to save options and paths to PDF
def save_options_to_pdf(output_folder):
    pdf = FPDF()
    pdf.add_page()

    pdf.set_font("Arial", size=12)
    pdf.cell(200, 10, txt="DEM Coregistration Options and Paths", ln=True, align="C")

    options = {
        "Coregistration Iterations": coregistration_iterations,
        "Buffer Distance (m)": buffer_distance_m,
        "Output EPSG": output_epsg,
        "Reference DEM Path": ref_dem_path,
        "To-be-aligned DEM Path": tba_dem_path,
        "Landcover Path": landcover_path,
        "Outlines Path": outlines_path,
        "Output Folder": output_folder,
    }

    for key, value in options.items():
        pdf.cell(200, 10, txt=f"{key}: {value}", ln=True)

    pdf_output_path = os.path.join(output_folder, "options_and_paths.pdf")
    pdf.output(pdf_output_path)
    print(f"{datetime.datetime.now()}: Saved options and paths to {pdf_output_path}")

# Main function
def main():
    clear_output_folder(output_folder)

    # Save options and paths to PDF
    save_options_to_pdf(output_folder)

    # Reproject DEMs
    ref_dem_path_reprojected = reproject_raster_to_epsg(ref_dem_path, os.path.join(output_folder,
"reprojected_ref_dem.tif"), output_epsg)
    tba_dem_path_reprojected = reproject_raster_to_epsg(tba_dem_path, os.path.join(output_folder,
"reprojected_tba_dem.tif"), output_epsg)

    ref_dem_filled_array, aligned_tba_dem_filled_array, ref_meta =
align_dem(ref_dem_path_reprojected, tba_dem_path_reprojected)

    # Create and save overlap mask
    overlap_mask_non_coreg = create_overlap_mask(ref_dem_filled_array, aligned_tba_dem_filled_array,
ref_meta['nodata'])
    save_mask(overlap_mask_non_coreg, os.path.join(output_folder, "mask_non_coreg.tif"), ref_meta)
```

```python
        ref_dem_filled_array[~overlap_mask_non_coreg] = np.nan
        aligned_tba_dem_filled_array[~overlap_mask_non_coreg] = np.nan

        # Reproject landcover and create stable terrain mask
        reprojected_landcover_path = reproject_landcover_to_dem(landcover_path, ref_meta, output_folder)
        outlines_mask, outlines_mask_path = rasterize_glacier_outlines(outlines_path, buffer_distance_m,
ref_dem_path_reprojected, ref_meta, output_folder)
        aligned_stable_mask, stable_mask_path =
create_and_save_stable_terrain_mask(reprojected_landcover_path, ref_meta, output_folder,
outlines_mask)

        # Perform coregistration using stable terrain mask
        coreg_dem_array = perform_coregistration(
            ref_dem_filled_array, aligned_tba_dem_filled_array, aligned_stable_mask, ref_meta,
coregistration_iterations
        )

        # Save the final coregistered DEM
        coreg_dem_path = os.path.join(output_folder, f"{output_folder_name}_coregistered.tif")
        save_dem(coreg_dem_array, coreg_dem_path, ref_meta)

        print('Final coregistered DEM saved to {}'.format(coreg_dem_path))

if __name__ == "__main__":
    main()
```

10.2 DEM differencing

```python
# ----------------------------------------------------------------------------
# DEM Differencing and Filtering Script
# Author: Andrin Schmidli
# Date: 31.01.2025
# Purpose: This script computes the differential DEM (dDEM) by subtracting two
#          coregistered DEMs, applies masks for overlap and glacier areas,
#          filters outliers based on standard deviation thresholds, and outputs
#          the final filtered differential DEM.
# ----------------------------------------------------------------------------

import os
import shutil
import numpy as np
import rasterio
from rasterio.warp import reproject, Resampling
import rasterio.features
import geopandas as gpd
import datetime

# Libraries used in this script:
# - os: For file and directory management.
# - shutil: For clearing and managing the output directory.
# - numpy: For numerical computations and handling arrays.
# - rasterio: For raster data manipulation and geometry-based operations.
# - geopandas: For handling shapefiles and spatial vector data.
# - datetime: For timestamping outputs and logging.

# Options
output_epsg = 32632
std_dev_multiplier = 3  # Multiplier for standard deviation (can be adjusted)

# Define paths for easy modification
```

```python
newer_dem_coreg_path = r"W:\Desktop\GIS_Selection\1_Spring_20Y_Ale\2021-03-
31_Aletsch_DEM_SGM_2m.tif"
older_dem_coreg_path = r"W:\Desktop\GIS_Selection\1_Spring_20Y_Ale\output_0\003-006_S5_054-256-
0_2003-03-26_DEM_5m\003-006_S5_054-256-0_2003-03-26_DEM_5m_coregistered.tif"
outlines_shapefile_path = r"\\geofiles.d.uzh.ch\private\aschmidl\windows\Desktop\Data\RGI2000-v7.0-
G-11_central_europe\RGI2000-v7.0-G-11_central_europe.shp"
output_folder = r"W:\Desktop\GIS_Selection\1_Spring_20Y_Ale\output_1"

# New: Specify the output file name
output_file_name = "ddem_final_filtered.tif"

# Function to clear output folder
def clear_output_folder(output_folder):
    if os.path.exists(output_folder):
        shutil.rmtree(output_folder)
    os.makedirs(output_folder)

# Function to create overlap mask
def create_overlap_mask(dem1, dem2, nodata):
    valid_dem1 = (dem1 != nodata) & ~np.isnan(dem1)
    valid_dem2 = (dem2 != nodata) & ~np.isnan(dem2)
    return valid_dem1 & valid_dem2

# Function to save DEM
def save_dem(data, path, meta):
    with rasterio.open(path, 'w', **meta) as dst:
        dst.write(data, 1)
    print("{}: Saved DEM to {}".format(datetime.datetime.now(), path))

# Function to create a glacier mask from shapefile
def create_glacier_mask(shapefile_path, ref_meta):
    glacier_gdf = gpd.read_file(shapefile_path)
    glacier_gdf = glacier_gdf.to_crs(ref_meta['crs'])  # Ensure it matches the DEM's CRS

    # Create a mask for the glacier area
    glacier_mask = rasterio.features.geometry_mask(
        [geom for geom in glacier_gdf.geometry],
        transform=ref_meta['transform'],
        invert=True,
        out_shape=(ref_meta['height'], ref_meta['width'])
    )
    return glacier_mask

# Main function
def main():
    clear_output_folder(output_folder)

    # Load the coregistered DEMs
    with rasterio.open(newer_dem_coreg_path) as newer_dem_src:
        newer_coreg_dem_array = newer_dem_src.read(1).astype(np.float32)
        ref_meta = newer_dem_src.meta.copy()
        nodata_value = ref_meta['nodata']

    with rasterio.open(older_dem_coreg_path) as older_dem_src:
        older_coreg_dem_array = older_dem_src.read(1).astype(np.float32)

    # Create an overlap mask
    overlap_mask = create_overlap_mask(newer_coreg_dem_array, older_coreg_dem_array, nodata_value)

    # Apply the mask to both DEMs
    newer_coreg_dem_array[~overlap_mask] = np.nan
    older_coreg_dem_array[~overlap_mask] = np.nan

    # Calculate the differential DEM by subtracting the older DEM from the newer DEM
    ddem_final = newer_coreg_dem_array - older_coreg_dem_array
```

```python
    # Create a glacier mask from the outlines shapefile
    glacier_mask = create_glacier_mask(outlines_shapefile_path, ref_meta)

    # Separate DEMs into glacier and off-glacier areas
    on_glacier_ddem = ddem_final[glacier_mask]
    off_glacier_ddem = ddem_final[~glacier_mask & overlap_mask]

    # Calculate the standard deviation and mean for on-glacier and off-glacier areas
    on_glacier_std_dev = np.nanstd(on_glacier_ddem)
    on_glacier_mean = np.nanmean(on_glacier_ddem)
    off_glacier_std_dev = np.nanstd(off_glacier_ddem)
    off_glacier_mean = np.nanmean(off_glacier_ddem)

    # Exclude values more than 3 times the standard deviation for on-glacier and off-glacier areas
    on_glacier_lower_bound = on_glacier_mean - std_dev_multiplier * on_glacier_std_dev
    on_glacier_upper_bound = on_glacier_mean + std_dev_multiplier * on_glacier_std_dev
    off_glacier_lower_bound = off_glacier_mean - std_dev_multiplier * off_glacier_std_dev
    off_glacier_upper_bound = off_glacier_mean + std_dev_multiplier * off_glacier_std_dev

    ddem_final_filtered = np.copy(ddem_final)
    ddem_final_filtered[(ddem_final < on_glacier_lower_bound) & glacier_mask] = np.nan
    ddem_final_filtered[(ddem_final > on_glacier_upper_bound) & glacier_mask] = np.nan
    ddem_final_filtered[(ddem_final < off_glacier_lower_bound) & ~glacier_mask & overlap_mask] = np.nan
    ddem_final_filtered[(ddem_final > off_glacier_upper_bound) & ~glacier_mask & overlap_mask] = np.nan

    # Save the final filtered differential DEM with the specified output file name
    output_post_coreg_final_path = os.path.join(output_folder, output_file_name)
    save_dem(ddem_final_filtered, output_post_coreg_final_path, ref_meta)

    print('Final filtered differential DEM saved to {}'.format(output_post_coreg_final_path))

if __name__ == "__main__":
    main()
```

10.3 DEM Analysis

```python
# ---------------------------------------------------------------------------
# DEM Analysis Script
# Author: Andrin Schmidli
# Date: 31.01.2025
# Purpose: This script calculates glacier surface elevation changes over time by analyzing
#          Digital Elevation Models (DEMs). It performs uncertainty analysis, hypsometric
#          analysis, and generates detailed PDF reports with statistical summaries and plots.
# ---------------------------------------------------------------------------

import os
import numpy as np
import matplotlib.pyplot as plt
import rasterio
from rasterio import features
from reportlab.lib.pagesizes import letter
from reportlab.pdfgen import canvas
from datetime import datetime as dt
from xdem.terrain import get_terrain_attribute
from xdem.spatialstats import (
    nd_binning,
    interp_nd_binning,
    nmad,
    sample_empirical_variogram,
    fit_sum_model_variogram,
    neff_circular_approx_numerical,
    plot_variogram,
)
import geoutils as gu
```

```python
import xdem
from scipy.stats import binned_statistic
import geopandas as gpd
import tempfile
from xdem.spatialstats import sample_empirical_variogram, fit_sum_model_variogram,
neff_circular_approx_numerical
from xdem.terrain import get_terrain_attribute
import xdem

# The tools and libraries used in this script are:
# - xDEM: For DEM differencing and statistical analysis.
# - GeoPandas: For handling shapefiles and spatial data.
# - Matplotlib: For plotting and visualizations.
# - Rasterio: For raster data handling.
# - NumPy: For numerical computations.

# User enters the two DEM dates for time difference calculation
date1_str = input("Enter the first DEM date (YYYY-MM-DD): ")
date2_str = input("Enter the second DEM date (YYYY-MM-DD): ")

# Define paths for easy modification
ddem_path =
r"W:\Desktop\GIS_Selection\1_Spring_20Y_Ale\output_1_archive\20030326_20210331_ddem_final_filtered.t
if"
stable_mask_path = r"W:\Desktop\GIS_Selection\1_Spring_20Y_Ale\output_0\2024-04-
11_Aletsch_DEM_SGM_2m\stable_terrain_mask.tif"
outlines_shapefile_path = r"\\geofiles.d.uzh.ch\private\aschmidl\windows\Desktop\Data\RGI2000-v7.0-
G-11_central_europe\RGI2000-v7.0-G-11_central_europe.shp"
ref_dem_path = r"W:\Desktop\GIS_Selection\Ref_DEM\2021-03-31_Aletsch_DEM_SGM_2m.tif"
glacier_shapefile_path = r"W:\Desktop\Data\RGI2000-v7.0-G-11_central_europe_Aletsch\RGI2000-v7.0-G-
11_central_europe_Aletsch.shp"
output_folder = r"W:\Desktop\GIS_Selection\1_Spring_20Y_Ale\output_2"

# Function to load masked DEM
def load_masked_dem(temp_path):
    with rasterio.open(temp_path) as src:
        data = src.read(1)
        data[data == src.nodata] = np.nan
    print("{}: Loaded and cleaned DEM from {}".format(dt.now(), temp_path))
    return data, src.meta

# Function to calculate statistics
def calculate_statistics(data, suffix):
    stats = {
        'median': np.nanmedian(data),
        'mad': np.nanmedian(np.abs(data - np.nanmedian(data))),
        'nmad': 1.4826 * np.nanmedian(np.abs(data - np.nanmedian(data))),
        'mean_error': np.nanmean(data),
        'std_dev': np.nanstd(data),
        'rmse': np.sqrt(np.nanmean(data ** 2)),
        'q1': np.nanpercentile(data, 25),
        'q3': np.nanpercentile(data, 75)
    }

    for key, value in stats.items():
        print(f'{key.capitalize()} {suffix} Terrain: {value:.2f} meters')

    return stats

# Function to plot histograms
def plot_histogram(data, title, suffix):
    valid_data = data[(data >= -8848) & (data <= 8848) & ~np.isnan(data)]

    fig, ax = plt.subplots(figsize=(10, 6))
    ax.hist(valid_data, bins=100, color='blue', edgecolor='black', alpha=0.7)
    ax.set_title(f'DEM Difference Histogram - {title} ({suffix})')
```

```python
    ax.set_xlabel('Elevation Difference (meters)')
    ax.set_ylabel('Frequency')
    ax.axvline(np.nanmedian(valid_data), color='red', linestyle='dashed', linewidth=2,
label=f'Median: {np.nanmedian(valid_data):.2f}')
    ax.axvline(0, color='green', linestyle='dashed', linewidth=2, label='0 meters')
    ax.legend()

    with tempfile.NamedTemporaryFile(delete=False, suffix=".png") as tmp_hist_file:
        fig.savefig(tmp_hist_file, format='png')
        hist_file_path = tmp_hist_file.name
    plt.close(fig)

    return hist_file_path


# Function to create a mask from a shapefile
def create_mask_from_shapefile(shapefile_path, ref_meta):
    shapefile_gdf = gpd.read_file(shapefile_path)
    shapefile_gdf = shapefile_gdf.to_crs(ref_meta['crs'])  # Ensure it matches the DEM's CRS

    mask = features.geometry_mask([geom for geom in shapefile_gdf.geometry],
                                  transform=ref_meta['transform'],
                                  invert=True,
                                  out_shape=(ref_meta['height'], ref_meta['width']))
    return mask, shapefile_gdf

def add_pdf_page(canvas_obj, title, stats):
    """Adds a page with statistics to a PDF."""
    canvas_obj.setFont("Helvetica", 14)
    canvas_obj.drawString(100, 750, title)
    canvas_obj.setFont("Helvetica", 12)
    y_pos = 730
    for key, value in stats.items():
        canvas_obj.drawString(100, y_pos, f'{key.capitalize()}: {value:.2f} meters')
        y_pos -= 20
    canvas_obj.showPage()

def uncertainty_analysis_and_visualization(ddem_path, stable_mask_path, outlines_shapefile_path,
glacier_shapefile_path, output_folder, suffix, date1_str, date2_str):
    """
    Perform uncertainty analysis on a DEM, including stable and glacier terrain, and save results as
a PDF.
    """
    # Load the dDEM
    ddem, ddem_meta = load_masked_dem(ddem_path)
    stable_mask = rasterio.open(stable_mask_path).read(1).astype(bool)

    # Create masks for glacier and stable terrain
    outlines_mask, _ = create_mask_from_shapefile(outlines_shapefile_path, ddem_meta)
    glacier_mask, _ = create_mask_from_shapefile(glacier_shapefile_path, ddem_meta)

    if np.isnan(ddem).all():
        print(f"The differential DEM ({suffix}) contains only NaN values.")
        return

    # Extract stable and glacier terrain data
    stable_valid_data = ddem[(ddem >= -8848) & (ddem <= 8848) & ~np.isnan(ddem) & stable_mask &
~glacier_mask]
    outlines_valid_data = ddem[(ddem >= -8848) & (ddem <= 8848) & ~np.isnan(ddem) & glacier_mask]

    # Calculate statistics for stable and glacier terrain
    stable_stats = calculate_statistics(stable_valid_data, 'Stable')
    outlines_stats = calculate_statistics(outlines_valid_data, 'Glacier')

    # Plot histograms with adapted color scheme
    def plot_adapted_histogram(data, title, color, suffix):
        valid_data = data[(data >= -8848) & (data <= 8848) & ~np.isnan(data)]
```

```python
        fig, ax = plt.subplots(figsize=(10, 6))
        ax.hist(valid_data, bins=100, color=color, edgecolor='black', alpha=0.7)
        ax.set_title(f'DEM Difference Histogram - {title} ({suffix})')
        ax.set_xlabel('Elevation Difference (meters)')
        ax.set_ylabel('Frequency')
        ax.axvline(np.nanmedian(valid_data), color='#E69F00', linestyle='dashed', linewidth=2,
label=f'Median: {np.nanmedian(valid_data):.2f}')
        ax.axvline(0, color='#009E73', linestyle='dashed', linewidth=2, label='0 meters')
        ax.legend()

        with tempfile.NamedTemporaryFile(delete=False, suffix=".png") as tmp_hist_file:
            fig.savefig(tmp_hist_file, format='png')
            hist_file_path = tmp_hist_file.name
        plt.close(fig)

        return hist_file_path

    hist_file_path_stable = plot_adapted_histogram(stable_valid_data, 'Stable Terrain', 'lightgray',
suffix)
    hist_file_path_outlines = plot_adapted_histogram(outlines_valid_data, 'Glacier Terrain',
'darkgray', suffix)

    # Store temporary files for cleanup
    temp_files = [hist_file_path_stable, hist_file_path_outlines]

    # Rename the output PDF
    output_pdf_path = os.path.join(output_folder, 'Glacier_Uncertainty_Report.pdf')
    c = canvas.Canvas(output_pdf_path, pagesize=letter)

    # Add a summary page
    c.setFont("Helvetica", 14)
    c.drawString(100, 750, "Glacier Uncertainty Report")
    c.setFont("Helvetica", 12)
    c.drawString(100, 730, f"First DEM Date: {date1_str}")
    c.drawString(100, 710, f"Second DEM Date: {date2_str}")
    c.drawString(100, 690, f"Reference DEM: {os.path.basename(ddem_path)}")
    c.drawString(100, 670, f"Stable Terrain Mask: {os.path.basename(stable_mask_path)}")
    c.drawString(100, 650, f"Glacier Outlines Shapefile:
{os.path.basename(glacier_shapefile_path)}")
    c.showPage()

    def add_pdf_page(c, title, stats):
        c.setFont("Helvetica", 14)
        c.drawString(100, 750, title)
        c.setFont("Helvetica", 12)
        y_pos = 730
        for key, value in stats.items():
            c.drawString(100, y_pos, f'{key.capitalize()}: {value:.2f} meters')
            y_pos -= 20
        c.showPage()

    add_pdf_page(c, f"DEM Uncertainty Analysis Report ({suffix}) - Stable Terrain DEM Statistics",
stable_stats)
    add_pdf_page(c, f"DEM Uncertainty Analysis Report ({suffix}) - Glacier DEM Statistics",
outlines_stats)

    c.drawImage(hist_file_path_stable, 50, 400, width=500, height=300)
    c.showPage()
    c.drawImage(hist_file_path_outlines, 50, 400, width=500, height=300)
    c.showPage()

    os.remove(hist_file_path_stable)
    os.remove(hist_file_path_outlines)

    c.save()
```

```python
    print('DEM Uncertainty Analysis PDF saved to {}'.format(output_pdf_path))

    def add_pdf_page(c, title, stats):
        c.setFont("Helvetica", 14)
        c.drawString(100, 750, title)
        c.setFont("Helvetica", 12)
        y_pos = 730
        for key, value in stats.items():
            c.drawString(100, y_pos, f'{key.capitalize()}: {value:.2f} meters')
            y_pos -= 20
        c.showPage()

    c.setFont("Helvetica", 14)
    c.drawString(100, 750, "DEM Processing Report")
    c.setFont("Helvetica", 12)
    c.drawString(100, 730, "Reference DEM: {}".format(os.path.basename(ref_dem_path)))
    c.drawString(100, 710, "TBA DEM: {}".format(os.path.basename(ddem_path)))
    c.drawString(100, 690, "Stable Terrain Mask Source:
{}".format(os.path.basename(stable_mask_path)))
    c.drawString(100, 670, "Glacier Shapefile: {}".format(os.path.basename(glacier_shapefile_path)))

    # Add the DEM date information
    c.drawString(100, 650, f"First DEM Date: {date1_str}")
    c.drawString(100, 630, f"Second DEM Date: {date2_str}")

    c.showPage()

    add_pdf_page(c, f"DEM Uncertainty Analysis Report ({suffix}) - Stable Terrain DEM Statistics",
stable_stats)
    add_pdf_page(c, f"DEM Uncertainty Analysis Report ({suffix}) - Glacier DEM Statistics",
outlines_stats)

    c.drawImage(hist_file_path_stable, 50, 400, width=500, height=300)
    c.showPage()
    c.drawImage(hist_file_path_outlines, 50, 400, width=500, height=300)
    c.showPage()

    os.remove(hist_file_path_stable)
    os.remove(hist_file_path_outlines)

    c.save()
    print('DEM Uncertainty Analysis PDF saved to {}'.format(output_pdf_path))

def analyze_glacier_height_bands(ddem_path, glacier_mask, ref_dem_path, output_folder,
pdf_report_path):
    """
    Analyze glacier elevation differences in 100m elevation bands and generate a PDF report.
    """
    ddem, _ = load_masked_dem(ddem_path)

    with rasterio.open(ref_dem_path) as ref_src:
        ref_dem = ref_src.read(1)
        transform = ref_src.transform

    ddem_glacier = ddem[(ddem >= -8848) & (ddem <= 8848) & glacier_mask]
    ref_dem_glacier = ref_dem[(ref_dem >= -8848) & (ref_dem <= 8848) & glacier_mask]

    min_elevation = int(np.nanmin(ref_dem_glacier) // 100 * 100)
    max_elevation = int(np.nanmax(ref_dem_glacier) // 100 * 100 + 100)

    temp_files = []
    elevation_bins = []
    medians = []
    means = []
    std_devs = []
    area_with_values = []
```

```python
        total_area_in_band = []

    for elevation in range(min_elevation, max_elevation, 100):
            band_mask = (ref_dem >= elevation) & (ref_dem < elevation + 100) & glacier_mask
            if not np.any(band_mask):
                print(f"No valid data for elevation band {elevation}-{elevation+100} meters.")
                continue

            ddem_band = ddem[(ddem >= -8848) & (ddem <= 8848) & band_mask]

            if np.isnan(ddem_band).all():
                print(f"No valid dDEM data for elevation band {elevation}-{elevation+100} meters.")
                continue

            elevation_bins.append(elevation)
            pixel_area = abs(transform[0] * transform[4]) / 1e6  # Convert pixel area to square
kilometers
            total_pixels_in_band = np.sum(band_mask)
            total_area_in_band.append(total_pixels_in_band * pixel_area)
            area_with_values.append(np.sum(~np.isnan(ddem_band)) * pixel_area)

            median_height = np.nanmedian(ddem_band)
            mean_height = np.nanmean(ddem_band)
            std_dev_height = np.nanstd(ddem_band)
            medians.append(median_height)
            means.append(mean_height)
            std_devs.append(std_dev_height)

            # Plot histogram for the current elevation band
            fig, ax = plt.subplots(figsize=(10, 6))
            ax.hist(ddem_band[~np.isnan(ddem_band)], bins=100, color='gray', edgecolor='black',
alpha=0.7)
            ax.axvline(median_height, color='#E69F00', linestyle='dashed', linewidth=2, label=f'Median:
{median_height:.2f}')
            ax.axvline(mean_height, color='#56B4E9', linestyle='dashed', linewidth=2, label=f'Mean:
{mean_height:.2f}')
            ax.axvline(0, color='#009E73', linestyle='dashed', linewidth=2, label='0 meters')
            ax.legend()
            ax.set_title(f'Elevation Band {elevation}-{elevation+100} [m]')
            ax.set_xlabel('Elevation Difference [m]')
            ax.set_ylabel('Frequency')
            with tempfile.NamedTemporaryFile(delete=False, suffix=".png") as tmp_hist_file:
                fig.savefig(tmp_hist_file, format='png')
                temp_files.append(tmp_hist_file.name)
            plt.close(fig)

    if len(elevation_bins) == 0:
        print("No valid elevation bins for glacier height analysis. Skipping combined plot.")
        return

    # Combined plot with separate axes for bars and lines
    fig, ax_bars = plt.subplots(figsize=(12, 8))
    ax_lines = ax_bars.twinx()

    # Plot area bars on the primary axis
    ax_bars.bar(elevation_bins, total_area_in_band, width=90, color='lightgray', alpha=0.5,
label='Total Area in Bin', zorder=1)
    ax_bars.bar(elevation_bins, area_with_values, width=90, color='darkgray', alpha=0.7, label='Area
with Data in Bin', zorder=2)
    ax_bars.set_ylabel('Area [km²]')
    ax_bars.legend(loc='upper right', fontsize=10)

    # Plot lines on the secondary axis
    ax_lines.errorbar(elevation_bins, medians, yerr=std_devs, fmt='o-', color='#E69F00',
label='Median Elevation Difference', linewidth=2, zorder=4)
```

```python
    ax_lines.errorbar(elevation_bins, means, yerr=std_devs, fmt='o-', color='#56B4E9', label='Mean
Elevation Difference', linewidth=2, zorder=3)
    ax_lines.axhline(0, color='#009E73', linestyle='dashed', linewidth=2, label='0 [m]', zorder=5)

    ax_lines.set_xlabel('Elevation [m]')
    ax_lines.set_ylabel('Elevation Difference [m]')
    ax_lines.legend(loc='upper left', fontsize=10)

    # Title and layout
    plt.title('Elevation Differences per 100m Bins', fontsize=14)
    plt.tight_layout()

    # Save combined plot
    mean_median_plot_path = os.path.join(output_folder, 'Mean_Median_Elevation_Difference_Bins.png')
    plt.savefig(mean_median_plot_path, dpi=300)
    plt.close()

    # Add all plots to a single PDF
    c = canvas.Canvas(pdf_report_path, pagesize=letter)
    plot_width = 250
    plot_height = 200
    x_positions = [50, 300]
    y_positions = [500, 280, 60]

    for i, temp_file in enumerate(temp_files):
        x = x_positions[i % 2]
        y = y_positions[i % 3]
        c.drawImage(temp_file, x, y, width=plot_width, height=plot_height)
        if i % 6 == 5:
            c.showPage()

    c.showPage()
    c.drawImage(mean_median_plot_path, 50, 300, width=500, height=400)
    c.save()

    for temp_file in temp_files:
        os.remove(temp_file)
    os.remove(mean_median_plot_path)

    print(f'Glacier Hypsometry Analysis report saved to {pdf_report_path}')

def glacier_analysis_report(ddem_path, glacier_mask, ref_dem_path, output_folder, date1_str,
date2_str):
    ddem, _ = load_masked_dem(ddem_path)
    ref_dem, ref_meta = load_masked_dem(ref_dem_path)

    # Filter out valid data within the glacier area
    ddem_glacier = ddem[(ddem >= -8848) & (ddem <= 8848) & glacier_mask]

    # Calculate data-only median and mean for the whole glacier area
    data_only_median = np.nanmedian(ddem_glacier)
    data_only_mean = np.nanmean(ddem_glacier)

    # Apply 3-sigma filter to remove extreme outliers
    glacier_std = np.nanstd(ddem_glacier)
    glacier_filtered = ddem_glacier[
        (ddem_glacier >= (data_only_mean - 3 * glacier_std)) &
        (ddem_glacier <= (data_only_mean + 3 * glacier_std))
    ]

    # Calculate filtered median and mean
    filtered_median = np.nanmedian(glacier_filtered)
    filtered_mean = np.nanmean(glacier_filtered)

    # Extrapolation over elevation bins (weighted mean and median)
    min_elevation = int(np.nanmin(ref_dem[glacier_mask]) // 100 * 100)
```

```python
    max_elevation = int(np.nanmax(ref_dem[glacier_mask]) // 100 * 100 + 100)
    total_glacier_area = np.sum(glacier_mask) * abs(ref_meta['transform'][0] *
ref_meta['transform'][4]) / 1e6

    weighted_median_sum = 0
    weighted_mean_sum = 0
    valid_band_count = 0

    bins = np.arange(min_elevation, max_elevation + 100, 100)
    for i in range(len(bins) - 1):
        band_mask = (ref_dem >= bins[i]) & (ref_dem < bins[i + 1]) & glacier_mask
        band_area = np.sum(band_mask) * abs(ref_meta['transform'][0] * ref_meta['transform'][4]) /
1e6

        if band_area == 0:
            continue

        band_ddem = ddem[(ddem >= -8848) & (ddem <= 8848) & band_mask]
        if np.isnan(band_ddem).all():
            print(f"No valid dDEM data for elevation band {bins[i]}-{bins[i+1]} meters.")
            continue

        band_median = np.nanmedian(band_ddem)
        band_mean = np.nanmean(band_ddem)

        weighted_median_sum += band_median * band_area
        weighted_mean_sum += band_mean * band_area
        valid_band_count += 1

    if valid_band_count == 0:
        print("No valid elevation bands were found for weighted calculations.")
        weighted_median = np.nan
        weighted_mean = np.nan
    else:
        weighted_median = weighted_median_sum / total_glacier_area
        weighted_mean = weighted_mean_sum / total_glacier_area

    # Parse the dates and calculate the time difference in years
    date1 = dt.strptime(date1_str, '%Y-%m-%d')
    date2 = dt.strptime(date2_str, '%Y-%m-%d')
    years = (date2 - date1).days / 365.25  # Convert the time difference into years

    # Calculate annual thickness change for both mean and median
    mean_annual_thickness_change = weighted_mean / years * 1000 if not np.isnan(weighted_mean) else
np.nan
    median_annual_thickness_change = weighted_median / years * 1000 if not np.isnan(weighted_median)
else np.nan

    # Rename the output PDF
    output_pdf_path = os.path.join(output_folder, 'Glacier_Heightchange_Report.pdf')
    c = canvas.Canvas(output_pdf_path, pagesize=letter)

    # Add results to the PDF
    c.setFont("Helvetica", 14)
    c.drawString(100, 750, "Glacier Heightchange Report")
    c.setFont("Helvetica", 12)

    # Data-only statistics
    c.drawString(100, 710, f"Data-only Glacier Median: {data_only_median:.2f} meters")
    c.drawString(100, 690, f"Data-only Glacier Mean: {data_only_mean:.2f} meters")

    # 3-Sigma filtered statistics
    c.drawString(100, 670, f"3-Sigma Filtered Glacier Median: {filtered_median:.2f} meters")
    c.drawString(100, 650, f"3-Sigma Filtered Glacier Mean: {filtered_mean:.2f} meters")

    # Extrapolated statistics
```

```python
        c.drawString(100, 630, f"Extrapolated Weighted Median: {weighted_median:.2f} meters")
        c.drawString(100, 610, f"Extrapolated Weighted Mean: {weighted_mean:.2f} meters")

        # Add Mean annual thickness change (Mean and Median)
        c.drawString(100, 590, f"Mean Annual Thickness Change (Mean): {mean_annual_thickness_change:.2f} mm/year")
        c.drawString(100, 570, f"Mean Annual Thickness Change (Median): {median_annual_thickness_change:.2f} mm/year")

        c.showPage()
        c.save()

        print(f'Glacier Heightchange Report saved to {output_pdf_path}')

        return weighted_mean, median_annual_thickness_change  # Return both values

def main():
    try:
        # Perform uncertainty analysis
        uncertainty_analysis_and_visualization(
            ddem_path=ddem_path,
            stable_mask_path=stable_mask_path,
            outlines_shapefile_path=outlines_shapefile_path,
            glacier_shapefile_path=glacier_shapefile_path,
            output_folder=output_folder,
            suffix="second",
            date1_str=date1_str,
            date2_str=date2_str,
        )
    except Exception as e:
        print(f"Error in uncertainty analysis: {e}")

    try:
        # Generate hypsometry plots
        ddem, ddem_meta = load_masked_dem(ddem_path)
        glacier_mask, _ = create_mask_from_shapefile(glacier_shapefile_path, ddem_meta)
        glacier_mask = glacier_mask.astype(bool)  # Ensure it is boolean

        hypsometry_pdf_path = os.path.join(output_folder, "Glacier_Hypsometry_Analysis.pdf")
        analyze_glacier_height_bands(
            ddem_path=ddem_path,
            glacier_mask=glacier_mask,
            ref_dem_path=ref_dem_path,
            output_folder=output_folder,
            pdf_report_path=hypsometry_pdf_path,
        )
    except Exception as e:
        print(f"Error in glacier height band analysis: {e}")

    try:
        # Perform glacier analysis report and retrieve required values
        extrapolated_weighted_mean, median_annual_thickness_change = glacier_analysis_report(
            ddem_path=ddem_path,
            glacier_mask=glacier_mask,
            ref_dem_path=ref_dem_path,
            output_folder=output_folder,
            date1_str=date1_str,
            date2_str=date2_str,
        )
    except Exception as e:
        print(f"Error in glacier analysis report: {e}")
        return  # Skip further analysis if this step fails

if __name__ == "__main__":
    main()
```

10.4 Package Versions and Availability

The following libraries were used to create the pipeline. The versions are listed based on the constellation that works together without any errors. For some packages newer versions are available. This led to conflicts when executing the code.

Library	Version	Last accessed	Link
datetime	Std. library	-	-
fpdf	1.7.2	19.01.2025	*https://anaconda.org/conda-forge/fpdf*
geopandas	1.0.0	19.01.2025	*https://geopandas.org/en/v1.0.0/getting_started.html*
geoutils	0.1.5	19.01.2025	*https://geoutils.readthedocs.io/en/stable/how_to_install.html*
matplotlib	3.9.2	19.01.2025	*https://matplotlib.org/stable/install/index.html*
numpy	1.26.4	19.01.2025	*https://numpy.org/install/*
os	Std. library	-	-
rasterio	1.3.10	19.01.2025	*https://rasterio.readthedocs.io/en/stable/installation.html*
reportlab	4.2.2	19.01.2025	*https://docs.reportlab.com/install/open_source_installation/*
scipy	1.12.0	19.01.2025	*https://scipy.org/install/*
shapely	2.0.4	19.01.2025	*https://shapely.readthedocs.io/en/2.0.4/installation.html*
shutil	Std. library	-	-
tempfile	Std. library	-	-
xdem	0.0.19	19.01.2025	*https://xdem.readthedocs.io/en/stable/how_to_install.html*

Personal declaration

I hereby declare that the submitted thesis is the result of my own, independent work. All external sources are explicitly acknowledged in the thesis. I also confirm that I have not used any AI for this thesis except for the part declared. The AI used is ChatGPT 4o.

AI has been used for the coding of the following parts:

10.1   Co-Registration Script

10.2   DEM Differencing Script

10.3   Analysis Script

With my signature, I confirm that the above information is true.

Zürich, January 2025   Andrin Schmidli